UNIVERSITAT POLITÈCNICA
DE CATALUNYA
BARCELONATECH

Departament de Matemàtiques

PhD Thesis

Novel consensus strategies applied to spacecraft formation flight

Fabrizio Paita

Advisors: Prof. Josep J. Masdemont and Prof. Gerard Gómez

Barcelona, May 2017

Memòria presentada per aspirar el grau de Doctor en Matemàtiques per la Universitat Politècnica de Catalunya. Programa de Doctorat de Matemàtica Aplicada.

UNIVERSITAT POLITÈCNICA DE CATALUNYA
BARCELONATECH
Escola de Doctorat

Assessment results for the doctoral thesis

Academic year:

Full name

Doctoral programme

Structural unit in charge of the programme

Decision of the committee

In a meeting with the examination committee convened for this purpose, the doctoral candidate presented the topic of his/her doctoral thesis entitled

_____

_____.

Once the candidate had defended the thesis and answered the questions put to him/her, the examiners decided to award a mark of:

☐ FAIL ☐ SATISFACTORY ☐ VERY GOOD ☐ EXCELLENT

(Full name and signature) Chairperson	(Full name and signature) Secretary	
(Full name and signature) Member	(Full name and signature) Member	(Full name and signature) Member

_____, _____

The votes of the members of the examination committee were counted by the Standing Committee of the Doctoral School, and the result is to award the CUM LAUDE DISTINCTION:

☐ YES ☐ NO

(Full name and signature) Chair of the Standing Committee of the Doctoral School	(Full name and signature) Secretary of the Standing Committee of the Doctoral School

Barcelona, _____

Abstract

In this dissertation we consider the problem of developing distributed control strategies for spacecraft formation flying. In light of possible interferometric applications, the study is conducted in two different contexts: formation acquisition and keeping, and attitude synchronization. Among others, elements of Graph and Lyapunov stability theory are employed to modellize the formation dynamics and to establish analytically basic convergence properties for the proposed control laws.

In the case of formation acquisition and keeping, the related strategy is designed to asymptotically cancel the spacecraft relative velocities, so that they may reach fixed values for their relative distances. Previously applied with success to spacecraft travelling along transfer orbits to Lagrangian points, we consider it here in two different situations. First, in order to clarify the dependence of the control's performance from the Newtonian differential acceleration, we employ the strategy in a toy model consisting of a formation orbiting around a primary and being subject only to its gravitational pull. Then, we exploit the informations obtained to design a mission objective suitable for an optimal application of our control. The latter builds upon the scientific goals of the LISA Pathfinder mission and corresponds to periodic visits of the Earth-Moon-Sun saddle point, with the control employed in a neighborhood of this point to maintain a rigid formation.

For attitude synchronization instead, a numerical framework is developed to complement rigorous stability analyses on the associated controls. We show that, in the case of a time-invariant network topology, by employing a hierarchical graph structure for the formation it is possible to conduct computationally fast Monte Carlo simulations to describe a control's parameter space and its dependence from the formation dimension and relative initial conditions. The method is then exploited to compare the performance increase given by a novel adaptive gains design when applied to a PD-like control with constant ones.

Contents

List of Figures

Chapter 1

Introduction

1.1 Preface

As an example of multi-agent system, a formation of spacecraft, intended as a group of satellites operating in close proximity and in the context of the same mission, offers a variety of control challenges related to its dimensionality and to the inherent cross-states coupling. This is complicated further by aspects that pertain to the most disparate fields, ranging from propulsion and architecture techniques to the correct modellization of the spacecraft natural dynamics.

Thus, while the primary concern of this dissertation lies in the development of adaptive, distributed and efficient formation control strategies, equal importance is given to the tools employed to analyze this controls, which have to be simple but also capable of capturing the different aspects mentioned in the previous paragraph. Consequently, this thesis is characterized by a predilection for developing numerical frameworks that can be reused to analyze different controls, regardless of the induced closed-loop dynamics, and that act as a complement to more rigorous stability analyses (in general and for those performed here).

In order to understand what aspects need to be considered, in the present chapter we offer an historical review of the literature associated to the concept of spacecraft formation flying and the means through which this can be realized (Section 1.2). The review is then extended to the literature pertaining the development of distributed controls, starting from aspects common to different fields (Section 1.3.1) and proceeding to outline more recent contributions specific to spacecraft formation flying (Section 1.3.2). Finally, in Section 1.4, we present the outline of the thesis, pointing out its specific contributions and their location in different scientific outputs.

1.2 Spacecraft formation flying

One of the main reasons behind the interest in the dynamics and control of multi-agent systems lies in the belief that the latter, whether in a natural or artificial context, can surpass the performance and possess enhanced characteristics with respect to one composed of a single unit.

Focusing for the moment on human-made structures, the key point behind the previous statement lies in the possibility of dividing the payload and the tasks among the agents that comprise the system, which leads to several advantages. First of all, since the total payload is being divided among several units it is possible to employ simpler and cheaper designs, which provide not only an inherent economical advantage but also allow to parallelize the agents manufacturing, thus significantly speeding up this process.

A second point shared by all the possible applications of multi-agent systems is related to the enhanced task stability offered by this paradigm. In fact, differently from the case of single monolithic agents, losing one in a formation does not necessarily compromise the entire endeavour. Again, this is due to the fact that the payload is being divided among the agents of the system.

Finally, the use of multiple agents in a cooperative formation opens up new application possibilities, with examples foreseen in a vast array of fields like surveillance missions, demining, planetary exploration, coordinated attack and so on. Some of these have already been successfully implemented in ground robots [1], unmanned air vehicles [2], autonomous underwater ones [3] and satellites [4]. It is this last field that is of interest for the present thesis.

In particular, one of the most important exclusive operations associated with formations of spacecraft is given by the construction of distributed interferometric arrays [5], where the data collected by the different sources is superimposed to obtain a coherent and upgraded output. Since the accuracy of such a structure is determined by the baseline, that is by the distance between the sources, it is easy to understand how employing a formation would allow to extend the aperture of the interferometer far beyond the capabilities of a single connected spacecraft. A first utilization of these structures is given by the life components detection in extra solar planets, like envisioned for the Stellar Imager Concept [6] and the Terrestrial Planet Finder [7].

Similarly, multi-aperture telescopes have been proposed [8], and, in addition to what discussed above, offer the advantage of being easily maintainable and upgradable with additional modules when the formation is in close proximity to the Earth.

The last examples associated with interferometric superimposition of multiple homogeneous waves include on one side the synthetic aperture radar (SAR) missions for Earth imaging and remote sensing [9, 10], which exploit multiple small antennas (distributed among the various spacecraft) to intercept the reflection of electromagnetic wavefronts from the Earth, and on the other missions for improved measurements of Earth's magnetosphere through the acquisition of simultaneous measurements at different locations separated by a few kilometers [11].

The previous are all practical examples of spacecraft formation flying. Instead, if we want to formally describe this concept, we can start by looking at the words of Scharf, Hadaegh and Ploen [12], who describe a formation as "a set of more than one spacecraft whose dynamic states are coupled through a common control law. In particular, at least one member of the set must 1) track a desired state relative to another member, and 2) the tracking control law must at the minimum depend upon the state of this other member."

While accurate enough for what we are going to discuss in the present thesis, the previous definition may be a little bit too restrictive, since it does not apply to several different means of realizing a formation (in the sense described in the previous section). In particular, there is not always need to track a desired relative state in order to accomplish the mission, since this can be realized more simply by maintaining the agents in a bounded region or even by applying some structural limitation which does not require any tracking at all.

A first way to avoid coupling the agents through a control is given by systems provided with multiple actuations possessing some level of coordination, which degree is determined by the particular architecture of the system. An easy example for this case is given by multiple actuators and sensors related to an actively controlled architecture [13].

A similar kind of structural constraint can be found in thetered systems [14], with the tethers linking the different agents of the formation, thus naturally imposing kinematic constraints on the spacecraft. Obviously, this implies that the state evolution of one vehicle depends on those of some of the others.

Finally, different agents of a formation may be linked without an active form of control through their actuation. This is done for example in electromagnetic formation flying [15], where electromagnetic forces are used to control the relative motion of multiple spacecraft. Obviously, when these forces are switched off, the formation is naturally decoupled. But if more than one vehicle activates them, then the states of some of the agents will end up depending on those of some of the others.

Regarding these controls, in the literature we can find roughly two approaches. On one side, we have the leader-follower one [16, 17], where every agent of the formation (follower) simply traces the state of a central unit (leader), thus reducing the problem of controlling the follower to a well known tracking one and allowing a direct exploitation of the natural dynamics (and this is true both for attitude and translational controls). Of course, the downside of such an approach lies in the fact that the leader becomes a single point of failure for the entire mission. From this observation arises the second approach, where the formation is driven towards a certain state through local information exchanges among the agents, and which is often referred in the space community as behavioural approach [18, 19]. The algorithms generated by the latter, which we refer to as distributed consensus algorithms, represent the focus of this thesis and offer a plethora of different techniques to analyze and classify.

1.3 Distributed consensus algorithms

1.3.1 General overview

As we have mentioned in the previous chapter, distributed consensus algorithms are iterative procedures through which neighboring agents exchange informations on their respective dynami-

cal state in order to reach an agreement on the value of some function of these states, with or without the support of a central unit.

Also known as the alignment or agreement problem [20], consensus was early studied in a coherent and general manner by Tsitsiklis [21, 22], although works about biological multi-agent systems [23, 24] can be easily found in the same time period and even before [25]. In later years, the subject gathered increasing attention due to its wide range of applications which, besides the already mentioned development of coordination techniques for autonomous agents [26–31] and understanding of flocking phenomena in different dynamical systems [32, 33], include fields like parallel computing [34–36] and data fusion [37–42]. On a more theoretical side, it is interesting to note that a good portion of the literature is dedicated to reconduct these phenomena to the self-synchronization dynamics of coupled oscillators [43–49].

Distributed consensus algorithms, linear and nonlinear, have been studied both in continuous and discrete form, and are generally constructed in order for the associated dynamical system to reach consensus either on a certain state or on its derivative. While the first have been proved robust with respect to changes in the connectivity of the network and possessing a bounded state value [50], the latter offer instead resilience to propagation delays or coupling noise [51, 52]. A good survey for state converging algorithms, both continuous and discrete, can be found for example in [53, 54] and references therein, while those converging on the state derivative are well studied in [47, 48, 55–57].

The above offers a first level of separation among the various algorithms. A second one comes from all the possible characteristics associated with the network topology, as constructed starting from the communication links among the agents. In general, these describe a synchronous algorithm, that is one where the agents update their state always at the same time instant. Albeit not considered in this thesis, it is worth noticing that there exist also asynchronous algorithms, like the so called gossip algorithm [58–60], where, for every time instant, a randomly chosen single node wakes up and broadcast its state to the rest of the network according to certain rules.

For synchronous algorithms, the most widespread structure in the literature is given by a time invariant and symmetric topology [38, 61], where every link between the nodes is bidirectional and does not change with time. The first aspect has been dropped either by subjecting the topology to a randomized presence/absence of links [31, 62, 63] or, as done in [50], by making it switching, that is deterministically selecting at every time instant a topology extracted from a finite known set. In addition, these changing topologies have been considered even in the presence of time delays [50, 50, 64] and under the effect of additive noise [40, 65, 66].

As for topologies derived from unidirectional or mixed links, due to the difficulties in analyzing non-symmetric structures, we find generally less examples than the symmetric case. Still, similarly to the case of symmetric topologies, much work has been done with random [49, 67–69] or time-varying [70, 71] directed structures, and with adaptive/robust consensus strategies [72, 73] over such topologies.

1.3.2 In spacecraft formation flying

The aspects that we have previously described characterize any distributed consensus algorithm, regardless of the field to which the latter refers to. However, oftentimes these algorithms are shaped in forms that depend on the natural dynamics that one is trying to influence. For example, we have mentioned that such algorithms may converge to a certain state or derivative of one such. Yet, similar effects derived from these kind of convergences can be achieved with slightly different techniques. If we limit ourselves to spacecraft formation flying, these algorithms can, for example, take the form of virtual structure approaches [74], where a virtual copy of the system is defined for the latter to follow, or generalizations of sliding mode techniques [75], where trajectories move across regions determined by different discrete control modes, or they can even be shaped via the use of artificial potential functions [76], where a series of of acctractive and repulsive fields is used to lead the formation towards a desired state.

Although not really specific for formation flying, many of these control techniques involve the use of time-varying gains which, most of the time, are designed simply in order to improve the consensus rate of a given algorithm [77−81]. However, their role can be extended by allowing them to decay smoothly towards zero [82, 83], reached at a certain threshold for the inter-agents distance, in such a way that the spacecraft are able to automatically deal with changes in time of the network topology due to communication breaks or similar reasons.

The use of adaptive gains that we have just described is strictly related to the dynamics that is being influenced by the algorithm, since these gains are usually designed as functions of the relative distances among some states of the spacecraft. While of course it is possible to design different kind of gains for the translational and rotational dynamics with all their possible declinations, in recent years there has been an effort to define a unified framework for all the dynamical influences of the spacecraft [83, 84], via an Euler-Lagrange formulation of the equations of motion [85], in order to simplify the process of constructing advantageous adaptive topologies for spacecraft formations.

Of course, this leads to a very complex and nonlinear formulation of the dynamics [86], which therefore require sophisticated tools for a stability analysis as complete as possible. One classical approach to this analysis is given by Lyapunov Function Theory [87], which is based on the construction and study of appropriate energy-like functions used to derive informations on the asymptotical behaviour of the dynamics. Similar in some of its aspects, and often used in combination with the Euler-Lagrange networks of before, is the so called Contraction Theory [88], whose main result provide sufficient conditions for a vector field to be “contracting” and that it is often used to analyze stability of multiple trajectories with respect to one another. Finally, a third approach is given by the so called Input-to-State stability analysis [89], which provides an useful framework to formulate stability notions with respect to input perturbations. Of course, besides other analysis frameworks, the previously mentioned have been extended in order to accommodate for communication time delays [90, 91] and different kind of disturbances [87].

1.4 Thesis outline and contributions

As previously stated, the focus of this thesis is the development and analysis of adaptive distributed consensus algorithms for spacecraft formation flying. Both translational and rotational dynamics of the formation are considered, and they are either treated separately or, when coupled, will see one relying on strict assumptions in order to study specific derived effects on the other. The analysis conducted to evaluate the algorithms has a twofold purpose: it is developed in order to derive a description as global as possible of the closed loop dynamics induced by the proposed procedures and, as a consequence, a quantitative description of the advantage given by these algorithms in the associated context. Besides the present introduction, the thesis is developed in five additional chapters.

Chapter 2 is devoted to construct an analytical frame of reference for the rest of the thesis. In particular, we first review some basic concepts of Algebraic Graph theory and its matricial formulation, which are used throughout the field to modellize the information exchange among the spacecraft and to derive informations on how this affects the performance of different distributed control strategies. Secondly, with the help of the notions just introduced, we present an organic review of the most important results associated with distributed systems, starting from classical, linear single and double integrators and arriving to more modern results on nonlinear systems.

In Chapter 3 we introduce the main tools employed in this thesis. First, in light of the results discussed in the previous chapter, we consider a specific translational double integrator model, whose features are exploited in later chapters to develop our control strategies. Then, we introduce some notions of Lyapunov Function theory, which is one of the main frameworks used in the literature to analyze nonlinear distributed systems, and that is employed extensively in Chapter 5 to derive informations for the construction of a suitable attitude synchronization strategy.

Chapter 4 concerns the translational problem of formation acquisition and maintenance for a group of spacecraft. Following a previous work [92], we show how it is possible to translate the model of the previous chapter in a fully fledged control for the purpose at hand. Furthermore, we improve on the analysis started in that paper by outlining how the efficiency of the proposed control depends strongly on the differential vector field in which the relative dynamics takes place. This information is first extrapolated by considering a formation orbiting around a primary, and then exploited when designing an optimal application of the control in the context of periodic visits of the Earth-Moon-Sun saddle point from a group of spacecraft. Part of the results given in this chapter have been presented at the 2013 International Astronautical Congress held in Beijing, China [93].

Chapter 5 instead is dedicated to the rotational problem of attitude synchronization in a formation of spacecraft, where we want to drive those towards a common value of attitude and spin rate. The first novelty of this chapter lies in the construction of an adaptive design derived

from the model introduced in Chapter 2, and that we prove improving on the performance of a baseline PD-like control for formations floating in free space and with a three-axis stabilized leader. To derive this conclusion, we complement a rigorous stability analysis via Lyapunov Function theory with numerical simulations based on averaging and that exploit particular network topologies for increased computational performance and analytical bounds on the results obtained. This represents the second contribution of this chapter which, along with the previous one, is the subject of two conference papers [94, 95].

Finally, the previous chapter concludes with an expansion of the previous study that considers formations with a leader subject to a time varying trajectory. In particular, in light of the results of Chapter 4, the formations are assumed synchronizing while orbiting a primary, thus being subject to a non-vanishing keplerian acceleration.

To conclude this thesis, in Chapter 6 we summarize the results obtained and we outline future research directions to expand on the ones presented here. A similar overview, albeit reduced in scope, can be found in [96].

Chapter 2

Analytical background (I)

2.1 Introduction

The present chapter is devoted to the construction of an analytical framework of reference for the rest of the thesis, which has the double purpose of highlighting the main techniques and results associated with distributed consensus strategies, and to infer from these, in terms of derived or complementary results, the tools used in the next chapters to construct our control strategies.

In particular, in Section 2.2 we introduce some important notions of Algebraic Graph theory, which are commonly used to modellize the information exchange of a distributed system in an easily readable graph. Furthermore, we describe how these informations can be encoded in matrix form by exploiting the Adjacency and Laplacian matrices associated with the graph, and we outline the associated spectral properties useful to construct distributed control algorithms.

Secondly, in Section 2.3 we discuss distributed consensus algorithms for single-integrator dynamics, starting from a basic linear consensus model for time-invariant communication graphs, and we present necessary and sufficient conditions over the Laplacian eigenvalues in order to achieve consensus. Subsequently, we show how these can be translated in terms of connectivity of the underlying graph. Finally, we consider this basic algorithm in a series of interesting situations from a control point of view (different control objectives, time-varying graph, ...) and we show how it can be extended in order to achieve consensus even in these situations.

In Section 2.4 instead, we tackle the problem of designing distributed consensus algorithms for double-integrator dynamics which, within some limits, can be seen as an extension of its equivalent for single-integrator dynamics. Similarly to Section 2.3, we define a basic algorithm (which encompasses the one presented in the next chapter) and we discuss some associated convergence results, showing how they generalize those discussed in Section 2.2 and what it is they lose in the process. Furthermore, we point out why attitude dynamics represent a particular example of double-integrator system for which the analysis developed here is not directly applicable.

Finally, in Section 2.5 we complement the analysis done in the previous two sections by

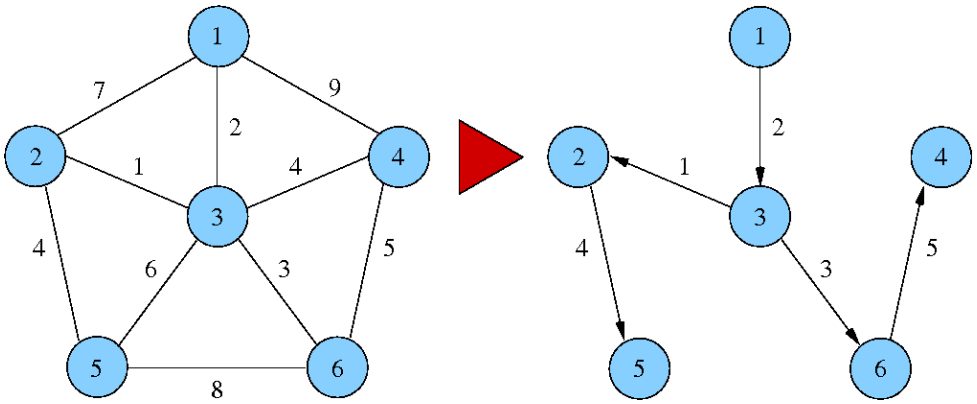

Figure 2.1: Weighted graphs topologies: undirected connected (left) and directed with a spanning tree (right).

discussing results concerning the convergence velocity of the algorithms presented, whether they arise from the spectral properties of the matrices involved or from advantageous communication graph designs.

2.2 Algebraic Graph theory

2.2.1 Graphs and connectivity

In the present subsection we recall the notion of graph along with some related concepts which we use throughout the thesis, and that offer a natural way to model interactions among multiple agents. A graphical example encompassing most of these notions is given in Figure 2.1, while a more extensive treatment of these concepts (along with those of the next subsection) can be found for example in [97].

First, we define a *graph* as a pair (X, Ω), where X is a finite non-empty set of indexed nodes (the agents) and $\Omega = X \times X$ is a set of pairs of nodes, which we call *edges* (the links determining the communication structure of the formation). These edges can have positive weights associated with them in order to specify the strength of each link in the graph. When this happens, we speak of a *weighted graph*. The following concepts are applicable to both kind of graphs, thus we draw no distinction and we continue using the graph denomination, albeit from now on we work only with weighted graphs. We also point out that, while a graph can be a time-varying structure, the following concepts still apply instantaneously. Therefore, without loss of generality, we can assume that our graph is time invariant.

That said, in an *undirected graph* the edges satisfy a symmetry property, that is if the nodes x_i and x_j are connected by an edge, then both nodes are passing informations to the other. In contrast, in a *digraph* (directed graph) every edge has a direction determined by the order of the pair (e.g., (x_i, x_j) means that x_i is passing information to x_j but not vice versa).

We say that a graph possesses a *path* if there exists a subset of Ω comprised of consecutive

edges, that is there exists an ordered subset of edges $(x_{i_1}, x_{i_2}), (x_{i_2}, x_{i_3}), \ldots, \left(x_{i_{N-1}}, x_{i_N}\right)$, with $\{i_1, \ldots, i_N\}$ denoting the indexes of the distinct nodes connected by the edges and where the order relation is determined by the first (parent) node of every edge being equal to the second (child) of the preceding one (with the possible exception of the first parent and the last child). We refer to this path as directed (undirected) if the corresponding graph is directed (undirected). Furthermore, we define as *root* the first parent of the path.

Starting from the concept of path it is possible to identify several ways in which informations spread across the graph. In particular we say that a directed (undirected) communication graph is *strongly connected* (*connected*) if there is a directed (undirected) path between any distinct pair of nodes. Moreover, we call *directed tree* a digraph where every node has exactly one parent, except for the root which we assume to have none. Finally, we say that a *directed spanning tree* of a digraph is a directed tree formed by edges that connect all the nodes in the graph. Such a structure is also a *subgraph* of the directed graph, that is a graph whose nodes set is a subset of the digraph one, and whose edges set equals that of the digraph restricted to the previous subset. Note that having a directed spanning tree is a weaker condition than being strongly connected, while in the case of an undirected graph the existence of an undirected spanning tree is actually equivalent to the graph being connected.

2.2.2 Matricial formulation

In the previous subsection we have seen how to use graphs to modellize interactions among multiple agents. However, in order to catch in an unitary fashion all the informations contained in a graph and to see how they affect consensus, it is useful to see things from a matricial point of view.

In particular, if $N \in \mathbb{N}$ indicates the number of nodes of a weighted graph G_N, then we define the *Adjacency matrix* $A_N = (a_{ij})$ of G_N as the matrix whose entries are the weights assigned to the edges of the graph. The rows correspond to the parent nodes and the columns to the child ones, with the order following the nodes indexation. Furthermore, we define the *Laplacian matrix* $L_N = (l_{ij})$ associated to a weighted graph as the matrix with diagonal entries $l_{ii} = \sum_{j \neq i} a_{ij}$ and out-of-diagonal ones $l_{ij} = -a_{ij}$.

As we are going to see in the next sections, the Laplacian matrix is an important informations repository when dealing with distributed consensus algorithms, and these informations are all encoded in its spectral properties. According to the Geršgorin circle theorem [98], in the complex plane the eigenvalues of the Laplacian L_N are located inside discs with centers l_{ii} and radii given by the row sums $\sum_{j \neq i} |l_{ij}|$. Since the diagonal entries of L_N are nonnegative and the row sums equal exactly these values, the Geršgorin circles lie on the right side of the plane and are tangent to the origin. Therefore, the eigenvalues of L_N have always nonnegative real parts and lie in a

complex circle of radius

$$d_M^+ = \max_{i\in\{1,\dots,N\}} d_i^+ = \max_{i\in\{1,\dots,N\}} \sum_{j\neq i} a_{ij}, \tag{2.1}$$

where the row sums d_i^+ are often referred in the literature as the *out-degrees* of the graph (with the *in-degrees* corresponding to the column sums).

Now, since $L_N \cdot \mathbf{1}_N = \mathbf{0}_N$, with $\mathbf{1}_N = [1, \dots, 1] \in \mathbb{R}^N$ and similarly for $\mathbf{0}_N$, we know that L_N has at least one zero eigenvalue with eigenvector $\mathbf{1}_N$. If the graph is undirected, then the Laplacian is positive semidefinite, its eigenvalues are real and therefore can be arranged as

$$0 = \lambda_1 \leq \lambda_2 \leq \cdots \leq \lambda_N \leq d_M^+. \tag{2.2}$$

Furthermore, the algebraic multiplicity of λ_1 which, as we are going to see in the next sections, determines whether consensus is reached or not, is one if and only if the undirected graph is connected [99]. In turn, this implies that the Laplacian L_N is irreducible, that is it does not exists a permutation making it similar to a block upper triangular matrix with more than one block of positive size.

The case of a digraph is a little bit more complex. First, the Laplacian is not symmetric. Yet, a necessary and sufficient conditions for λ_1 to be an eigenvalue of algebraic multiplicity one still exists, and it is that the digraph possesses a directed spanning tree [100]. However, the necessary and sufficient condition for the Laplacian being irreducible is different and requires for the associated graph to be strongly connected [99]. As we are going to show, in certain situations this implies a different behaviour of a given algorithm.

To conclude, let us note that in the previous statements we have implicitly assumed that the Laplacian was operating on $\mathbb{R}^N$, with the vectors components living in $\mathbb{R}$. The latter is in general not true, thus, while the previous statements continue to hold regardless of the space dimension, a different notation must be adopted to describe what follows in the next sections. That is, let x denote the column vector $x = [x_1, \dots, x_N]$, where $x_i \in \mathbb{R}^m$. Then, under the conditions previously mentioned, $(L \otimes I_m)\, x = 0$ if and only if $x = \mathbf{1}_N \otimes \alpha$ (i.e, $x_1 = \cdots = x_N = \alpha$), with $\alpha \in \mathbb{R}^m$ and $\mathbf{1}_N = [1, \dots, 1]$ belonging to $\mathbb{R}^N$, and where $\otimes$ denotes the Kronecker product. The latter, if A is a $m \times n$ matrix and B is a $p \times q$ matrix, is defined by the $mp \times nq$ block matrix

$$A \otimes B = \begin{bmatrix} a_{11}B & \dots & a_{1n}B \\ \vdots & \ddots & \vdots \\ a_{m1}B & \dots & a_{mn}B \end{bmatrix}. \tag{2.3}$$

2.3 Consensus for single integrator dynamics

2.3.1 Time invariant topology

The continuous case

Single integrator or first order differential systems are used to represent dynamical models where, given a set of describing coordinates, we are interested only in the values of these coordinates and not on that of their derivatives (i.e., for a set of moving particles we would be interested only in their positions and not their velocities). In continuous time, and without the presence of any external force, these systems can be described by the equations of motion

$$\dot{x}_i(t) = u_i(x,t), \quad i = 1,\ldots,N, \tag{2.4}$$

where the states x_i and the control inputs u_i both belong to $\mathbb{R}^m$, $t \in \mathbb{R}^+$ and x denotes the column vector $x = [x_1, \ldots, x_N]$ (with N being the dimension of the formation).

One of the simplest consensus algorithms for the previous system is given by the linear equation [50]

$$u_i = -\sum_{j=1}^{N} a_{ij}(x_i - x_j), \quad i = 1, \ldots, N, \tag{2.5}$$

where the gains $a_{ij} = a_{ij}(x,t) \geq 0$ represent the (i,j) entries of the Adjacency matrix $A_N(x,t) \in \mathbb{R}^N \times \mathbb{R}^N$ at time t. Thus, as seen at the end of the previous section, we can write the previous equations in matrix form as

$$\dot{x} = -\left[L_N(x,t) \otimes I_m\right] x, \tag{2.6}$$

where L_N denotes the Laplacian matrix at time t, I_m the m-dimensional identity matrix and $\otimes$ the Kronecker product. We say that consensus for system (2.6) is achieved if, for all $x(0)$ and $(i,j) \in \{1, \ldots, N\}^2$, $\|x_i(t) - x_j(t)\|_2 \to 0$ for $t \to \infty$.

Assuming a time invariant communication graph, in light of the results on the Laplacian eigenvalues presented in the previous section, it is convenient to split our analysis of consensus with respect to the structure of the graph. In particular, for a digraph we have [101]

Theorem 1. *Suppose that A_N is a time invariant matrix and the associated graph G_N is directed. Then system* (2.6) *achieves consensus if and only if G_N possesses a directed spanning tree. Furthermore, $x_i(t) \to \sum_{j=1}^{N} \nu_j x_j(0)$ as $t \to \infty$, where $\nu_j \geq 0$ for all j, $\mathbf{1}_N^T \cdot \nu = 1$ and $L_N \nu = 0$.*

The convergence to a consensus value can be proved to be exponential [54] and it follows from the properties of the solution $x(t) = e^{-L_N t} x(0)$ of system (2.6). The undirected connected

case is similar and it can actually be posed as a corollary of the directed one [50], giving the result

Theorem 2. *Suppose that A_N is a time-invariant matrix and the associated graph G_N is undirected. Then system* (2.6) *achieves consensus if and only if G_N is connected. Furthermore, $x_i(t) \to \frac{1}{N}\sum_{j=1}^{N} x_j(0)$ as $t \to \infty$.*

As you can see, in the case of an undirected connected graph, the consensus value is defined and it corresponds to the average of the initial states. Thus, in the literature this condition is often referred to as *average consensus*.

In the direct case the values of the ν_j's, which in turn determine the consensus one, are directly related to the connectivity of the graph. For example, if there exists a node k in G_N without an incoming edge (and since G_N has a spanning tree, only one node of this kind can exist), then it will result $\dot{x}_k(t) = 0$ and therefore $x_k(t) = x_k(0)$ for all $t \in \mathbb{R}^+$. Thus, all nodes will converge to $x_k(0)$, that is $\nu_k = 1$ and $\nu_j = 0$ for all j.

On the other side of the spectrum, given a digraph it is still possible to reach average consensus, but the graph has to be strongly connected and balanced [54] (that is $\sum_{j=1}^{N} a_{ij} = \sum_{j=1}^{N} a_{ji}$ for all i). Intuitively, if there is no path from node i to node j it is impossible for $x_j(t)$ to be influenced by $x_i(t)$. Thus, in order for every agent to be influenced by every other, the digraph has to be strongly connected. The latter also implies that the consensus value is given by $\left(\gamma^T x(0)\right) / \sum_{i=1}^{N} \gamma_i$, where γ is the left eigenvector of L_N corresponding to the null eigenvalue (which is also simple). If the graph is balanced then $\gamma_i = 1$, which in turn implies average consensus. Finally, with a counterexample [50] it can be shown that balance is also a necessary condition.

We conclude this analysis with a remark on the consensus velocity of algorithm (2.5). We have mentioned before that the convergence is exponential. In Section 3.1 we are going to see that, for an undirected connected graph (or a strongly connected, balanced digraph) and a double integrator system, the consensus velocity, defined through a deviation function from average consensus, is at least of the order of $O\left(e^{-\lambda_2 t}\right)$. The same [50] can be proved for system (2.6) (of course, for a general digraph things are much more complicated). A well known observation regarding λ_2 for the undirected case is that this eigenvalue is relatively large for dense graphs and relatively small for sparse ones [102]. Thus, it is sometimes referred to in the literature as *algebraic connectivity* of a graph.

Extensions of the continuous case

The system (2.6) represents a fundamental model for consensus in single integrator dynamics. However, depending on the application, this may be extended to deal with different situations. Here we discuss three such extensions which are often encountered in formation control.

In the first case, instead of states being equal at consensus one may want for their differences to reach certain desired values, that is $x_i(t) - x_j(t) \to \Delta_{ij}(t)$, with $\Delta_{ij} = \Delta_{ij}(t)$ denoting the requested time-varying distance. To reach this state, one can consider the algorithm [101]

$$u_i = \dot{\delta}_i - \sum_{j=1}^{N} a_{ij} \left[(x_i - x_j) - (\delta_i - \delta_j) \right], \quad i = 1, \ldots, N, \tag{2.7}$$

where $\delta_i - \delta_j = \Delta_{ij}$. Do note that algorithm (2.6) can be seen as a particular case of (2.7) where $\Delta_{ij}(t) = 0$ for all $t \in \mathbb{R}^+$ and $i \neq j$. In particular, one can reconduct (2.7) to (2.6) by imposing $\hat{x}_i(t) = x_i(t) - \delta_i(t)$ and consequently derive

$$\dot{\hat{x}}_i = -\sum_{j=1}^{N} a_{ij} \left(\hat{x}_i - \hat{x}_j \right), \quad i = 1, \ldots, N. \tag{2.8}$$

By applying theorems 1 and 2 one can conclude, under conditions appropriate for those results, that $\hat{x}_i(t) \to \hat{x}_j(t)$ for every i and j, and therefore that $x_i(t) - x_j(t) \to \Delta_{ij}(t)$.

Another situation often encountered when controlling a formation of artificial agents, is given by the presence of perturbations in the dynamics. Thus, under these perturbations, system (2.6) becomes [101]

$$u_i = -\sum_{j=1}^{N} a_{ij} \left(x_i - x_j \right) + w_i, \quad i = 1, \ldots, N, \tag{2.9}$$

where $w_i = w_i(t) \in \mathbb{R}^m$ denotes the perturbation term for agent i. Under the previous signal, and with the usual notation for w, the model (2.4) can be rewritten in matrix form as

$$\dot{x} = -\left[L_N \otimes I_m \right] x + \mathbf{1}_N \otimes w. \tag{2.10}$$

If the perturbations are all equal, that is $w_i = w_j$ for all $i \neq j$, then it can be proved that [101]

Theorem 3. *Suppose that A_N is constant and that G_N is directed. Then algorithm* (2.9) *achieve consensus asymptotically if and only if G_N has a directed spanning tree. In particular $x_i(t) \to \sum_{i=j}^{N} \nu_j x_j(0) + \int_0^t w(\tau)\, d\tau$ as $t \to \infty$, where $\nu_j \geq 0$ for all j, $\mathbf{1}_N^T \cdot \nu = 1$ and $L_N \nu = 0$.*

The previous result follows from the fact that the solution for (2.10) is given by $x(t) = \left(e^{-L_N t} \otimes I_m \right) x(0) + \int_0^t \left(e^{-L_N (t-\tau)} \otimes I_m \right) \left(\mathbf{1}_N \otimes w(\tau) \right) d\tau$. Thus, similarly to what said for theorem 1, one can exploit the properties of the Laplacian exponential matrix to prove consensus [101].

The general case can be reconducted to the previous one by imposing $\tilde{x} = [x_{12}, \ldots, x_{1N}]$ and $\tilde{w} = [w_{12}, \ldots, w_{1N}]$, where $x_{ij} = x_i - x_j$ and similarly for w_{ij}, which leads to (2.4) becoming

$$\dot{\tilde{x}} = -\left[Q \otimes I_m \right] \tilde{x} + \mathbf{1}_N \otimes \tilde{w}, \tag{2.11}$$

where $Q \in \mathbb{R}^{(N-1)} \times \mathbb{R}^{(N-1)}$ is constant. This is a linear time invariant system, therefore asymptotical stability (which follows from the previous theorem) implies bounded input, bounded state stability [101], that is, if $\tilde{w}$ is uniformly bounded, so is $\tilde{x}$. This is equivalent to state that if $\|w_i - w_j\|$ is uniformly bounded, then the same is true for $\|x_i - x_j\|$. Do note that, as in the case of $w_i = w_j$ for all $i \neq j$, there cannot be a steady state, since the perturbation vector w is assumed to be non vanishing.

The final modification of model (2.6) that is of interest for practical applications happens when there are time delays in the information exchanges between the agents. If we denote with τ_{ij} the information delay between agents i and j, and we assume that $\tau_{ij} = \tau_{ji}$ for all i and j, then algorithm (2.5) becomes [50]

$$u_i(t) = -\sum_{j=1}^{N} a_{ij}\left(x_i(t-\tau_{ij}) - x_j(t-\tau_{ij})\right), \quad i = 1, \ldots, N. \tag{2.12}$$

Thus, if we consider system (2.4) equipped with control (2.12), after a Laplace transform of both sides the former can be written for every i as

$$sX_i(s) - x_i(0) = \sum_j a_{ij} h_{ij}(s)\left(X_j(s) - X_i(s)\right), \tag{2.13}$$

with $X_i(s)$ denoting the Laplace transform of $x_i(t)$. In a matricial form, the previous equation gives

$$X(s) = \left(sI + L^{\star}(s)^{-1}\right) x(0), \tag{2.14}$$

where $L^{\star}(s)$ denotes the Laplacian associated with the Adjacency matrix $A^{\star}(s) = [a_{ij}h_{ij}(s)]$ and $h_{ij}(s)$ the transfer function of edge (i,j).

The discussion on time-delayed systems is rather involved, thus we limit ourselves to consider the simplest case possible, where the time-varying graph is undirected and connected and the time delay in all communications is equal to $\tau > 0$. The first consequence of these assumptions is, similarly to the non-delayed undirected connected case, that the sum of the signals (2.12) is zero and therefore the average $\frac{1}{N}\sum_{j=1}^{N} x_j(t)$ is time invariant [103]. In addition, the Laplacian $L^{\star}(s)$ becomes

$$L^{\star}(s) = e^{-\tau s} L_N, \tag{2.15}$$

with L_N denoting the Laplacian associated to the undirected connected graph. With these observations in mind one can prove that [50]

Theorem 4. *Consider the system* (2.4) *equipped with control* (2.12)*, where $\tau_{ij} = \tau$ for all $(i,j) \in \{1, \ldots, N\}^2$. Additionally, assume that the underlying graph is time invariant, undirected and connected. Then consensus is achieved if and only if one of the following conditions is satisfied:*

- $\tau \in (0, \tau^\star)$ *with* $\tau^\star = \frac{\pi}{2\lambda_N}$ *and* $\lambda_N = \lambda_{max}$.
- *The Nyquist plot of* $\Gamma(s) = \frac{e^{-\tau s}}{s}$ *has a zero encirclement around* $\frac{-1}{\lambda_k}$, $\forall k > 1$.

Moreover, for $\tau = \tau^\star$ *the system has a globally asymptotically stable oscillatory solution with frequency* $\omega = \lambda_N$.

Leaving aside the second condition, let us focus on the consequences of the first one. The latter is saying that the time delay cannot be greater that a certain quantity in order to achieve global consensus. This bound can be further refined by observing that, for the Geršgorin Circle theorem, $\lambda_N \leq 2d_M^+(G_N)$, where $d_M^+(G_N)$ is again the maximal outdegree of graph G_N. Thus, we have the sufficient condition

$$\lambda_N \leq \frac{\pi}{4d_M^+(G)} \tag{2.16}$$

This means that if the nodes have relatively high outdegrees, they cannot stand relatively high communication time delays. On the other hand, let $\tilde{A} = kA$ be the Adjacency matrix of the new graph $\tilde{G}$, with $k > 0$. Similarly, denote with $\tilde{L}_N$ the associated Laplacian, and observe that $\lambda(\tilde{L}_N) = k\lambda(L_N)$. Thus, for any arbitrary delay $\tau > 0$, there exists a sufficiently small $k > 0$ such that $\tau < \pi/(2k\lambda_N)$. Therefore, in principle, one could rescale the weights of the graph in order to tolerate any delay $\tau > 0$. The problem is that the value of λ_2, which determines the consensus velocity, degrades by a factor of $1/k > 0$. Therefore, in the presence of time delays there appears to be a tradeoff between the robustness of a protocol and its performance.

The discrete case

When interaction among vehicles occurs at discrete time instants, the information state is updated using a difference equation. In particular, fundamental algorithm (2.5) becomes [101]

$$x_i[k+1] = \sum_{j=1}^{N} a_{ij}[k]\, x_j[k], \tag{2.17}$$

where $k \in \{0, 1, \dots\}$ denotes the discrete time and where $A_N[k]$ is assumed to be a row-stochastic matrix (that is $\sum_{j=1}^{N} a_{ij} = 1$ for all i) satisfying $a_{ii} > 0$ for all $i \in \{1, \dots, N\}$ (besides $a_{ij} > 0$ whenever i and j are connected by an edge and $a_{ij} = 0$ otherwise). We remark that the model (2.17) is actually slightly more general than a real discretization of (2.6), since it allows the contribution of $x_i[k]$ to be arbitrarily rescaled. Similarly, given a time invariant nonnegative matrix, it can be made row-stochastic by rescaling the gains of the rows by $\| \sum_{j=1}^{N} a_{ij} \|_2$.

In a manner formally equal to the continuous case, one may rewrite the previous system in matrix form and define consensus for it. In order to derive connectivity conditions to achieve the latter with algorithm (2.17), we first need to observe some things about the spectral properties of

nonnegative matrices (with some of them having been discussed in Section 2.1.2). Assuming that the associated graph is directed, we have [101]

Lemma 1. *If a nonnegative matrix $A = [a_{ij}] \in \mathbb{R}^N \times \mathbb{R}^N$ has the same positive constant row sums given by $\mu > 0$, then μ is an eigenvalue of A with associated eigenvector $\mathbf{1}_N$ and the spectral radius $\rho(A)$ actually equals μ. In addition, the eigenvalue μ of A has algebraic multiplicity one if and only if the underlying digraph has a directed spanning tree. Finally, if $a_{ii} > 0$ for all $i \in \{1, \dots, N\}$, then $|\lambda| < \mu$ for every other eigenvalue of A.*

From the previous lemma, we know that, in the presence of a spanning tree, a row-stochastic matrix with a positive diagonal has as largest (and simple) eigenvalue 1. It can be proved [101], as a consequence of more general properties, that this implies $\lim_{m\to\infty} A^m = \mathbf{1}_N \nu^T$, where ν satisfies $A^T\nu = \nu$ and $\mathbf{1}_N^T \nu = 1$. Similarly to the continuous case, the previous properties allow to state the consensus result [101]

Theorem 5. *Suppose that A_N is a time-invariant matrix and the associated graph G_N is directed. Then system* (2.17) *achieves consensus if and only if G_N possesses a directed spanning tree. Furthermore, $x_i[k] \to \sum_{i=1}^N \nu_i x_i[0]$ as $k \to \infty$, where $\nu_i \geq 0$ for all i, $\mathbf{1}_N^T \cdot \nu = 1$ and $A_N \nu = \nu$.*

Results similar to the continuous case can be obtained for balanced digraphs and undirected connected ones, in terms of necessarity and sufficiency for consensus achievement (for the latter) and convergence to average consensus (for both of them) [54]. Note that in the reference given, in order to make the spectral radius of the Adjacency matrix a simple eigenvalue, the digraph is assumed to be strongly connected (which, as we have seen before, is equivalent to ask for an irreducible matrix). Of course, this is a weaker condition than the one asked here.

To conclude, we want to remark that, in system (2.17) we have implicitly assumed that the discretization step h of the method equalled one. If we write $x_i[k] = x_i(kh)$, then we can consider the more general algorithm [54]

$$x_i[k+1] = x_i[k] + h \sum_{j \neq i} a_{ij}[k] (x_i[k] - x_j[k]) = [(I_N - hL_N) x[k]]_i , \tag{2.18}$$

where in the last equation we have dropped the Kronecker product notation for commodity. Do note that here we are assuming $a_{ii} = 1$ for every i, but we are not yet imposing any hypothesis on the Perron matrix $P = I - hL$. The importance of the previous algorithm lies in the fact that some properties of P, sufficient to achieve consensus, depend on the size of the discretization step h with respect to the maximal outdegree d_M^+ of the graph. In particular [54]

Lemma 2. *Let G_N be a digraph with maximal outdegree d_M^+. Then, if the discretization step h of the Perron matrix satisfies $h \in \left(0, \frac{1}{d_M^+}\right]$, it results*

- *P is a row-stochastic matrix*

- *If G_N is a balanced graph, then P is also column-stochastic*
- *If G_N is strongly connected, then P is also primitive, that is there exists $k \in \mathbb{N}$ such that the entries of P^k are all positive*

Thus, as long as the discretization step is properly bounded, one can recover the same results of (2.17). Furthermore, again following a path similar to that of the continuous case, if the graph G_N is strongly connected and balanced, and as long as the previous bound on h remains true, average consensus can be proved [54].

2.3.2 Dynamically changing topology

In this subsection we consider the problem of achieving consensus for system (2.4) under the effects of a time varying graph. More specifically, in a control context, this means that the distribution of the edges and/or the associated gains vary with time (either deterministically or stochastically), while the nodes remain the same. Roughly speaking, in the deterministic approach one tries to limit the set of the possible states that a graph can assume by imposing bounds on some relevant quantities, up to defining a priori the states themselves. Conversely, in the stochastic approach the graph is usually assumed to vary according to some probability distribution, thus making the states random variables and the system stochastic.

Now, in a deterministic modelling the starting point is usually the frequency with which the graph changes its structure. This observation standing, the continuous system (2.4) can be rewritten as [101]

$$\dot{x}(t) = -\left[L_N(t_i) \otimes I_m\right] x(t), \quad t \in [t_i, t_i + \tau_i), \tag{2.19}$$

where $\tau_i > 0$ denotes the *dwell time* [104], that is the period between two consecutive switchings, and $t_0, t_1, \ldots$ is the infinite time sequence such that $t_{i+1} - t_i = \tau_i$. Do note that, since A_N is assumed constant between switchings, then both $A_N(t)$ and $L_N(t)$ are piecewise continuous functions. This kind of topologies are aptly known in the literature as *switching topologies*.

By limiting ourselves to discuss only the general case of a digraph, consensus for the model (2.19) can be described by the following result

Theorem 6. *Suppose that $A_N(t) \in \mathbb{R}^N \times \mathbb{R}^N$ is piecewise continuous and that its positive entries are both uniformly lower and upper bounded, that is $a_{ij} \in [\underline{a}, \bar{a}]$ $(0 < \underline{a} < \bar{a})$ if i and j are connected by an edge, and $a_{ij} = 0$ otherwise. Let $t_0, t_1, \ldots$ be the time sequence corresponding to the times at which A_N switches, where, for all i, it is assumed that $t_i - t_{i-1} \geq t_L$, with t_L being a positive constant. Continuous time algorithm* (2.5) *achieves consensus asymptotically if there exists an infinite sequence of contiguous, nonempty, uniformly bounded time intervals $\left[t_{i_j}, t_{i_{j+1}}\right)$ $(j \in \mathbb{N})$ starting at $t_{i_0} = t_0$, with the property that the union of directed graphs $G_N(t)$ across each such interval has a directed spanning tree.*

The previous theorem is telling us that a sufficient requisite for consensus is that the system does not switch "infinitely" fast, both in time (with the switching times having a minimum distance) and in the gains value (which cannot change too drastically). Furthermore, the union of the graphs derived by considering G_N on the intervals $\left[t_{i_j}, t_{i_{j+1}}\right)$ has to present a directed spanning tree often enough. This is required in the proof [105] in order for the zero eigenvalue of the Laplacian to present algebraic multiplicity one often enough, which, as we have seen in the previous sections, is a fundamental requirement in the time invariant case.

In line with what we have seen in the latter case, different, mainly stronger, conditions can be asked to the union of the graphs $G_N(t)$ in order to achieve consensus. For example, in [26] undirected graphs are considered and it is shown, as consequence of a slightly more general result, that a sufficient condition for consensus is for this union (and not necessarily the single graphs) to be connected "often" enough, so that the Laplacian remains irreducible for a sufficient amount of time. On the side of digraphs, irreducibility is exploited also in [50], where hypotheses stronger than those of the theorem above are made. In particular, not only the graph has always to be strongly connected and balanced, but also, at every time instant, it is assumed to belong to a finite set of predefined topologies. Clearly, this result is weaker than the one presented in [26] (due to the requirement on the topologies set), which in turn can be seen as a particular case of Theorem 6. We remark that these results can be readily extended to the discrete case and these extensions can be found in the corresponding works mentioned before. In what follows we are going to mention a discrete version of Theorem 6 (with slightly different hypotheses), and we use it to draw a comparison with some results associated with random networks.

Speaking of the latter, the underlying idea behind their study lies in the fact that when one tries to control a formation of automated vehicles, there are several "random" factors that may cause the communication graph to change, of which mechanical or electronic failures in the agents are the primary example. As we have mentioned at the beginning of the subsection, these imply that the Adjacency matrix A_N becomes random and therefore the states $x_i[k]$ can be seen as random variables. Although here we limit ourselves to treat only the discrete case, it should be noted that, by considering models similar to (2.19), it is possible to introduce random elements also for continuous control algorithms [106].

The first thing to observe is that the consensus objective can be now better phrased in terms of almost sure convergence, that is we say that system (2.17) achieves consensus if $x[k]$ converges almost surely to a certain vector $\hat{x}$ or equivalently

$$Pr\left\{\lim_{k\to\infty} x[k] = \hat{x}\right\} = 1. \tag{2.20}$$

We remark however that sometimes it is more convenient to rephrase consensus in a different manner or ask for a weaker condition. Thus, we have the two following definitions

Definition 1. *We say that $x[k]$ converges to $\hat{x}$ in the mean square sense if*

$$\lim_{k\to\infty} \mathbb{E}\left[\|x[k] - \hat{x}\|_2^2\right] = 0. \tag{2.21}$$

and

Definition 2. *We say that $x[k]$ converges to $\hat{x}$ in probability if, for any $\delta > 0$,*

$$\lim_{k\to\infty} Pr\left[\|x[k] - \hat{x}\|_2 > \delta\right] = 0. \tag{2.22}$$

Do note that both almost sure and mean square convergence imply the probability one, and that mean square convergence can be in principle generalized to an r-th mean convergence.

In the continuous time, switching topology case, we have seen that it is not necessary for the connectivity properties to hold always but only often enough. This remains true also in the discrete case, where the following theorem can be stated [107]

Theorem 7. *Consider the deterministic sequence of row-stochastic Adjacency matrices $\{A_N[k]\}_{k=0}^{+\infty}$. Then algorithm* (2.17) *solves the consensus problem if and only if there exits a finite positive integer number K such that, for $k \in \mathbb{N}$, the graphs $\bar{G}_N(k) = G_N(k) \cup G_N(k+1) \cup \cdots \cup G_N(k+K-1)$ all possess a directed spanning tree. Furthermore, if the Adjacency matrices are also column stochastic, then the consensus problem is automatically solved.*

Similarly to the continuous case, the requested connectivity conditions over a definite time window guarantee that information travels, possibly with some time delay, from at least one node to any other node infinitely many times. Still, the convergence rate defined in the proof is based on a worst case scenario, thus making this theorem not very practical to employ in the analysis of real systems.

The previous result has been stated by several authors, oftentimes with some modifications attached. One of the different directions considered is in finding tighter bounds on the rate of convergence while adding only general constraints on the topology of the underlying graph or on the numerical values of the edges (as it has been done for example in the references mentioned before). Of course, another one concerns the search for a similar result when random sequences of stochastic matrices are used. In this context, Theorem 7 can be restated as [108]

Theorem 8. *Consider a random sequence of independent and identically distributed row-stochastic matrices $\{-L_N[k]\}_{k=0}^{+\infty}$, drawn according to some probability distribution from a given set, along with their expectation $\bar{L}_N = \mathbb{E}[-L_N[k]]$. If the graphs $G_N[k]$, for all k, and $\bar{G}_N$ all possess a directed spanning tree, then the probabilistic consensus problem is solved. Furthermore, the rate of convergence in the mean square sense, defined as $\rho = \sup_{x(0)} \limsup_{k\to\infty} \left(\mathbb{E}\left[\|x[k] - x[\infty]\|^2\right]\right)^{\frac{1}{k}}$, is bounded by*

$$esr\left(\left(\bar{L}_N\right)^2\right) \leq \rho \geq sr\left(\mathbb{E}\left[L_N[k]^T \Omega L_N[k]\right]\right), \tag{2.23}$$

where $\Omega = I_N - \frac{1}{N}\mathbf{1}\mathbf{1}^T$, while $esr(P)$ and $sr(P)$ denote respectively the essential and spectral radius of P, that is their smallest and largest eigenvalue respectively. In addition, if the Laplacians L_N are double stochastic, then the average consensus problem is solved.

As it can be seen, similarly to Theorem 7, convergence to consensus is guaranteed if the graph is connected on average. However, differently from the same result, the randomized framework provides tighter bounds on the rate of convergence. Finally, the previous result can be further extended in the sense of weakening the i.i.d hypothesis to simple ergodicity [109] or adding additional hypotheses on the entries of the Laplacians [110].

To conclude this subsection, we look briefly at models where "randomness" takes a slightly different form with respect to what discussed up to now. Due to the increasing distance from the main problems of the thesis, no results are given and we limit ourselves to point out the relevant literature of the respective fields. The first extension that we present concerns consensus processes subject to $quantization$ [111], and in particular quantized communications. Quantization can be described as a nonlinear process applied to physical quantities in order to represent them numerically. A practical application of this concept can be found in wireless sensor networks, which are exposed not only to power constraints to reduce the energy consumption, but also to bandwidth constraints, which lead to the common practice of quantizing the information before transmitting it. Analytically, a quantizer is usually a staircase function $\psi_d : \mathbb{R} \to Q_d$, with Q_d being a finite or countable set, that transforms a continuous set of values into a discrete one by rounding these values to their nearest unit or quantization level (thus, a simple quantizer is given by the integer part). Consequently, one can rewrite for example the consensus model (2.17) as [112]

$$x_i[k+1] = \sum_{j=1}^{N} \psi_d\left(a_{ij}[k]\, x_j[k]\right),\ i = 1, \ldots, N. \tag{2.24}$$

The main problem of these systems is that quantization acts similarly to noise by introducing an error between the original and the quantized data, which in turn destabilizes the consensus matrices, thus making convergence no longer guaranteed. Yet, when it is, these systems act similarly to the corresponding time invariant ones, with the convergence speed being almost the same as long as the quantization step is much smaller than the distance from consensus [113]. Consequently, we can find research directions similar to those presented here for time invariant systems, ranging from the inclusion of noise into the model [65] to the modification of quantization in a probabilistic sense [114], up to the introduction of random link failures [115].

A second variation comes from consensus scenarios subject to lossy communication, that is scenarios where communication scheduled between two nodes fails due to random interference or noise. Although this instance may fit the randomized framework of Theorem 8 above, it also requires a compensation mechanism when the packet is lost. A simple example of the latter (but several others have been proposed [63, 116, 117]) consists in replacing the lost value x_j from

node j with the self value of the receiver x_i. This can be written formally as [116]

$$x_i[k+1] = \left(a_{ii}[k] + \sum_{j \neq i} (1 - \gamma_{ij}[k]) a_{ij}[k] \right) x_i + \sum_{j \neq i} \gamma_{ij}[k] a_{ij}[k] x_j[k], \; i = 1, \ldots, N, \tag{2.25}$$

where $\gamma_{ij}[k]$ is a Bernoulli random variable. At time k, transmission success between nodes i and j is denoted by 1. In general, packet loss does not affect convergence to consensus, but it can reduce the convergence speed and change the final consensus value with respect to the "perfect" case of $\gamma_{ij} = 1$ at every time instant.

Finally, in the same manner of what done in Section 2.3.1 for the continuous case, one can study a model of a discrete system subject to additive noise. In its simplest form this obviously reads as [65]

$$x[k+1] = A[k] x[k] + w[k]. \tag{2.26}$$

Differently from the previous case, here also convergence itself is an issue, and the main objective lies in modifying the standard consensus algorithm in order to avoid noise accumulation. The general approach is to design adaptive algorithms aimed to dampen the effect of neighbours noise [118, 119], but there exist also alternative strategies (for example, in [120] the noise is decreased through the use of error correcting codes of increasing length).

2.4 Consensus for double integrator dynamics

In this section we consider distributed consensus algorithms for double integrator dynamics, that is for systems where the motions of the states and their derivatives are both taken into account. Similarly to what done in the single integrator context, we consider a baseline model in order to describe the relevant features of this kind of systems. However, differently from what done in the previous section we do not extend this model in order to take into account different consensus objectives. Instead, we focus on showing how the model the we present here can be seen as a natural extension of (2.6) and what are the differences between the two. As a consequence, it will be perfectly clear how to adapt the different modifications of (2.6) to the new model and its characteristics.

The prototype for a double integrator system is given by the equations

$$\dot{x}_i = v_i, \quad \dot{v}_i = u_i, \tag{2.27}$$

where $x_i \in \mathbb{R}^m$ denotes the information state, $v_i \in \mathbb{R}^m$ its derivative and $u_i \in \mathbb{R}^m$ the control input associated with the i-th agent. Most often, (2.27) is what one encounters when controlling the translational dynamics of a group of particles moving in free space. Furthermore, under the appropriate parametrization, attitude dynamics can be described by a similar set of equations.

However, as we are going to see, not only the inherent nonlinearity of the dynamics reflects itself in the equations, but it also prevents a direct application of the following discussion.

Coming back to (2.27), in order to understand the differences with the single integrator case, we introduce the general linear control algorithm [101]

$$u_i = -\sum_{j=1}^{N} a_{ij}(t)\left[(x_i - x_j) + \gamma(t)(v_i - v_j)\right], \tag{2.28}$$

where the notations of the single integrator case still holds and $\gamma(t) > 0$.

The most important difference between consensus algorithms for single and double integrator dynamics comes from the proliferation of possible consensus objectives that one can achieve. In fact, if in the single integrator case one could only have the states converging to the same value (a change in control is required to achieve some definite relative distances), for the model (2.27) not only one has to take into account the consensus behaviour of the states derivative, but also how the latter interacts with the states themselves (as we are going to see, this mechanism is exploited in the construction of the control considered in the next two chapters).

Here we limit ourselves to consider only the more educational consensus objectives. As a first step, we say that consensus is achieved if, for all $(i,j) \in \{1, \ldots, N\}^2$, it results $\|x_i - x_j\|_2 \to 0$ and $\|v_i - v_j\|_2 \to 0$.

Now, following the notation of the previous section, we write system (2.27), equipped with algorithm (2.28), in matrix form as

$$\begin{bmatrix} \dot{x} \\ \\ \dot{v} \end{bmatrix} = (\Theta \otimes I_m) \begin{bmatrix} x \\ \\ v \end{bmatrix}, \tag{2.29}$$

where the matrix Θ is defined as

$$\begin{bmatrix} 0_n & I_n \\ \\ -L_n & -\gamma(t) L_n \end{bmatrix}. \tag{2.30}$$

We remark that here we are implicitly assuming that the underlying graph and the associated weights are the same for the states and their derivatives, but generally they may differ.

In order to proceed with the analysis of system (2.29), we need to remember an important fact. Assuming that both A_N and γ are constant, let's consider the block matrix

$$M = \begin{bmatrix} A & B \\ \\ C & D \end{bmatrix}. \tag{2.31}$$

Then it is known that the determinant is given by $det(M) = det(AD - BC)$ if A and C commute. In our case, it is convenient to try and describe the dynamics of the system in terms

of the eigenvalues of Θ, which leads us to solve the equation $det\left(\lambda I_{2N} - \Theta\right) = 0$ for the characteristic polynomial of Θ. Thus, the previous observation leads us to the chain of equalities

$$det\left(\lambda I_{2N} - \Theta\right) = det\left(\begin{bmatrix} \lambda I_N & I_N \\ L_N & \lambda I_N + \gamma L_N \end{bmatrix}\right) = det\left(\lambda^2 I_N + \left(1 + \gamma\lambda\right) L_N\right) \tag{2.32}$$

Furthermore, since

$$det\left(\lambda I_N + L_N\right) = \prod_{i=1}^{N} \left(\lambda - \mu_i\right), \tag{2.33}$$

with μ_i denoting the i-th eigenvalue of L_N, by exploiting additivity and multiplicativity of the determinant, one can show that the eigenvalues of Θ are given by

$$\lambda_i^{\pm} = \frac{\gamma\mu_i \pm \sqrt{\gamma_2\mu_i^2 + 4\mu_i}}{2}. \tag{2.34}$$

Since we know that $-L_N$ has at least one zero eigenvalue with associated eigenvector 1_N (see previous sections), then we also know that Θ has at least two zero eigenvalues which, without loss of generality, we will suppose being λ_1^+ and λ_1^-. Furthermore, all the non-zero eigenvalues have negative real parts. Therefore, we have the following necessary and sufficient condition for achieving consensus under system (2.27) [101].

Lemma 3. *Algorithm* (2.28) *asymptotically achieves consensus if and only if* Θ *has exactly two zero eigenvalues and all the other eigenvalues have negative real parts. Specifically,* $x_i\left(t\right) \rightarrow \sum_{j=1}^{N} p_j x_j\left(0\right) + t\sum_{j=1}^{N} p_j v_j\left(t\right)$ *and* $v_i\left(t\right) \rightarrow \sum_{j=1}^{N} p_j v_j\left(0\right)$ *for large* t*, where* $p = [p_1, \ldots, p_N] \geq 0$*,* $1_N^T p = 1$ *and* $L_N p = 0$*.*

Now, if all of the nonzero eigenvalues of $-L_N$ are real and hence negative, it is straightforward using (2.34) to verify that all nonzero eigenvalues of Θ have negative real parts. Thus, we can state that [101]

Lemma 4. *If* $-L_N$ *has a simple zero eigenvalue and all other eigenvalues are real and hence negative, then algorithm* (2.28) *achieves consensus asymptotically for any* $\gamma > 0$*.*

In turn, if we look back to the conditions required for single integrator dynamics, the previous lemma implies [101]

Corollary 1. *Suppose that the underlying graph is undirected. Then algorithm* (2.28) *achieves consensus asymptotically for any* $\gamma > 0$ *if and only if the graph is also connected.*

If the graph is not undirected, things become a little bit more complicated. On the obvious side, we still depend on the multiplicity of the zero eigenvalue of L_N. For example, if the graph has two or more disconnected subgroups, then obviously $-L_N$ has at least two zero eigenvalues,

and therefore Θ has at least four of them. The same situation happens if there are two or more graph nodes that possess only outgoing edges, since then the Laplacian $-L_N$ will have two or more rows with all zero entries.

Yet, we can observe that when we are at consensus, by Lemma 3 the matrix Θ has exactly two zero eigenvalues, which in turn implies that $-L_N$ has exactly one of this kind. Thus, G_N has a directed spanning tree and the following result can be stated [101]

Theorem 9. *If algorithm* (2.28) *achieves consensus asymptotically, then directed graph G_N has a directed spanning tree.*

Do note that in the single integrator case, the existence of a directed spanning tree is also a sufficient condition for consensus achievement. For double integrator dynamics however, since we know that consensus is achieved if ad only if Θ has only two zero eigenvalues and all the rest have a negative real part, we have to check when these conditions hold for the eigenvalues (2.34). For these, the following result is fundamental ([101], with the case $\alpha = 0$ first treated in [121])

Lemma 5. *Let*

$$\rho_{\pm} = \frac{\gamma\mu - \alpha \pm \sqrt{(\gamma\mu - \alpha)^2 + 4\mu}}{2}, \tag{2.35}$$

where $\rho, \mu \in \mathbb{C}$. If $\alpha \geq 0$, $Re(\mu) < 0$, $Im(\mu) > 0$ and

$$\gamma > \sqrt{\frac{2}{|\mu| \cos\left[\tan^{-1}\left(\frac{Im(\mu)}{-Re(\mu)}\right)\right]}}, \tag{2.36}$$

then $Re(\rho_{\pm}) < 0$, where $Re(\cdot)$ and $Im(\cdot)$ represent respectively the real and imaginary part of a number.

To conclude, in light of the previous result, one has the following sufficient condition to achieve consensus in double integrator systems subject to algorithm (2.28) [101].

Theorem 10. *For all $i \in \{1, \ldots, N\}$ let μ_i be the i-th eigenvalue of $-L_N$. Algorithm* (2.28) *asymptotically achieves consensus if the underlying digraph has a directed spanning tree and*

$$\gamma > \bar{\gamma}, \tag{2.37}$$

where $\bar{\gamma} = 0$ if all $n-1$ nonzero eigenvalues of $-L_N$ are negative and

$$\bar{\gamma} = \max_{\{\mu_i | Re(\mu_i) < 0 \text{ and } Im(\mu_i) > 0\}} \sqrt{\frac{2}{|\mu_i| \cos\left[\tan^{-1}\left(\frac{Im(\mu_i)}{-Re(\mu_i)}\right)\right]}} \tag{2.38}$$

otherwise.

2.5 Consensus velocity

2.5.1 Spectral approaches

Although the consensus velocity of the algorithms presented in this thesis is overshadowed by more important aspects of the treated problems, it still pops up here and there. So, in this subsection and the next one we give a brief review of previous results that concern the convergence speed of common algorithms for single and double integrator dynamics. In particular, here we consider analysis approaches that focus on the spectral properties of the "influence" matrix, be it a Laplacian or some other one. We remark that some of these results appear again, obviously in a more detailed fashion, in Section 3.1. Finally, we limit ourselves to treat the case of fixed topologies, which are those considered in this thesis.

Of course, when we speak of spectral properties, due to the linearity of the model considered, we refer to the values of the matrices eigenvalues. A well known result from graph theory states that the *algebraic connectivity* of an undirected graph, that is the second smallest eigenvalue λ_2 of the Laplacian matrix, reflects the degree of connectivity of the graph, meaning that a more connected graph has a larger λ_2 [102]. Furthermore, for many linear Laplacian based models (included those presented up to now), λ_2 can be seen as a measure of the algorithm convergence speed [50]. Thus, it is only natural that many algorithms have been designed with the idea of maximizing the value of λ_2. In the next subsections we see how this can be achieved by different means.

For weighted graphs, things are usually more complicated and additional hypotheses have to be made. As an example, Olfati-Saber and Murray [50] managed to prove that if (and only if) a digraph G_N with associated Laplacian L_N is balanced, then the matrix

$$\hat{L}_N = \frac{L_N + L_N^T}{2} \tag{2.39}$$

is a valid (symmetric) Laplacian for the *mirror graph* $\hat{G}_N$ of G_N, that is the undirected graph with the same set of nodes of G_N and (symmetric) Adjacency matrix

$$\hat{A}_N = \frac{A_N + A_N^T}{2}, \tag{2.40}$$

where A_N denotes the Adjacency matrix of G_N. More importantly, it can be proved that the *Laplacian disagreement functions* of the two graphs coincide, that is

$$x^T L_N x = x^T \hat{L}_N x \tag{2.41}$$

for all $x \in \mathbb{R}^N$. With the appropriate control algorithm ((2.5) is an example, as is the Cucker-Smale model of the next chapter), and if the Laplacian L is symmetric, estimates of the corresponding Laplacian disagreement functions lead to a convergence rate of $O\left(e^{-\lambda_2 t}\right)$, where t

denotes the time. An instance of this kind of calculation can be found in Section 3.1 for the Cucker-Smale model [122].

The approach of maximizing the value of λ_2 has been used for example in [123], where it has been coupled with concepts related to *small world networks*, that is graphs where the number of edges connecting two nodes is at most $O(\log N)$, in order to obtain very fast consensus velocities. A similar strategy has been employed in [124] to design both the topology and the weights to be assigned to each edge.

For the discrete model (2.17), Kar and Moura [125] observed that the following inequality can be stated for an undirected connected graph

$$\|x\left[k\right]-\bar{x}\|_2 \leq \|x\left[0\right]-\bar{x}\|_2 \gamma_2^k. \tag{2.42}$$

Here $\bar{x}$ stand for the average consensus value, while

$$\gamma_2 = \frac{1-\gamma}{1+\gamma}, \tag{2.43}$$

where $\gamma = \lambda_2/\lambda_N$. Thus, instead of maximizing simply λ_2, the authors focus on maximizing the ratio γ. The same kind of observations have led the authors of [61] to offer a global description of average consensus for system (2.17) in terms of an *asymptotic convergence factor* and the associated *convergence time*, which are defined respectively as

$$r_a = \sup_{x[0]\neq\bar{x}} \lim_{k\to\infty} \left(\frac{\|x\left[k\right]-\bar{x}\|_2}{\|x\left[0\right]-\bar{x}\|_2}\right)^{\frac{1}{k}} \tag{2.44}$$

and

$$\tau_a = \frac{1}{\log\left(1/r_a\right)}, \tag{2.45}$$

where the relation with (2.42) is crystalline. Similarly, the previous quantities can be restricted to describe the *per step* behaviour as

$$r_s = \sup_{x[k]\neq\bar{x}} \frac{\|x\left[k+1\right]-\bar{x}\|_2}{\|x\left[k\right]-\bar{x}\|_2} \tag{2.46}$$

and

$$\tau_s = \frac{1}{\log\left(1/r_s\right)}. \tag{2.47}$$

Based on the per step convergence factor above, the authors propose a method to obtain the optimum Adjacency matrix that achieves the average consensus in time invariant, balanced topologies as the solution of a semi-definite convex programming problem. The particular aspect of this matrix is that it is allowed to have negative entries, and it is considered optimum in terms of the minimization of $\rho\left(A_N - J_N\right)$, where J_N is an N dimensional square matrix whose entries all equal $\frac{1}{N}$ and ρ denotes the second largest eigenvalue of the matrix. A time varying case is

addressed in [126], where the mean square convergence rate is considered as the optimization criterion to assign the optimum weights in random networks with correlated links.

As we have said before, (2.17) is a particular case of (2.18), and spectral analyses like the ones above can be conducted also for other instances of the latter. For example, in [127], the author considers the particular Perron matrix P_N defined by the entries

$$(P_N)_{ij} = \begin{cases} h, & j \in \mathcal{N}_i \\ 1 - h|\mathcal{N}_i|, & i = j \\ 0, & \text{otherwise} \end{cases} \tag{2.48}$$

in such a way that the model (2.18) becomes

$$x_i[k+1] = x_i[k] + h \sum_{j \in \mathcal{N}_i} (x_i[k] - x_j[k]), \tag{2.49}$$

where $\mathcal{N}_i$ denotes the set of agents linked to agent i. Albeit here we briefly consider only the case with a constant and positive h, it must be remarked that the previous model have been extended to cover different cases. For example, in the presence of additive noise, [128] introduces a decreasing link weight in order to reduce the variance of the consensus value, and a similar approach is employed in [66]. Finally, [67] studies the consensus with link weights that are not necessarily positive.

That said, it can be shown that the eigenvalues of P_N are related to those of the corresponding Laplacian L through the equality

$$\lambda_i(P_N) = 1 - h\lambda_{N-i+1}(L_N). \tag{2.50}$$

In light of the discrete results of Section 2.3.1, consensus is then achieved as long as $h \in (0, 2\beta)$, where

$$\beta = \min_{i=2,\ldots,N \text{ and } \lambda_i(L_N) \neq 0} \frac{Re[\lambda_i(L_N)]}{\lambda_i^2(L_N)}. \tag{2.51}$$

Thus, for example, if the graph is undirected and connected, it will result $\beta = \frac{1}{\lambda_N(L_N)}$, since the eigenvalues of L_N are all real and nonnegative. Similarly to what done for the restriction (2.17), one focuses on minimizing the quantity $\rho(P_N - J_N)$, and therefore maximizing the second smallest eigenvalues $\lambda_2(L_N)$ of the graph Laplacian.

Since the eigenvalues of P_N are real (of course, this may be obtained also with a digraph), its second largest eigenvalue in magnitude will be the maximum between $\lambda_{N-1}(P_N)$ and $-\lambda_1(P_N)$ or, expressed in terms of the Laplacian,

$$\rho(P_N - J_N) = \max\{1 - h\lambda_2(L_N), h\lambda_N(L_N) - 1\}, \tag{2.52}$$

with $h \in \left(0, \frac{2}{\lambda_N(L_N)}\right)$. Therefore, one can explicitly find the optimum link weight minimizing $\rho\left(P_N - J_N\right)$ as

$$h^\star = \frac{2}{\lambda_2\left(L_N\right) + \lambda_N\left(L_N\right)}, \tag{2.53}$$

which is attained at the intersection of two lines [61, 129]. Furthermore, one can restrict the living domain of h to $\left(0, \frac{1}{N-1}\right]$ (this still satisfies the convergence criterions since $d_M^+ \leq N-1$ and $\lambda_N\left(L_N\right) \leq 2d_M^+$ [102]), so that the choice of h guaranteeing consensus depends only on the knowledge of the number of nodes (albeit in this case the convergence time would not be minimized).

2.5.2 Topology designs

In the previous subsection we have seen that, for linear consensus algorithms, it is possible to define the consensus velocity by maximizing or minimizing the appropriate eigenvalues of the influence matrix, and therefore the values of the graph edges. However, there exists scenarios where it is possible to design the graph topology (and not just defining the edges weights) in such a way to achieve high convergence velocity.

Of course, this possibility becomes increasingly important when the number of nodes, and thus the formation dimension, reaches very high values. The latter represent just one instance of the fact that, in many situations, the definition of an appropriate graph topology is more important than the actual choice of the weights. For example, Xiao et al. [65] studied consensus over random geometric graphs [130] and compared optimal designs (like those considered in the previous subsection) with "suboptimal" decentralized strategies involving adaptive gains (in particular, the so called Metropolis weights [129]). What they found can be resumed by observing that not only the difference in convergence time is far from being dramatic as the number of nodes increases, but also that for large graphs this difference tends to shrink very fast with the number of edges considered.

Although other examples like the previous one exist, ultimately asking what is the best graph in terms of consensus speed without any further constraint is fruitless, since one can just take a complete graph where every pair of nodes is connected by an edge [106]. More interesting, and this is something that is usually asked in computer science, is what have been asked by Delvenne et al. [131], that is what is the best graph under the constraint that each agent is a child for at most ν edges at each iteration (i.e., G_N has a bounded in-degree). The answer is given by a family of graphs known as *de Bruijn graphs*, which are capable of achieving average consensus in a finite time $\bar{t}$, and with $\bar{t}$ being the smallest possible consensus time with the constraint on the number of edges.

This kind of performance is certainly one of the most useful traits when dealing with large networks, especially when compared with other, more common classes of graphs. An example is given by the *Abelian Cayley graphs* [132], which are grids on d-dimensional tori, and whose

algebraic structure (a generalization of circulant matrices) allows to compute the eigenvalues of the influence matrix Q and to prove that $esr\,(Q) \geq 1 - cN^{\nu+1}$, where ν denotes the degree of the nodes and c is a positive scalar independent of the graph. The problem with the previous inequality lies in the observation that, for $N \to \infty$, $esr\,(Q) \to 1$, which in turn implies a severely slowed down convergence.

Yet, what we have just stated is not always the case. Besides the de Bruijn graphs that we have mentioned before, there exists another interesting class of graphs, aptly referred to as *expander graphs* [133], such that $esr\,(Q)$ is bounded away from 1 when $N \to \infty$. A similar property, that is a small diameter despite a small in-degree, holds for the so called *small-world graphs*, which are considered a basic model for many social interactions (including those on the Internet); as we have seen in the previous subsection, in the context of consensus algorithms they have been extensively studied by Olfati-Saber [134] and Tahbaz-Salehi et al. [135].

The difference in performance between Abelian Cayley graphs and the rest lies in the combined smallness of the neighbours number and in their forced "local" position in a geometric sense, which reflects in the fact that symmetric graphs scale badly with the number of the nodes. It should be remarked however, that this kind of graphs are still important from a representation point of view, since they modellize well many of the geometrical constraints to which the nodes may be subject to in a realistic setting.

To conclude, we come back for a moment to the random geometric graphs mentioned at the beginning of the subsection. These are undirected graphs obtained by randomly generating points in the Euclidean space according to a Poisson point process, that is the number of points in any bounded region is a Poisson random variable with average proportional to the area and their position is uniformly distributed in the region. Subsequently, an edge is drawn between two nodes if and only if their relative distance is within a predefined radius r. Thus, although they may be an overshoot for autonomous vehicle control, where dynamical constraints and adjustments are always exploitable, they still represent a step forward (with respect to Abelian graphs) to a more realistic and less structured family of graphs.

Chapter 3

Analytical background (II)

3.1 The Cucker-Smale model

3.1.1 The undirected connected case

Equations of motion

In this subsection we introduce the Cucker-Smale model as was originally described in [122], that is as a translational consensus model for point-mass agents subject to an all-to-all communication topology. Additionally, we discuss the analytical results presented there and how they relate to our problem.

This model has been inspired by studies done on flocks of animals like birds or fishes, which have been observed to converge to a state where all the animals are moving with the same velocity. In particular, the postulate at the base of the Cucker-Smale system is that any agent of the flock adjust its velocity by adding to it weighted differences between this velocity and those of the other agents. That is, following the notation of Cucker and Smale ($v\left(t\right) = v\left(th\right)$), at time $t \in \mathbb{N}$ and for a step $h \in \mathbb{N}$, for agent i we have

$$v_i\left(t+1\right) - v_i\left(t\right) = h \sum_{j=1}^{N} a_{ij}\left(v_j\left(t\right) - v_i\left(t\right)\right), \tag{3.1}$$

where v_i and v_j denote the three-dimensional velocities of agents i and j in a flock of N companions, while the gains a_{ij} determine the weights associated to the underlying communication graph. In particular, these gains are defined as

$$a_{ij} = \eta\left(\|x_i - x_j\|^2\right), \tag{3.2}$$

where x_i and x_j stand for the three-dimensional position of agents i and j respectively, $\|\cdot\|$

denotes the standard Euclidean norm and the non-increasing function $\eta : \mathbb{R}^+ \to \mathbb{R}^+$ is given by

$$\eta(y) = \frac{K}{(\sigma^2 + y)^\beta}, \tag{3.3}$$

where $K > 0$, $\sigma^2 > 0$ and $\beta \geq 0$ are a given set of constants. Scaling the weights with respect to the relative distances between the agents ensures that every agent pays more attention to its closest companions (since $\|x_i(t) - x_j(t)\| \leq \|x_i(t) - x_k(t)\|$ implies $a_{ij} \geq a_{ik}$). Additionally, the term σ^2 helps avoiding singularities, while β is used to control the rate of decay of the gains with respect to the relative distances and, as we are going to see, is a fundamental parameter to determine whether consensus is reached unconditionally or if additional hypotheses are required.

In order to proceed with the analysis, we need to do a couple of remarks. The first concerns the underlying communication graph. Specifically, we can see that the sum adopted in (3.1) spans the entire formation, and this obviously implies an all-to-all communication structure, which in turn corresponds to an undirected connected graph. Although in a later work [136] this has been generalized to accommodate for a general undirected connected structure (furthermore, with gains satisfying $a_{ij} \geq \eta(\|x_i - x_j\|^2)$) we find the original results more descriptive and easier to understand.

The second, necessary to proceed with an analysis of the consensus process induced by this model, is that the equations (3.1) can be rewritten matricially as

$$\begin{aligned} v_i(t+1) - v_i(t) &= -h\sum_{j=1}^{N} a_{ij}(v_i(t) - v_j(t)) = h\left(-\left(\sum_{j=1}^{N} a_{ij}\right)v_i(t) + \sum_{j=1}^{N} a_{ij}v_j(t)\right) = \\ &= h\left(-\left[(D_N \otimes I_3)\,v(t)\right]_i + \left[(A_N \otimes I_3)\,v(t)\right]_i\right) = -h\left[(L_N \otimes I_3)\,v(t)\right]_i, \end{aligned} \tag{3.4}$$

where $v = (v_1, \ldots, v_N) \in \mathbb{R}^{3N}$, D_N denotes the diagonal matrix with entries $d_{ii} = \sum_{j=1}^{N} a_{ij}$, I_3 the three dimensional identity matrix, while A_N and L_N stand respectively for the Adjacency and Laplacian matrices as defined in the previous section. Do note that in the last equation we have implicitly taken advantage of the Kronecker product associativity. Furthermore, in order to lighten the writing, from now on we will drop the Kronecker product notation.

That said, following the previous series of equalities, (3.1) can be rewritten as

$$v(t+1) = (I_N - hL_N)\,v(t). \tag{3.5}$$

By adding the natural equation for the positions

$$x(t+1) = x(t) + hv(t), \tag{3.6}$$

we obtain a complete discrete dynamical model, which can then be translated naturally to continuous time as

$$\dot{x} = v, \quad \dot{v} = -L_N v. \tag{3.7}$$

Besides the Kronecker product, in the previous equation we have also dropped the time dependence in order to improve readability even further. We remark that for spacecraft formation flying both (3.1) and (3.7) are important, since, depending on the task at hand, both continuous and discrete propulsion systems can be employed.

The continuous case

As a first step for the analysis of the model's properties, we are going to discuss what happens with the continuous system (3.7). If we denote with $\Gamma(t)$ and $\Lambda(t)$ the quantities

$$\Gamma(t) = \frac{1}{2}\sum_{i\neq j}\|x_i - x_j\|^2 \quad \text{and} \quad \Lambda(t) = \frac{1}{2}\sum_{i\neq j}\|v_i - v_j\|^2, \tag{3.8}$$

then we can state the following theorem

Theorem 11. *Assume that, for some $K > 0$, $\sigma > 0$ and $\beta \geq 0$, for system* (3.7) *it holds*

$$a_{ij} = \frac{K}{(\sigma^2 + \|x_i(t) - x_j(t)\|^2)^{\beta}}. \tag{3.9}$$

Assume also that one of the following three hypotheses hold true

- $\beta < \frac{1}{2}$
- $\beta = \frac{1}{2}$ *and* $\Lambda_0 < \left((\nu K)^2/8\right)$
- $\beta > \frac{1}{2}$ *and*

$$\left[\left(\frac{1}{2\beta}\right)^{\frac{1}{2\beta-1}} - \left(\frac{1}{2\beta}\right)^{\frac{2\beta}{2\beta-1}}\right]\left(\frac{(\nu K)^2}{8\Lambda_0}\right)^{\frac{1}{2\beta-1}} > 2\Gamma_0 + \sigma^2. \tag{3.10}$$

Then there exists a constant B_0 (independent of t and specific for any case) such that $\Gamma(t) \leq B_0$ for all $t \in \mathbb{R}^+$. In addition, $\Lambda(t) \to 0$ for $t \to \infty$ and there exists $\hat{x} \in X$ such that $x(t) \to \hat{x}$ for $t \to \infty$.

At a first glance, the previous result is telling us three things. First, since $\Lambda(t) \to 0$, we know that the agents velocities need to converge asymptotically to the same value. As a consequence, the relative distances between the agents should reach a fixed value determined by $\hat{x}$. Of course, these results imply that asymptotically the formation will move as a sort of single rigid body, with the relative distances remaining bounded during the entire process. This is achieved unconditionally, that is independently from the formation initial conditions, for $\beta < \frac{1}{2}$, while it requires additional constraints in the other cases.

The last point to discuss in regards to the theorem stated above concerns the definition and role of the factor ν appearing in the second and third case. This factor ν originates from the inequality

$$\nu\|x\|^2 \leq \|x\|_Q^2 \leq \bar{\nu}\|x\|^2, \tag{3.11}$$

where ν and $\bar{\nu}$ are positive quantities, $x \in \Delta^\perp = \left\{x = (x_1, \ldots, x_N) \in \mathbb{R}^{3N} \mid x_i = x_j,\ \forall i, j\right\}^\perp$ and $\|\|_Q$ denotes the norm induced by the form $Q : \mathbb{R}^{3N} \to \mathbb{R}$ defined as

$$Q\left(u, v\right) = \frac{1}{2}\sum_{i,j=1}^{N}\langle u_i - u_j, v_i - v_j\rangle. \tag{3.12}$$

This form is bilinear, symmetric and, when restricted to $\Delta^\perp \times \Delta^\perp$, definite positive. Although we do not discuss in detail the definition of this form (or the reduction to $\Delta^\perp$), we remark that the possibility of defining it is at the base of the approach adopted by Cucker and Smale, and it is exclusive for the case of an undirected connected graph.

The bound (3.11) is useful to prove several stepping stones leading to the main theorem (11), but the most important point lies in the lemma

Lemma 6. *For all $N \geq 2$, $\nu = \nu\left(N\right) \geq 1/\left(3N\right)$ and $\bar{\nu} = \bar{\nu}\left(N\right) \leq 2N\left(N-1\right)$,*

which put into relation the factor ν and $\bar{\nu}$ with the dimension of the formation through the symmetric form Q. To understand the importance of the previous lemma, the latter has to be considered in relation with the propositions

Proposition 1. *Let $\mathbf{\Phi}_t = \min_{\tau\in[0,t]}\phi_\tau$, with ϕ being the smallest non-zero eigenvalue of L_N (also referred to as the Fiedler number of the associated Adjacency matrix). Then, for all $t \geq 0$, it results*

$$\Lambda\left(t\right) \leq \Lambda\left(0\right)e^{-2t\mathbf{\Phi}_t}. \tag{3.13}$$

and

Proposition 2. *Let A be a non-negative symmetric matrix, L its Laplacian, ϕ the former Fiedler number and $\mu = min_{i\neq j}a_{ij}$. Then, $\phi \geq \frac{1}{2}\nu\mu$. Furthermore, if $a_{ij} = \eta\left(\|x_i - x_j\|^2\right)$ then*

$$\phi \geq \frac{1}{2}\nu\eta\left(\Gamma\left(t\right)\right). \tag{3.14}$$

If we now consider a time interval $[0, t]$, putting together the three results yield

$$\Lambda\left(t\right) \leq \Lambda\left(0\right)e^{-2t\mathbf{\Phi}_t} \leq \Lambda\left(0\right)e^{-2t\frac{\nu K}{2\left(\sigma^2+\Gamma(t^\star)\right)^\beta}}, \tag{3.15}$$

where $t^\star$ indicates the point maximizing Γ in $[0, t]$. The previous result follows from

$$\mathbf{\Phi}_t = \min_{\tau \in [0,t]} \phi_\tau \geq \min_{\tau \in [0,t]} \frac{\nu K}{2\left(\sigma^2 + \Gamma\left(\tau\right)\right)^\beta} = \frac{\nu K}{2\left(\sigma^2 + \Gamma\left(t^\star\right)\right)^\beta}. \tag{3.16}$$

Additional results allow to obtain an estimate which is independent of t, but from the previous points we can already obtain some interesting informations. In particular, the bound (3.15) arises directly from the properties of the Laplacian, with the convergence rate and the presence of the factor ν in the exponential being a direct consequence of the Laplacian being a symmetric positive definite matrix, while the other factors are related to the definition of the weights a_{ij}. Since the first property follows from the communication graph being undirected and connected, this seemingly indicates that the dependence of the convergence process from the initial relative conditions and the dimension of the flock are connaturated in the way in which the spacecraft exchange information, and has therefore a very loose connection with the dynamics or the control.

As a final remark for the continuous case, we want to point out that, as discussed in [92], the bounds on ν and $\bar{\nu}$ can be made exact by observing that the inner product Q can be written as $u^T Q v$, with the matrix Q defined as

$$Q = \begin{pmatrix} N-1 & -1 & -1 & \dots \\ -1 & N-1 & -1 & \dots \\ -1 & -1 & N-1 & \dots \\ \vdots & \vdots & \vdots & \end{pmatrix} \otimes I_3. \tag{3.17}$$

From this representation it is straightforward to prove $\nu = \bar{\nu} = \frac{N}{2}$.

The discrete case

A result similar to Theorem 11 can be proved for the model (3.1). In particular, we have

Theorem 12. *Assume that, for some constants $\sigma > 0$, $\beta \geq 0$ and $K < \sigma^{2\beta} / \left((N-1)\sqrt{N}\right)$ it results*

$$a_{ij} = \frac{K}{\left(\sigma^2 + \|x_i\left(t\right) - x_j\left(t\right)\|^2\right)^\beta} \tag{3.18}$$

Assume also that one of the following hypotheses hold true

- $\beta < \frac{1}{2}$
- $\beta = \frac{1}{2}$ *and* $\|v\left(0\right)\| \leq \nu K / \left(2\bar{\nu}^{\frac{1}{2}} h\right)$

- $\beta > \frac{1}{2}$ *and*

$$\left(\frac{1}{\boldsymbol{a}}^{\frac{2}{\alpha-1}}\right)\left[\frac{1}{\alpha}^{\frac{2}{\alpha-1}} - \frac{1}{\alpha}^{\frac{\alpha+1}{\alpha-1}}\right] > \bar{\nu}\left(V_0^2 + 2V_0\left((\alpha\boldsymbol{a})^{-\frac{2}{\alpha-1}} - \sigma^2\right)\bar{\nu}^{-\frac{1}{2}}\right) + \boldsymbol{b}, \tag{3.19}$$

where $\alpha = 2\beta$, $V_0 = h\|v\,(0)\,\|$,

$$\boldsymbol{a} = \frac{2\bar{\nu}^{\frac{1}{2}}}{\nu K}V_0 \quad and \quad \boldsymbol{b} = \nu^{\frac{1}{2}}\|x\,(0)\,\| + \sigma. \tag{3.20}$$

Then there exists a constant B_0 *(independent of* t *and different for the various cases) such that* $\|x\,(t)\,\| \leq B_0$ *for all* $t \in \mathbb{N}$. *In addition,* $\|v\,(t)\,\| \to 0$ *when* $t \to \infty$. *Finally, there exists* $\hat{x} \in \Delta^{\perp}$ *such that* $\|x\,(t)\,\| \to \hat{x}$ *for* $t \to \infty$.

As it can be seen, the previous result has the same main characteristics of the one proved for the continuous case, with the notable exception of the hypothesis $K < \sigma^{2\beta}/\left((N-1)\sqrt{N}\right)$. The latter has the function of giving an exact bound on $\|L_N\|$ as specified in the following lemma.

Lemma 7. *For all* $x \in \Delta^{\perp}$

$$\|L_N\| < \frac{2\,(N-1)\sqrt{N}K}{\sigma^{2\beta}}. \tag{3.21}$$

In particular, if $K < \sigma^{2\beta}/\left((N-1)\sqrt{N}\right)$, *then* $\|L_N\| < 2$.

What is interesting to note about the previous bound is that seemingly it is not needed due to the approach adopted by the authors, but it is instead an at least sufficient requirement to obtain consensus, as explained in the following example (discussed in greater detail in [122]).

Example 1. *For* $\beta > 0$, *consider* $K > \sigma^{2\beta}$ *and* $\gamma = \frac{\sqrt{K^{\frac{1}{\beta}} - \sigma^2}}{2} > 0$, *so that*

$$\frac{K}{\left(\sigma^2 + 4\gamma^2\right)^{\beta}} = 1. \tag{3.22}$$

For $\beta = 0$ *instead, let* $K = \sigma^{2\beta} = 1$ *and* $\gamma > 0$ *be arbitrary. Furthermore, assume* $h = 1$.

Now, consider the case of two agents moving on a line, that is $N = 2$ *and with* $\mathbb{R}^3$ *reducible to* $\mathbb{R}$. *If we assume that* $x\,(0) = (-\gamma, \gamma)$ *and* $v\,(0) = (2\gamma, -2\gamma)$, *then it results*

$$A_{x(0)} = \begin{pmatrix} 0 & 1 \\ 1 & 0 \end{pmatrix} \; and \; L_{x(0)} = \begin{pmatrix} 1 & -1 \\ -1 & 1 \end{pmatrix}. \tag{3.23}$$

It can be verified that $\|L_N\| = 2$. *Correspondingly, the equations of motion become*

$$x\,(1) = x\,(0) + v\,(0) = \begin{pmatrix} -\gamma \\ \gamma \end{pmatrix} + \begin{pmatrix} 2\gamma \\ -2\gamma \end{pmatrix} = \begin{pmatrix} \gamma \\ -\gamma \end{pmatrix} \tag{3.24}$$

and

$$v(1) = I_2 - L_{x(0)} = \begin{pmatrix} 0 & 1 \\ 1 & 0 \end{pmatrix} \begin{pmatrix} 2\gamma \\ -2\gamma \end{pmatrix} = \begin{pmatrix} -2\gamma \\ 2\gamma \end{pmatrix} \tag{3.25}$$

It is easy to check that, by iterating the map (3.1)*, for every* $r \in \mathbb{N}$*, besides* $\|L_{x(r)}\| = 2$*, we have on one side*

$$x(2r) = (-\gamma, \gamma) \ and \ v(2r) = (2\gamma, -2\gamma), \tag{3.26}$$

while on the other, at time $2r + 1$*, the exact opposite values of the previous ones. Thus, we can conclude that* $v(r)$ *does not asymptotically converge to* 0*, since it results* $\|v(r)\| = 4\gamma$ *for all* $r \in \mathbb{N}$*.*

3.1.2 The directed case: hierarchical leadership

The continuous case

In this subsection we summarize the work of J. Shen [137], where some aspects of the Cucker-Smale model are investigated further and which represent the second keystone work taken into account in this thesis.

The main contribution of this work, at least for what concerns this thesis, lies in considering a different graph structure for the Cucker- Smale model. In particular, standing the notations of the previous subsection, we can rewrite equations (3.7) in a more general form as

$$\dot{x}_i = v_i, \quad \dot{v}_i = -\sum_{j \in \mathcal{L}(i)} a_{ij} (v_i - v_j), \tag{3.27}$$

where the sets $\mathcal{L}(i) = \{j | a_{ij} > 0\}$, to which from now on will refer to as *leadership sets*, individuate the agents that are passing informations to agent i. Instead, the weights a_{ij} are defined as in (3.2), with σ^2 being equal to one.

For the original Cucker-Smale model it obviously results $\#\mathcal{L}(i) = N$. The structure considered by Shen instead, represent a particular example of a digraph with a spanning tree, and it abides to the conditions

$$a_{ij} \neq 0 \Rightarrow j < i, \quad \forall i > 0, \ \mathcal{L}(i) \neq \emptyset.$$

These conditions define a *hierarchical leadership* for the flock in the following sense. If we look at the second condition, this is saying that every element in the flock has to communicate with someone. However, consider the natural order induced by the indexation of the flock as $[0, 1, \ldots, N]$. Then, according to the first condition, every element i in the flock can communicate only with the elements j such that $j < i$. Note that this is not true for the element 0 which,

according to the second condition, acts independently from the rest of the flock, thus justifying the name of hierarchical leadership. When coupled, these conditions obviously imply that graph is directed (due to the unidirectionality of the hierarchy) and that there exists a spanning tree, whose root is exactly the leader of the formation.

From a control point of view, the importance of a hierarchical leadership is twofold: on one side, the presence of a leader, either real or virtual, ensures that a predefined trajectory for the formation to follow can be defined (see next theorem); on the other, due to the reduced number of connections required for every agent, it allows the formation to reach consensus with a low computational load for every spacecraft.

Of course, given a hierarchical leadership, convergence of the agents to a consensus state can be proved, and this is true both for the continuous model (3.7) and its discrete version (3.1). In particular, for the continuous model (3.27) we have

Theorem 13. *Let $[0, 1, \dots, N]$ be a Cucker-Smale flock acting under hierarchical leadership with $\beta < \frac{1}{2}$. Then for some $B > 0$ which depends only on the initial configuration and all the system parameters, it results*

$$\max_{0 \leq i,j \leq N} \|v_i(t) - v_j(t)\| = O\left(e^{-Bt}\right),\ t > 0. \tag{3.28}$$

The previous result quantifies the rate of convergence towards a consensus state in the case of a non-accelerating leader, thus describing a rigid body-like formation moving around a predefined trajectory defined by the leader's velocity (or lack thereof). But what happens instead if the leader is accelerating, thus possibly changing this predefined trajectory? A first answer is offered by the following theorem

Theorem 14. *Consider an $N+1$ elements flock subject to the Cucker-Smale continuous dynamics* (3.27)*, with the exception of agent* 0*, which, for $t > 0$, acts according to the equations of motion*

$$\dot{x}_0 = v_0, \quad \dot{v}_0 = f(t). \tag{3.29}$$

Assume that $\beta < \frac{1}{2}$ and

$$\|f(t)\| = O\left((1+t)^{-\mu}\right),\ \mu > N. \tag{3.30}$$

Then the flock reaches consensus at the rate

$$\max_{0 \leq i,j \leq N} \|v_i - v_j\|(t) = O\left((1+t)^{-(\mu - N)}\right). \tag{3.31}$$

There are a series of observation that need to be done with respect to the previous result. First, as already observed by Shen, intuitively speaking, if the leader changes continuously its

velocity (up to the extreme hypothesis of a drunken leader following some Brownian motion) it will be naturally more difficult for the rest of the flock to synchronize with its movement.

This difficulty in synchronization is also reflected in the fact that the decaying constraint $\mu > N$ depends on the dimension of the flock. This means that the larger the formation, the less degree of free-will the leader will be able to exercise. This is because, given a hierarchy, for large formations the agents at the end of the indexation have to wait for the information flow to pass through several agents before being able to act.

Finally, keeping in mind the previous comments, this theorem hints at the possibility of steering the formation mid-flight without compromising its rigid body state and, by acting solely on the leader, without the need of defining a computationally expensive control law for the rest of the flock.

The discrete case

Similarly to what described for the case $\#\mathcal{L}(i) = N$, consensus for discrete time can be proved even under a hierarchical leadership. In this case, following the notation introduced by Shen, fixed a time step $h > 0$ we can write the equations of motion as

$$\begin{aligned} x[k+1] &= x[k] + hv[k] \\ v[k+1] &= S[k]\, v[k], \end{aligned} \tag{3.32}$$

where $x[k] = x(kh)$, $v[k] = v(kh)$ and $S[k] = S^h[k] = Id - hL_k$, with $L_k = L_{x[k]}$.

In order to state the theorem previously mentioned, we first need to review the concept of dominant matrix along with an associated result. In particular

Definition 3. *We say that a matrix $B = (b_{ij})$ is dominated by a matrix $C = (c_{ij})$ of the same size if*

$$|b_{ij}| \leq c_{ij},\ \forall i, j. \tag{3.33}$$

In that case we write $B \prec C$.

The previous definition allows us to state the following proposition, which establishes a bound on the elements of $S[k]$ (acting on the reduced space $\mathbb{R}^{3(N+1)}/\Delta$, with Δ defined in the previous section) as a function of the iteration step h.

Proposition 3. *For $0 < h < \frac{1}{2NK}$, $S_{ij}[k] \geq 0$ for any i and j. Furthermore*

$$\max_{i,j} S_{ij}[k] \leq 1 - hd_* := \rho_h,\ \forall k \geq 0. \tag{3.34}$$

Here d_* is defined as

$$d_* = \frac{K}{(1+B_h)^\beta}, \tag{3.35}$$

where B_h represent an uniform bound on the vector $x[k] = [(x_i - x_0)[k]]_{i=1,\dots,N}$, in the sense that

$$\|x[k]\|^2 \geq B_h, \ \forall k \geq 0. \tag{3.36}$$

This is the same B_h which we find at the base of the results of Cucker and Smale, and similarly to that case its definition is related to a critical threshold in the value of β. As explained in the next theorem, this threshold is what separate this result from that of Cucker and Smale.

Theorem 15. *Given an $N+1$ flock acting according to the discrete Cucker-Smale equations of motion and subject to a hierarchical leadership, for any sufficiently small step h (as defined in Proposition 3) there exists some $\rho_h \in (0,1)$, under conditions similar to Theorem 12 but with $\beta <, =,$ or $> \beta_c = \frac{1}{2N}$, such that*

$$\Pi_{l=0}^k S[l] \prec O\left(\rho_h^k k^{N-1}\right) T, \tag{3.37}$$

where T denotes the $N \times N$ triangular inferior matrix with non-zero entries equal to 1. In particular, it results

$$\|v[k]\| \leq O\left(\rho_h^k k^{N-1}\right) \|v[0]\|, \ \forall k \geq 0. \tag{3.38}$$

Again, although not explicitly stated, given the adaptive character of the model and the approach adopted, some sufficient-like conditions on the parameters and initial conditions need to be defined. Of course, these are all aimed to show that it is possible to control the growth rate of the iterated map $S[n] \dots S[0]$.

To conclude, we remark that the critical value $\frac{1}{2N}$ for the parameter β has been subsequently improved to $\frac{1}{2}$ by Dong and Cucker [138]. In particular the following result holds

Theorem 16. *Let $\{0,1,\dots,N\}$ be an Hl-flock with $\beta < \frac{1}{2}$. Furthermore, assume that the marching step h satisfies the same condition of Proposition 3. Then, there exist $P, Q > 0$ (dependent on h, the initial conditions and the parameters K and β) such that*

$$\max_{0 \leq i,j \leq N} \|v_i[k] - v_j[k]\| \leq Qe^{-Pk}. \tag{3.39}$$

Furthermore, for all $\beta > \frac{1}{2}$ there exists an initial state $(x[0], v[0])$ whose orbit under the dynamics fails to converge to a common velocity.

3.1.3 Further developments

In this subsection we summarize briefly some of the improvements that have been introduced for the Cucker-Smale model over the years, but that are not considered in this thesis. In particular, we focus on those that cover aspects relevant for Astrodynamics, starting from extensions or alternative approaches to the study of the model, and then proceeding in order with works related to collision avoidance, robustness with respect to time-varying communication graphs and extensions of the particle model to the continuum case.

Notations may change slightly with respect to the previous subsections in order to facilitate the comparison with the references given. Furthermore, we remark that, albeit by means of direct application the following analysis is more appropriate for the control presented in Chapter 4, most of these modifications can be translated with some work to the context of attitude synchronization.

Extensions of the Cucker-Smale model

Here we mention just a couple of extensions for the original Cucker-Smale model (3.7) which, like the Shen's one considered in the previous subsection, primarily aim to extend the validity of the associated results to more general graph structures and influence functions. As we are going to see, the last one offers also an approach to prove consensus seemingly alternative to those that we have discussed in this section and in Chapter 2.

As a first step, we mention again the extension of the Cucker-Smale model considered by the eponymous authors in [136]. The main result of that work concern the extension of the results given for (3.7) to the general undirected connected case, without requiring an all-to-all communication. This is proved to be true also for a time-varying undirected graph, as long as the latter remains connected for all $t \geq 0$ (in the author's words, this has also a discrete equivalent in Theorem 1 of [26]), and in both cases flocking is unconditional for $\beta < \frac{1}{2}$. Furthermore, these results have been proved to hold with gains a_{ij} satisfying

$$a_{ij} \geq \eta\left(\|x_i - x_j\|^2\right), \tag{3.40}$$

with η defined in (3.3). We remark that these results can also be reconducted to the analysis of double-integrator systems outlined in [101].

The second extension that we take into account here is given by [139], where the authors consider the CS model written in a slightly different form as

$$\dot{x}_i = v_i, \quad \dot{v}_i = \alpha \sum_{j=1}^{N} a_{ij}\left(v_j - v_i\right), \tag{3.41}$$

where α is a positive constant and $\sum_{j=1}^{N} a_{ij} \leq 1$ (which of course can always be obtained with a proper rescaling of α). Differently from [122], there is no symmetry requirement on the gains, that is $a_{ij} \neq a_{ji}$. However, they still require an all-to-all communication in the flock, which, differently from Shen's hierarchy, represents a strongly connected digraph.

The main point of this work lies in their approach for proving consensus, which relies on the concept of *active set*, where the latter, fixed an arbitrary constant $\theta > 0$, is defined for agent i as the set

$$\Lambda_i(\theta) = \{j | a_{ij} \geq \theta\}, \tag{3.42}$$

that is the set of agents which *directly* influences agent i more than θ. By considering intersections of the different Λ_i, one can easily generalize the notion to more than one agent (e.g., for two agents we have $\Lambda_{ij}(\theta) = \Lambda_i(\theta) \cap \Lambda_j(\theta)$).

With the notion above, the authors are able to bound the rate of consensus as

$$\frac{d}{dt} d_X(t) \leq d_V(t), \quad \frac{d}{dt} d_V(t) \leq -\alpha \min_{i,j} \lambda_{ij}^2(\theta)\, \theta^2 d_V(t), \tag{3.43}$$

where $d_X(t) = \max_{i,j} |x_i(t) - x_j(t)|$ and $d_V(t) = \max_{i,j} |v_i(t) - v_j(t)|$. If one defines $\Lambda(\theta) = \cap_{i=1}^{N} \Lambda_i(\theta)$ as the *global active set*, then $\Lambda(\theta) \subset \Lambda_i(\theta)$ for all i, and therefore $\lambda(\theta) \leq \lambda_{ij}(\theta)$ for all i and j. Thus

$$\frac{d}{dt} d_V(t) \leq -\alpha \lambda^2(\theta)\, \theta^2 d_V(t). \tag{3.44}$$

In the particular case of (3.41), a judicious selection of θ allows one to prove flocking under the condition

$$d_V(0) \leq \int_{d_X(0)}^{\infty} \phi^2(r)\, dr, \tag{3.45}$$

where $a_{ij} = \phi(\|x_j - x_i\|)$ (here ϕ denotes a general influence function). Furthermore, flocking results unconditional as long as $\int^{\infty} \phi^2(r)\, dr = \infty$, which is a slightly more restrictive result than the original CS model, where the authors argue it is sufficient for the influence function ϕ to satisfy $\int^{\infty} \phi(r)\, dr = \infty$.

The importance of the previous result lies in the fact that it allows to prove consensus without resorting explicitly to the spectral properties of the Laplacian matrix, which in turn may be useful for intrinsic nonlinear dynamics (i.e.,attitude synchronization) where sophisticated nonlinear stability tools are usually required. However, as it is, its uselfuness is limited by the assumption of an all-to-all communication, which may be too strict when analyzing consensus for robotic systems.

Collision avoidance

As it is, the Cucker-Smale model can be readily translated to a translational control. However, it should be noted that, without proper modifications, it cannot deal with some important aspects of formation control. Prominent among these is the fact that while asymptotic consensus of the velocities ensures that eventually the formation will behave as a rigid body-like structure, it does not say anything about possible collisions among the agents during the interphase.

In the literature, this problem is tackled through the addition of additional terms aimed to take care of the collision avoidance part. An example is given in [140] where, albeit collision avoidance is not formally proved, it is argued by the authors that it follows naturally from the structure of the possible equilibrium configurations generated by their control. For every agent i in a formation of N elements, the latter reads as

$$\dot{x}_i = v_i, \quad \dot{v}_i = \frac{\lambda}{N} \sum_{j=1}^{N} a_{ij} \left(v_j - v_i \right) + f \left(x, v \right), \tag{3.46}$$

where λ is a positive constant. As it can be seen, this control is actually the sum of a Cucker-Smale term and an inter-particle bonding force defined as

$$f \left(x, v \right) = \frac{\sigma}{N} \sum_{j=1}^{N} \left(\frac{K_1}{2 \| r_{ij} \|^2} \langle v_i - v_j, x_i - x_j \rangle \left(x_j - x_i \right) + \frac{K_2}{2 r_{ij}} \left(r_{ij} - 2R \right) \left(x_j - x_i \right) \right), \tag{3.47}$$

where $r_{ij} = \| x_j - x_i \|_2$, the K's and σ are positive constants, and $R \in \mathbb{R}^+$ is a predefined value used to control the inter-particle distances. The idea behind this model is to drive the distance $e = 2R - r_{ij}$ to zero when the system is subject to an all-to-all communication structure. This is possible in the case $N = 2$ (in fact the control is derived by differentiating twice e in this instance). For larger dimensions the interparticle distances satisfy the uniform bound

$$\sup_{0 \leq t < \infty} \| x_i - x_j \|_2 < 2R + \sqrt{\frac{4NE \left(0 \right)}{\sigma K_2}}, \tag{3.48}$$

where $E \left(0 \right)$ is the initial value of an appropriate energy functional. Still, the authors subsequently show numerical evidence that for $N > 2$ distances are generally smaller than $2R$, and that this is related with the equilibrium configurations that the agents tend to assume (themselves seen as local minimizers of $E \left(t \right)$).

More formally, in [141], the authors manage to prove analytically flocking with collision avoidance for their extension of the CS model, unconditionally for $\beta \leq \frac{1}{2}$ and conditionally otherwise. The model that they used is defined as

$$\dot{x}_i = v_i, \quad \dot{v}_i = \sum_{j=1}^{N} a_{ij} \left(v_j - v_i \right) - \Lambda \left(v \right) \sum_{j \neq i} f \left(\| x_j - x_i \|_2^2 \right) \left(x_j - x_i \right), \tag{3.49}$$

where $\Lambda \left(v \right) = \sqrt{\frac{1}{N} \sum_{i>j} \| v_i - v_j \|_2^2}$. The function $f : \left(d_0, \infty \right) \to \left[0, \infty \right)$ is a differentiable one satisfying, for all $d_1 > d_0 > 0$, the conditions

$$\int_{d_0}^{d_1} f \left(r \right) dr = \infty \quad \text{and} \quad \int_{d_1}^{\infty} f \left(r \right) dr < \infty. \tag{3.50}$$

Intuitively, the conditions above guarantee respectively collision avoidance (with a time-independent $d > d_0$) and convergence to alignment, while the alignment measure $\Lambda \left(v \right)$ is used to moderate the repelling force.

These results have later been extended by the same authors to a more general flocking model with collision avoidance [142, 143]. The latter can be described by the equations

$$\dot{x}_i = v_i, \quad \dot{v}_i = \sum_{j=1}^{N} \phi\left(\|x_i - x_j\|_2\right) G\left(v_j - v_i\right) + \Lambda\left(v\right)^{2\alpha-1} \sum_{j\neq i} f\left(\|x_j - x_i\|_2^2\right)\left(x_i - x_j\right), \tag{3.51}$$

where Λ and f satisfy the same conditions of before, the *strength* function ϕ is nonincreasing and the *coupling* one G satisfies

- For all $w \in \mathbb{R}^3$, we have $G\left(w\right) = -G\left(-w\right)$ and $\left\langle G\left(w\right), w\right\rangle \geq 0$,
- There exist constants C and α (both in $\left[1, \frac{3}{2}\right]$) such that

$$\sum_{1\leq i,j\leq N} \left\langle G\left(v_i - v_j\right), v_i - v_j\right\rangle \geq C\Lambda\left(v\right)^{2\alpha}. \tag{3.52}$$

However, differently from the Cucker-Smale model with collision avoidance, the more general (3.51) brings the velocities to alignment only if the initial conditions satisfy some bounds. In particular it must result $\|x_i\left(0\right) - x_j\left(0\right)\|_2^2 > d_0 > 0$ (so the particles do not start too close) and

$$\frac{C}{2}\int_{\Gamma(x(0))}^{\infty} \phi\left(2\sqrt{r}\right) dr > \frac{\Lambda\left(v\left(0\right)\right)^{3-2\alpha}}{3-2\alpha} + \frac{1}{2}\sum_{i>j}\int_{\|x_i(0)-x_j(0)\|^2}^{\infty} f\left(r\right) dr, \tag{3.53}$$

with $\Gamma\left(x\right) = \sqrt{\frac{1}{N}\sum_{i>j}\|x_i - x_j\|_2^2}$. In practice, the previous formula constrains the initial conditions so that positions are not too spread and the differences in the velocities too high.

Robustness under a time-varying topology

Another aspect relevant for an application to Astrodynamics lies in how to allow the formation to deal with different kinds of inner perturbations (that is not related to environmental effects like those caused by third body perturbations or solar radiation pressure). As we have seen in the Introduction, one of the most common problems is given by the possible loss of some of the communication links, which reflects itself in a time varying communication graph.

Many of the approaches adopted in the Astrodynamics community can be found also in works related to the Cucker-Smale model (or other biology-derived systems). Here we mention just two, which cover the different topologies considered for the CS model considered here.

The first one, authored by F. Dalmao and E. Mordecki [144], consider the discrete Cucker-Smale model under hierarchical leadership (3.32), but with the gains a_{ij} chosen semi-randomly at every time step, as long as the conditions

$$h \leq \frac{1}{N-1} \quad \text{and} \quad 0 \leq a_{ij} \leq 1 \tag{3.54}$$

remain satisfied (h denotes again the time step). In particular, the gains are subject to the inequality

$$\mathbb{E}\left(a_{ij}\left[t+1\right]|\mathcal{F}_t\right) \geq \frac{p}{\left(1+\|x_i\left[t\right]-x_j\left[t\right]\|\right)^{\alpha}}, \tag{3.55}$$

where $p \in (0,1]$, $j \in \mathcal{L}(i)$ for all i and $\mathbb{E}$ denotes the conditional expectation over the past state of the system $\mathcal{F}_t = \{x\left[0\right], v\left[0\right], \ldots, x\left[t\right], v\left[t\right]\}$. Flocking follows and it is proved unconditional for $\alpha < 1$.

A simple, interesting model satisfying the previous conditions can be constructed by allowing the gains a_{ij} to be constant and to take as values either p or 0 with probability

$$\mathbb{P}\left(a_{ij}\left[t+1\right]=p|\mathcal{F}_t\right) = 1-\mathbb{P}\left(a_{ij}\left[t+1\right]=0|\mathcal{F}_t\right) = \frac{1}{\left(1+\|x_i\left[t\right]-x_j\left[t\right]\|\right)^{\alpha}}. \tag{3.56}$$

As in other models, the interesting point here lies in the fact that the probability that agents i and j actually communicate depends on their distance, and it shrinks down to zero when the latter goes to infinity, thus simulating the difficulty in communicating for two very distant agents.

A second work worth mentioning is given again by S. Motsch and E. Tadmor [145]. The authors pick up the general model introduced in [139], but this time focus on showing how tight-knit subgroups of the formation which barely communicate with each other lead asymptotically to the formation of clusters, characterized by different consensus states. More formally, consider the first order model (similar results hold for second order ones, even for a discrete dynamics)

$$\dot{x}_i = \sum_{j=1}^{N} a_{ij}\left(x_j - x_i\right), \quad a_{ij} = \frac{1}{\sigma_i}\phi\left(\|x_i - x_j\|\right), \tag{3.57}$$

where the influence function ϕ is compactly supported by $[0,R]$ and σ_i satisfies

$$\begin{cases} \sigma_i = N, \text{ if } a_{ij} = a_{ji} \text{ for all } j, \\ \sigma_i = \sum_{j\neq i} a_{ij}, \text{ otherwise.} \end{cases} \tag{3.58}$$

A cluster $\mathcal{C} = \mathcal{C}(t) \subset \{1, \ldots, N\}$ is dictated by the finite diameter of the influence function ϕ according to the conditions

- $\max_{i,j\in C(t)} \|x_j(t) - x_i(t)\| \leq R$,
- $\min_{i\in C(t), j\notin C(t)} \|x_j(t) - x_i(t)\| > R$.

Do note that if $R >> x(0)$, then the dynamics is *global* and the formation can be seen as one giant cluster. Now, given a solution $x(t)$ of (3.57) which possesses a bounded time-variation

$$\int^{\infty} \|\dot{x}(s)\| ds < \infty, \tag{3.59}$$

then $x(t)$ asymptotically approaches a solution $\hat{x}$ which is partitioned in K clusters $\{\mathcal{C}_k\}_{k=1}^K$ (that is, $\{1, \ldots, N\} = \cup_{k=1}^K \mathcal{C}_k$). Furthermore, either

$$x_i(t) \to \hat{x}_{\mathcal{C}_k}, \text{ for all } i \in \mathcal{C}_k \tag{3.60}$$

or

$$\|\hat{x}_i - \hat{x}_j\| > R, \text{ if } i \in \mathcal{C}_k, j \in \mathcal{C}_l, \text{ with } k \neq l. \tag{3.61}$$

Additionally, these clusters are countable. In fact, their number equals exactly the geometrical multiplicity of the unitary eigenvalues of the Adjacency matrix $A = \{a_{ij}\}$. Thus, when there is only one such eigenvalue we recover the cases treated in [139], where a key role is played by the global connectivity of the graph. However, for the *local* models that we have just described, which do not rely on a defined topology but instead see it determined by the profile of the influence function ϕ, the authors show through different numerical simulations that an influence function ϕ *increasing* over the distances $\|x_j - x_i\|$ may actually reduce the number of clusters up to global consensus for the formation, and that the steeper the increase over its compact support is, the smaller is the number of clusters formed.

Extension to a continuum model

The last aspect of the CS model that we want to discuss concerns its applicability to very large and very dense formations (like those that are planned to be used in conjunction with chipsats or spacecraft of similar dimensions and capabilities [146]). Several authors have pointed out how in this case the particle formalism employed in the previous subsections should be dropped in favor of a kinetic or hidrodynamical formulation, in large part due to the fact that it is no longer economical keeping track of every single particle in the system.

Staying close to the Cucker-Smale model we mention only [147] (itself partly a continuation of [148]), where a continuum version of the equations is presented and results similar to the particle formulation are obtained. Without going into too many details, the starting point is to consider the N-particle distribution function

$$\tilde{f}^N(x_1, v_1, \ldots, x_N, v_N, t), \quad (x_i, v_i) \in \mathbb{R}^d \times \mathbb{R}^d, \quad i = 1, \ldots, N \tag{3.62}$$

and the corresponding one-particle marginal distribution

$$f^N(x_1, v_1, t) = \int_{\mathbb{R}^{2d(N-1)}} \tilde{f}^N(x_1, v_1, \tilde{x}, \tilde{v})\, d\tilde{x} d\tilde{v}, \tag{3.63}$$

where $\tilde{x} = (x_2, \ldots, x_N)$ and similarly for $\tilde{v}$. Through specific formal techniques based on the Liouville equation (see [148], Section 3.1), it can be proved that the discrete Cucker-Smale

model (3.1) can be translated as

$$\partial_t \tilde{f}^N + \sum_{i=1}^{N} v_i \cdot \nabla_{x_i} \tilde{f}^N + \frac{\lambda}{N} \sum_{i=1}^{N} \nabla_{v_i} \cdot \left(\sum_{j=1}^{N} r\left(x_i, x_j\right)\left(v_j - v_i\right) \tilde{f}^N \right) = 0, \tag{3.64}$$

where $r\left(x_i, x_j\right) = r\left(\|x_i - x_j\right)$ denotes a non-increasing influence function. By integrating the terms of (3.64) with respect to $d\tilde{x}d\tilde{v}$ one can study the behaviour of the marginal distribution $f^N\left(x_1, v_1, t\right)$.

If we assume $\tilde{f}^N$ symmetric with respect to its phase-space arguments, that is

$$\tilde{f}^N\left(\ldots, x_i, v_i, \ldots, x_j, v_j, \ldots, t\right) = \tilde{f}^N\left(\ldots, x_j, v_j, \ldots, x_i, v_i, \ldots, t\right), \tag{3.65}$$

after some computations one can consider the mean-field limit $N \to \infty$, which leads to the equation

$$\partial_t f + v_1 \cdot \nabla_{x_1} f + \lambda_{v_1} \cdot \left(\int_{\mathbb{R}^{2d}} r\left(x_1, x_2\right)\left(v_2 - v_1\right) g dx_2 dv_2 \right) = 0, \tag{3.66}$$

where $f = \lim_{N\to\infty} f^N\left(x_1, v_1\right)$ and $g = \lim_{N\to\infty} g^N\left(x_1, v_1, x_2, v_2\right)$, with g^N denoting the two-particle marginal density. Assuming g satisfies the independence hypothesis

$$g\left(x_1, v_1, x_2, v_2, t\right) = f\left(x_1, v_1, t\right) f\left(x_2, v_2, t\right) \tag{3.67}$$

and relabeling $\left(x_1, v_1\right) \to \left(x, v\right)$ and $\left(x_2, v_2\right) \to \left(y, v^\star\right)$, the continuum CS model can be written as

$$\begin{gathered} \partial_t f + v \cdot \nabla_x f + \lambda_v \cdot Q\left(f, f\right) = 0 \\ Q\left(f, f\right)\left(x, v, t\right) = \int_{\mathbb{R}^{2d}} r\left(x, y\right)\left(v^\star - v\right) f\left(x, v, t\right) f\left(y, v^\star, t\right) dy dv^\star. \end{gathered} \tag{3.68}$$

It can be shown, in a manner similar to the particle-based Cucker-Smale model, that system (3.68) admits the Lyapunov functional [148]

$$\Lambda\left(f\right)\left(t\right) = \int_{\mathbb{R}^{2d}} |v - m|^2 f\left(x, v, t\right) dx dv, \tag{3.69}$$

where

$$m\left(f\right) = \int_{\mathbb{R}^{2d}} v f\left(x, v, t\right) dx dv. \tag{3.70}$$

In [148] the authors managed to prove that the previous functional converges *subexponentially* to zero for $\beta \leq \frac{1}{4}$ but, differently for what happens in the particle case, couldn't give an uniform bound for the spatial support of the density. These results have to be complemented with those given in [149], where the authors characterize rigorously the gap between the particle and kinetic CS model, and also discuss a particular class of solutions for the latter. Finally, these works have later been extended in [147], where the main result lies in the *exponential* decay of Λ towards zero for the entire range $\beta \leq \frac{1}{2}$.

3.2 Lyapunov stability

3.2.1 Definitions

As we have seen before, a desirable consensus process for applications should be characterized by the asymptotical convergence of the agents states towards a particular one, which is then kept indefinitely. Thus, since this state can be characterized as an equilibrium one, when analyzing these processes it is natural to check the (asymptotical) stability of this state as a first step.

In this subsection we are going to review the concept of stability (in the sense of Lyapunov) for autonomous non-linear systems, along with the associated results which are exploited in this thesis. We remark that, albeit here it is enough to limit ourselves to the previous kind of systems, in spacecraft formation flying we can find also non-autonomous ones (typically as a consequence of the controls adopted or of some particular perturbations). Furthermore, it is not uncommon to consider linearized dynamics to describe operations that are fairly contained in terms of the spacecraft relative distances (for example, reconfiguring a formation orbiting around a central body). We remark that the results presented in this section are treated in a deeper fashion inside [87].

That said, in the present work we work with stability both for points and regions of space. In the following, $\mathbb{N}$ denotes the set of natural numbers, $\mathbb{R}$ that of the reals and $\mathbb{R}^n$ ($n \in \mathbb{N}$) the n-dimensional Euclidean space. Additionally, $x \in \mathbb{R}^n$ denotes a column vector of dimension n, i.e. $x = [x_1, ..., x_n]$ with $x_i \in \mathbb{R}$, $\dot{x} = \frac{dx}{dt}$ the corresponding first time derivative and $\ddot{x}$ the second time one.

Now, consider the autonomous dynamical system

$$\dot{x} = f(x), \tag{3.71}$$

with $f : D \to \mathbb{R}^n$ being a locally Lipschitz map from a domain $D \subset \mathbb{R}^n$ to $\mathbb{R}^n$. Suppose $\bar{x} \in D$ is an equilibrium point for f ($f(\bar{x}) = 0$). As usual, for commodity one can shift this equilibrium to the origin of $\mathbb{R}^n$ by imposing $y = x - \bar{x}$ (of course, as long as $\bar{x} \neq 0$), so that it results

$$\dot{y} = \dot{x} = f(x) = f(y + \bar{x}). \tag{3.72}$$

By imposing $f(y + \bar{x}) = g(y)$, we have that $g(0) = 0$. Therefore, without loss of generality, we can always assume $f(0) = 0$ and study the stability of $x = 0$ according to the following definition.

Definition 4. *The equilibrium point* $x = 0$ *of* (3.71) *is*

- *stable if, for every* $\epsilon > 0$*, there exists* $\delta = \delta(\epsilon) > 0$ *such that*

$$\|x(0)\| < \delta \Rightarrow \|x(t)\| < \epsilon, \ \forall t \geq 0 \tag{3.73}$$

- *unstable if it is not stable*
- *asymptotically stable if it is stable and we can choose δ such that*

$$\|x(0)\| < \delta \Rightarrow \lim_{t\to\infty} x(t) = 0. \tag{3.74}$$

As we are going to see in the next subsection, due to the complicated forms that formation flying controls can take, sometimes it is easier to reason in terms of sets instead of points. In particular, let $x(t)$ be a solution of (3.71). A point p is said to be a *positive limit point* of $x(t)$ if there exists a sequence $\{t_n\}$, with $t_n \to \infty$ when $n \to \infty$, such that $x(t_n) \to p$ as $n \to \infty$. Correspondingly, the set of all the limit points of $x(t)$ is called the *positive limit set* of $x(t)$. Furthermore, a set M is said to be *invariant* with respect to (3.71) if

$$x(0) \in M \Rightarrow x(t) \in M,\ \forall t \in R. \tag{3.75}$$

That is, if a point is in M then it stays there for any past and future time. As a particular case, we say that a set M is *positively invariant* if

$$x(0) \in M \Rightarrow x(t) \in M,\ \forall t \geq 0. \tag{3.76}$$

We also say that $x(t)$ approaches M for $t \to \infty$ if, for every $\epsilon > 0$, there exists $T > 0$ such that

$$d(x(t), M) < \epsilon,\ \forall t > T, \tag{3.77}$$

where d denotes the distance from a point p to a set M, that is the smallest distance from p to any point in M. Formally, this is defined as

$$d(p, M) = \inf_{x\in M} \|p - x\|. \tag{3.78}$$

While we do not discuss the matter in depth, it is worth noticing that working with points and working with sets present a fundamental difference. To understand it, let's consider a $stable\ limit\ cycle$, that is the positive limit set of every solution starting sufficiently close to it. In an analogous manner, an asymptotically stable equilibrium point is by definition the positive limit set of every solution starting nearby. In both cases, this near solutions will approach the objects in question. However, in the case of a stable limit cycle, the solution is not approaching any particular point, which means that $x(t)$ approaching M for $t \to \infty$ does not imply that $\lim_{t\to\infty} x(t)$ exists.

3.2.2 Theorems

In the previous subsection we have discussed stability concepts both for equilibrium points and invariant sets. In this subsection instead, we are going to look at a classical approach to determine

the stability type of the object in question. In particular, we focus on a partial list of results aimed to individuate asymptotically stable items.

This approach relies, given the autonomous system (3.71), on the construction of a continuous differentiable energy-like function $V : D \to \mathbb{R}$, with $D \subset \mathbb{R}^n$. The idea is for this function to be a non-increasing one along the solutions of system (3.71) ($\dot{V}(x) \leq 0$, with $x = x(t)$ being a solution of the autonomous system). Assuming that we can restrict to a compact subset of D, then this function will converge to some limit on the $x(t)$ trajectory. What these results aim to prove is that when you stop you have reached a point or a set for which the solution $x(t)$ is at the equilibrium that you wanted to achieve. From this follows asymptotical stability by different means.

The main result that employ the previous approach is the so called second Lyapunov's theorem, which gives sufficient conditions for the origin of the system (3.71) to be stable and asymptotically so. In particular, the theorem states that

Theorem 17. *Let $x = 0$ be an equilibrium point for* (3.71) *and $D \subset \mathbb{R}^n$ a domain containing it. Let $V : D \to \mathbb{R}$ be a continuously differentiable function such that*

$$\begin{gathered} V(0) = 0 \text{ and } V(x) > 0,\ x \in D - \{0\}, \\ \dot{V}(x) \leq 0,\ x \in D. \end{gathered} \tag{3.79}$$

Then $x = 0$ is stable. Moreover, if

$$\dot{V}(x) < 0,\ x \in D - \{0\}, \tag{3.80}$$

then $x = 0$ is also asymptotically stable.

To clarify the idea previously described in the context of Theorem 17, let us consider the level surfaces $V(x) = c$ (for some $c > 0$) of the function V. The condition $\dot{V} \leq 0$ implies that when a trajectory crosses a level surface $V(x) = c$, it moves inside the set $\Omega_c = \{x \in \mathbb{R}^n | V(x) \leq c\}$ and can never come out again. If additionally $\dot{V} < 0$, the trajectory moves from a level surface to an inner one with a smaller c. As c decreases, the surface $V(x) = c$ shrinks to the origin, showing that the trajectory approaches the origin as time progresses. Thus, if we only know that $\dot{V} \leq 0$, we cannot be sure that the trajectory will approach the origin, but we can conclude that the origin is stable since the trajectory can be contained inside any ball B_ϵ, as long as the initial state $x(0)$ lies on a level surface contained in that ball.

The previous discussion allows us to focus on an important aspect of the preceding theorem, that is the extension of the *basin of attraction* of system (3.71), where the latter is defined as the set of all points x such that a solution $\phi(t; x)$, starting at x when $t = 0$, is defined for all $t \geq 0$ and $\lim_{t\to\infty} \phi(t; x) = 0$. In particular, we focus on understanding under what conditions the basin of attraction is given by the entire space $\mathbb{R}^n$.

It will be the case if we can show that for any initial condition x, the trajectory $\phi(t; x)$ approaches the origin as $t \to \infty$, no matter how large $\|x\|$ is. An asymptotically stable

equilibrium point having this property is called *globally asymptotically stable*. Recalling what has been said before, we can see that global asymptotic stability can be established if any point $x \in \mathbb{R}^n$ can be included in the interior of a bounded set Ω_c. For this condition to hold, obviously it must result $D = \mathbb{R}^n$. However, this is not enough, since, for example, for large c the set Ω_c is not necessarily bounded. An extra condition assuring the needed boundness is given by

$$V(x) \to \infty \text{ as } \|x\| \to \infty, \tag{3.81}$$

which usually goes under the name of *radial unboundness*. With this condition in tow, Theorem 17 can be restated as

Theorem 18. *Let $x = 0$ be an equilibrium point for system 3.71 and $V : \mathbb{R}^n \to \mathbb{R}$ a continuous differentiable function such that*

$$\begin{gathered} V(0) = 0 \text{ and } V(x) > 0,\ \forall x \neq 0, \\ V(x) \to \infty \text{ as } \|x\| \to \infty, \\ \dot{V}(x) \leq 0,\ \forall x \neq 0. \end{gathered} \tag{3.82}$$

Then, the point $x = 0$ is globally asymptotically stable.

The previous result is known as Barbashin-Krasovskii theorem. Similarly to Theorem 17, this one, albeit definitive in theory, may be of difficult application. This is due to the fact that there exist systems (an example being the pendulum with friction) for which we can find easily a non-increasing Lyapunov function, which is then difficult to prove being strictly decreasing.

A possible solution to this problem is to observe that, given a non-increasing Lyapunov function V defined in some domain around the origin, if we can establish that no trajectory of system (3.71), except for $x = 0$, can stay in the set of points where $\dot{V}(x) = 0$ for all times, then the origin is asymptotically stable.

The previous idea can be seen as an application of the so called LaSalle's Invariance Principle, exploiting the fact that an asymptotically stable equilibrium point is not only the positive limit set of every solution starting sufficiently close to it, but it is also clearly an invariant set. The Invariance Principle generalizes this fact, and this generalization rests on the properties of positive limit sets outlined in the following lemma

Lemma 8. *If a solution $x(t)$ of (3.71) is bounded and belongs to D for $t > 0$, then its positive limit set L_+ is a nonempty, compact and invariant set. Moreover, $x(t)$ approaches L_+ as $t \to \infty$.*

With this property in tow, we are assured that our solution will arrive in a certain set. Therefore, the first thing to do is verify that this set has the characteristics that we are looking for. Since we know that a function V like before has a limit in a compact Ω (since it is non-increasing and continuous) and that the trajectories along which we are evaluating it asymptotically approach L_+ (which is in Ω due to the latter being a closed set), it must result that V is constant on this set

and consequently $\dot{V} = 0$. Thus, since L_+ may be a difficult set to pinpoint, we can be happy by enlarging ourselves to the largest invariant set for which $\dot{V} = 0$. The latter, as can be seen below, is exactly the statement of the LaSalle's Invariance Principle.

Theorem 19. *Let $\Omega \in D$ be a compact set which is positively invariant with respect to* (3.71). *Let $V : D \to \mathbb{R}$ be a continuously differentiable function such that $\dot{V}(x) \leq 0$ in Ω. Furthermore, let $E = \left\{ x \in \Omega | \dot{V}(x) = 0 \right\}$ and M be the largest invariant set contained in E. Then every solution starting in Ω approaches M as $t \to \infty$.*

Chapter 4

On the translational Cucker-Smale control

4.1 Introduction

In the present chapter we consider the problem of formation acquisition and maintenance for a group of autonomous or semi-autonomous agents, that is, given different initial conditions for these agents, we want them to asymptotically achieve a rigid configuration, characterized by time invariant relative distances. Furthermore, we want for this state to be kept indefinitely or at least for a useful period of time. Although the underlying theory is valid for any group of agents acting according to some translational dynamics, here we limit ourselves to consider the problem in the context of spacecraft formation flying.

The main purpose of this chapter is to expand on the work done in [92], where the Cucker-Smale model previously introduced was used as a template to design a formation flying control aimed to achieve the objectives described in the previous paragraph. In particular, the control was employed in that paper with three spacecraft travelling along a transfer orbit to the Sun-Earth L_2 libration point, allowing them to achieve and maintain fixed relative distances for the entire transfer.

Thus, the expansion mentioned in the previous paragraph goes along two consecutive directions. First, we consider a simpler dynamical model with respect to [92] in order to outline what are the aspects of the natural dynamics that more affect the application of the Cucker-Smale control (and more in general any distributed control strategy). This model is given by a formation acting only under the influence of a central force field (and supposedly performing different interferometric operations), with the main difference from Perea et al.'s work being the non-vanishing character of the vector field affecting the formation dynamics.

Secondly, we exploit the informations obtained in this toy model to design a more complex application of the Cucker-Smale strategy, showing how it can act as a fundamental wheel in a multi-layered mission scenario. The example presented here is given by the use of the CS control

to maintain a formation in a neighborhood of one of the Earth-Moon-Sun saddle points, which are periodically visited by this formation as it travels along eccentric elliptic orbits having Earth as one of the foci.

In conclusion, the chapter is organized as follows. In Section 4.2 we discuss how to adapt the Cucker-Smale model in order to define a formation control and how to implement numerically said control. Section 4.3 is dedicated to the study of the introductory case of a formation achieving consensus in the presence of a single central force field. Following the results obtained, in Section 4.4 we construct a favourable instance for the control application in the context of a four body problem and outline the major features of the control in such a case. Finally, in Section 4.5 we present our conclusions and summarize the results outlined in the chapter.

4.2 Methodology

4.2.1 Control definition

As previously explained, a first attempt to implement the Cucker-Smale control to spacecraft formation flying was done in [92]. In this subsection we discuss the approach adopted in that work, since it actually constitutes the basis for the present one. Note that the discussion presented here is slightly more general than the one in [92]. This is required to highlight some aspects of both the problems and the approach that are relevant for our settings and methodology.

Assume to have a formation of N satellites. If $x_i(t)$ and $v_i(t)$ denote respectively the three-dimensional position and velocity of the i-th satellite in a given reference frame, we can define

$$x = (x_1, \ldots, x_N), \quad v = (v_1, \ldots, v_N). \tag{4.1}$$

In general, given a force function $f(x, v)$ and a control function $u(x, v)$, the dynamics of the fleet can be described by the continuous system

$$\dot{x} = v, \quad \dot{v} = f(x, v) + u(x, v). \tag{4.2}$$

If we define the extension of the Cucker-Smale control law as

$$u(x, v) = -L_N v + f(x_0, v_0) - f(x, v), \tag{4.3}$$

where $(x_0, v_0) \in \mathbb{R}^{3N} \times \mathbb{R}^{3N}$ denotes the N-replica of a reference orbit $(\tilde{x}_0, \tilde{v}_0) \in \mathbb{R}^3 \times \mathbb{R}^3$, system (4.2) reduces to

$$\dot{x} = v, \quad \dot{v} = -L_N v + f(x_0, v_0). \tag{4.4}$$

This system is actually equivalent to a Cucker-Smale like one. In fact, by writing positions and velocities as

$$x = x_0 + \Delta x, \quad v = v_0 + \Delta v, \tag{4.5}$$

the first of equations (4.4) can be rewritten as

$$\frac{d}{dt}\left(x_0 + \Delta x\right) = \dot{x} = v = v_0 + \Delta v. \tag{4.6}$$

Furthermore, if we assume that the underlying communication graph is either undirected connected or directed with a spanning tree, we have that $L_N v_0 = 0$. Thus, the second equation in (4.4) becomes

$$\frac{d}{dt}\left(v_0 + \Delta v\right) = \dot{v} = f\left(x_0, v_0\right) - L_N v = f\left(x_0, v_0\right) - L_N\left(\Delta v\right). \tag{4.7}$$

Finally, the system defined by the last equation is equivalent to the union of the systems

$$\dot{x}_0 = v_0, \quad \dot{v}_0 = f\left(x_0, v_0\right), \tag{4.8}$$

and

$$\begin{aligned} \frac{d}{dt}\left(\Delta x\right) &= \Delta v, \\ \frac{d}{dt}\left(\Delta v\right) &= -L_N\left(\Delta v\right). \end{aligned} \tag{4.9}$$

By analogy between equations (3.27) and (4.9), Theorems 11 and 13 give sufficient conditions for the system described by the latter to achieve full cancellation of the relative velocities and converge to a flight formation.

A couple of remarks must be done on this implementation. First of all, as we are going to discuss in greater detail in the next section, one has to take care of what is the the reference frame where the spacecraft coordinates are taken, paying particular attention of whether eventual fictitious forces are taken into account.

A second consideration must be done on the introduction of the concept of leadership. With the previous paragraph in mind, let's consider as leader of the formation a point travelling on the chosen reference orbit. In the associated relative reference frame, this point corresponds to the origin and therefore has null velocity. This implies that, if the procedure above is considered in the relative frame, the control will eventually cancel the relative velocities of the other satellites and paint (in the frame relative to the reference, of course) a cloud of fixed points (at least after a certain amount of time). Furthermore, in case of a continuous application of the control, results like Theorem 14 lose importance with the previous approach, since by construction the relative accelerations are cancelled.

4.2.2 Numerical implementation

As already discussed in [92], the extension of the CS control presented in the previous subsection relies implicitly on two assumptions: the possibility of exercising a continuous control and the continuous availability of relative data (distance, velocity and acceleration) from the satellites of the formation. Since one (or both) of these assumptions may not be feasible for a real space mission, it is necessary to discretize the continuous control. In what follows, we present a possible way to do this.

Let t_{i-1} and t_i be the instants of two consecutive maneuvers and

$$\pi_n = \{t_{i-1} = t_{i,0}, t_{i,1}, \ldots, t_{i,n} = t_i\}, \tag{4.10}$$

a partition of the interval defined by them, where, for each epoch $t_{i,j}$, each satellite can measure relative positions, velocities and accelerations. Then, denoting by $\Delta t_{i-1,j} = t_{i,j} - t_{i,j-1}$ the time span between two consecutive estimates of the relative data, we can consider as approximation for an impulsive maneuver Δu_{i-1} at time t_{i-1} the expression

$$\Delta u_{i-1} = \int_{t_{i-1}}^{t_i} u(t)\, dt \approx \sum_{j=1}^{n} u(t_{i-1,j})\, \Delta t_{i-1,j}, \tag{4.11}$$

where u denotes the modified control defined in equation (4.3). An easy way to improve this approximation is to use some step-size control. That is, if $\tilde{x}(t_i)$ is the solution of system (4.4) and $\hat{x}(t_i)$ is the result of using equation (4.11) with boundary conditions x_{i-1} and v_{i-1} at time t_{i-1}, the difference between the two values can be used to modify the size of the interval $t_i - t_{i-1}$.

Note that the considerations done in this subsection and in the previous one are very general, in the sense that they are valid for any kind of force field, not only gravitationally generated ones. This means that the control that we are designing can be applied in a vast array of fields (for example, it could be used to control swarms of nanobots flowing in the human organism).

4.3 Application in a central force field

4.3.1 Dynamical model

As stated in the introduction, the main goal is the design of a control law which needs to operate in an orbital environment, that is under the presence of a central force field. Therefore, to understand if the extended Cucker-Smale control performs well under these circumstances, it is natural to consider a simple keplerian problem as a starting point, with the central body supposed to be Earth and the satellites masses being neglected. For the numerical simulations that we are going to present in the next subsections no perturbative effect (oblateness, atmospheric drag, ...) has been considered.

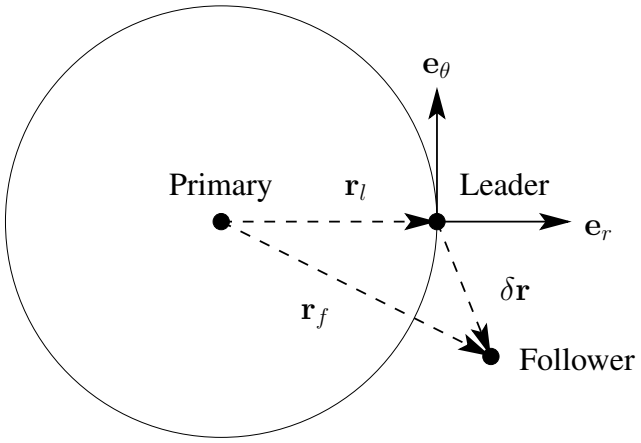

Figure 4.1: Top-down view of the Hill's frame for a circular reference orbit.

Still, for reference, it should be noted that their presence may alter significantly the analysis. On one side, they will probably represent obstacles to overcome (for example, the control will have to be able to compensate also for the J_2 effect). On the other side, they may represent a source of fuel-free implementation for the control (for example, as it as been done in [150], the solar radiation pressure could be used in such a manner). Note that, in the last case, different kind of propulsion tools can be used to achieve the same result, ranging from solar sails to ion thrusters.

That said, to simplify the setting in which we are going to operate, the reference orbit $(\tilde{x}_0, \tilde{v}_0)$ is always considered to be circular. This constraint allows us to restrict our considerations solely on the relative data of the satellites, without worrying about the position of the leader on its orbit. Of course, this observation is relevant only when control (4.3) is applied discretely.

Thus, in light of the previous restrictions, to describe a formation's dynamics we can introduce the so called Hill's reference frame, which, as shown in Figure 4.1, is nothing more than a rotating frame which origin travels along the reference orbit with angular velocity equal to its mean motion. The frame itself is defined by the unitary vectors

$$\mathbf{e}_r = \frac{\mathbf{r}_l}{\|\mathbf{r}_l\|}, \quad \mathbf{e}_c = \frac{\mathbf{r}_l \wedge \dot{\mathbf{r}}_l}{\|\mathbf{r}_l \wedge \dot{\mathbf{r}}_l\|}, \quad \mathbf{e}_\theta = -\mathbf{e}_r \wedge \mathbf{e}_c, \tag{4.12}$$

where $\mathbf{r}_l$ denotes the vector radius of the reference point and $\dot{\mathbf{r}}_l$ its time derivative.

The equations of motion in this reference frame, which describe the relative motion of a satellite (follower) with respect to another one (leader), are [151]

$$\begin{aligned} X'' - 2nY' - n^2 (X + r_l) &= -\frac{\mu}{r_f^3} (X + r_l), \\ Y'' + 2nX' - n^2 Y &= -\frac{\mu}{r_f^3} Y, \\ Z'' &= -\frac{\mu}{r_f^3} Z, \end{aligned} \tag{4.13}$$

	K	σ	β	$\|\Delta x_0\|$ (m)	$\|\Delta v_0\|$ (m/s)	θ (rad)	ϕ (rad)	a (km)
Baseline values	10^{-1}	10^{-10}	0.4	10^3	10^{-4}	$\frac{\pi}{2}$	$\frac{\pi}{2}$	42168
Intervals	$\left[10^{-10}, 1\right]$	$\left[10^{-10}, 1\right]$	$[0, 2]$	$[50, 5000]$	$\left[10^{-8}, 10^2\right]$	$[0, 2\pi)$	$[0, 2\pi)$	$[6778.14, 46378.14]$

Table 4.1: Values for the simulation parameters (brackets denote the intervals of the parameter values used for the simulations of Section 4.3). From left to right: control parameters (K, σ and β), initial relative distance and velocity w.r.t. the leader, in plane and out of plane angles defining the direction of the relative velocity vector, semi-major axis of the reference orbit.

where (X, Y, Z) denote the relative coordinates of the follower, n the mean motion of the leader, μ the gravitational parameter while r_l and r_f indicate respectively the distance of the leader and the follower from the central mass. Note that, considering our hypotheses on the setting, the Hill's frame seems to be a natural choice to describe the dynamics of a formation. However, it is not the only possibility and may not be a good choice in case other hypotheses are added or different tasks for the formation are planned.

4.3.2 Simulations design

The main goal of the simulations performed in this section is to understand how (and how well) the extended CS control behaves under the effect of a central force field, in particular when it is used to achieve and maintain a loose formation driven by a leader moving on a keplerian circular orbit. To achieve this goal, the simulations have been limited to the dynamics of couples leader-follower. This essentially means studying, in a flock under hierarchical leadership, the dynamics of the satellites that communicate directly with the leader and that, consequently, should offer the better performances.

Note that the extended CS control law has been designed as a stabilization law (i.e., to cancel intervehicle velocities and accelerations). Therefore, one must be aware that, due to the process of convergence (and the approximation previously described), there may exist variations in the relative distances (from the initial position, between the satellites of the formation, ...). Part of the purpose of the simulations lies in trying to understand how these variations respond to different values of the parameters involved. Clearly, for a real space mission, these variations may violate specific requirements, such as minimal/maximal intervehicle separation. To solve this, the CS control law may be combined with other control strategies to meet the required mission specifications.

To better evaluate the performances of the control, some additional constraints have been imposed when performing the simulations. First of all, due to the considerable number of parameters involved in the simulations, a baseline scenario has been selected for all them (see Table 4.1). Depending on the purpose of the simulation performed (in particular when running simple data propagations), some of the baseline values may have been modified. Where

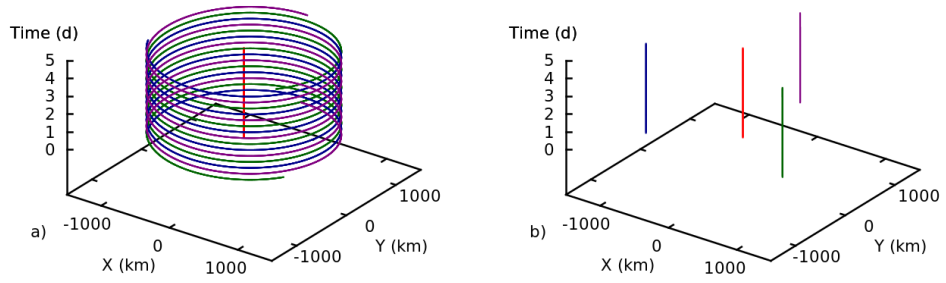

Figure 4.2: Time evolution of a coplanar triangular formation subject to a non-hierarchical Cucker-Smale control. The reference orbit is depicted in red. (a) Output of the integration of equations (4.4). (b) Output of the integration of equations (4.9).

appropriate, it will be remarked.

A second point comes from the time interval between two consecutive maneuvers. For the set of experiments described in the next two subsections, this time interval has been set as 10^{-1} seconds (with n of equation (4.11) equal to 1), which corresponds to an idealized low-thrust propulsion regime for the satellites of the formation. The regime is idealized in the sense that no restriction on the thrust is imposed. While this choice may seem to be in contrast with the observations done in the previous section, one must remember that the CS control has been designed to operate in free space. Therefore this choice is the most natural, in terms of performance understanding, since it allows the control to operate in a very favorable regime (close to the continuous case), while at the same time permitting the evaluation of the impact of a gravitational acceleration.

Finally, we arrive at the description of the simulations. In Section 4.3.2 we are going to discuss a little bit about the geometry of the CS control by comparing our approach (based on the presence of a leader) with the one presented in [92] and discussed in Section 4.2 (which relies on the original work from Cucker and Smale). Instead, in Section 4.3.3 we will evaluate the performance of the CS control with respect to a certain sets of parameters (CS control parameters, initial relative distance, magnitude and orientation of the initial relative velocity, altitude of the reference orbit). This analysis will be carried out by comparing the evolution of two metrics (maximal deviation from the initial leader-follower relative distance and total thrust employed to keep the formation) with respect to every parameter indicated previously.

4.3.3 Strategies comparison

This subsection aims to provide a comparison between the strategy presented in [92] and the improvements previously discussed (see 3.2). In particular, we focus on how the CS control (with and without leadership) influences the geometry of a formation.

In the previous section we have shown how to implement the CS control under the presence

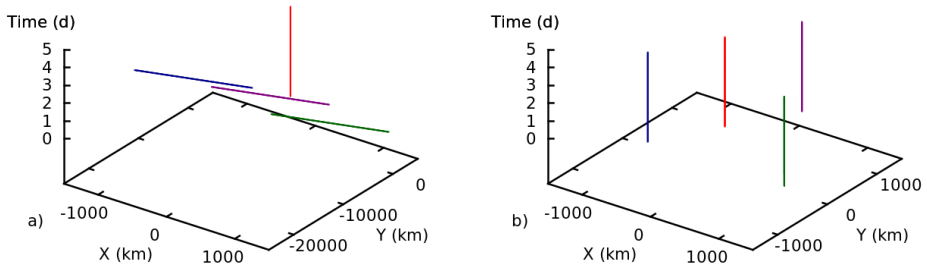

Figure 4.3: Time evolution of the same formation of Figure 4.2. The only difference is that the reference is moved on the left side of the triangle. (a) The reference is not a leader. (b) The reference is imposed as leader of the formation.

of an acceleration. However, a quick clarification must be done. If we look at equation (4.7) it is obvious that working with the absolute equations of motion puts into play the effect of the fictitious forces. This is made clear in Figure 4.2, where a triangular formation has been selected alongside a reference orbit (indicated in red). Initial conditions have been chosen as for the satellites to move in the plane defined by the reference orbit. The plots depict the time evolution of the orbits of the satellites as seen in Hill's frame (with respect to the reference). The integration has been done both in an Earth-centered reference frame (left) and in the Hill's frame (right). As it can be seen, the presence of the fictitious forces causes the circularization of the relative orbits of the satellites (with the relative circular orbits having a period close to the reference's one) which, however, technically achieve a flocking state (in the sense of relative positions being constant and relative velocities being the same). More formally, we have that

$$\mathbf{r}_f = \mathbf{r}_l + \delta\mathbf{r}, \tag{4.14}$$

and therefore

$$\frac{d}{dt}\mathbf{r}_f = \frac{d}{dt}\left(\mathbf{r}_l + \delta\mathbf{r}\right) = \mathbf{v}_l + \left(\frac{d}{dt}\delta\mathbf{r}\right)_r + \Omega \times \delta\mathbf{r}, \tag{4.15}$$

where in the last equation we have applied the Transport theorem (with $\left(\frac{d}{dt}\right)_r$ denoting the rate of change as observed in the Hill's frame and Ω the angular velocity of the latter). If we consider what said for equation (4.9), we have $\lim_{t\to\infty}\left(\mathbf{v}_f - \mathbf{v}_l\right) = 0$, and therefore

$$\left(\frac{d}{dt}\delta\mathbf{r}\right)_r = -\Omega \times \delta\mathbf{r}, \tag{4.16}$$

where $\delta\mathbf{r}$ remains constant and the limit notation has been dropped for commodity. A similar computation for the accelerations proves our point. Of course, picking coordinates directly in the rotating frame (where $f\left(x_0, v_0\right)$ equals zero) gives the correct consensus behaviour (which can be observed on the right of Figure 4.2).

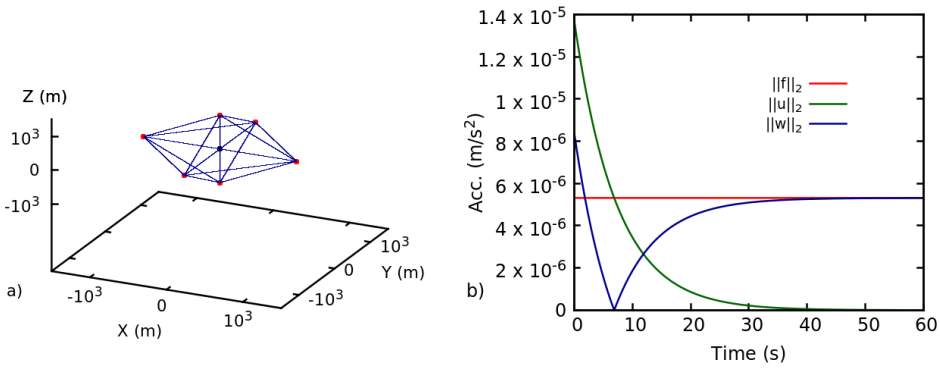

Figure 4.4: Example of formation (a) and corresponding time evolution of the control terms (satellite on $Z > 0$) (b). Final integration time is 30 days.

A second point that must be clarified comes from the presence (or absence) of a leader. In Figure 4.3 we plot the time evolution of the same formation depicted in Figure 4.2. Now however, the reference orbit has been moved on one of the sides of the triangle formed by the flock. On the left, one can observe what happens when the reference is not considered as a leader and the agents communicate only between themselves. As could be expected, the flock achieves a common velocity different from the one of the reference. Instead, if the reference is considered as the leader of the formation (plot on the right) then the satellites achieve its velocity and therefore follow it for the whole time interval. These plots, in combination with the ones in Figure 4.2 (where the reference is not considered as leader, but it is conveniently placed at the spatial barycenter of the formation) actually show that, while true that correct deployment of a formation and choice of the reference path can substitute the presence of a leader, they actually give a less flexible strategy since the chosen path cannot be customized (think, for example, at the instants that follow deployment through a carrier, where the agents possess different initial velocities).

We conclude this subsection by showing a more general example of a formation alongside the associated behavior of the control terms. On the left side of Figure 4.4 the evolution of a formation in a time span of 30 days (as seen in the Hill's frame) is shown, where the red dots denote the followers of the formation while the black one indicates the leader (the blue lines are there to give a crystal-like aesthetic flavor to the formation). As it can be noted, when the control can operate under favorable conditions, the satellites essentially behave as fixed points in the Hill's frame. Of course, as shown on the right side of the same figure, where the evolution in time of the various components of the control is shown, this is not completely true. In fact, what happens is that, as time goes by, the CS term of the control (in green) goes to zero as the relative velocities are canceled, thus leaving as the only relevant term of the control the one determined by the relative acceleration felt by the chosen follower (in red). Indeed, this is the only relevant term for the control (blue curve) when it comes to keep the formation (while the CS term is still present due to the sensitivity to the initial conditions of the problem, its contribution, thanks also to the small time delay between maneuvers, is significantly smaller).

4.3.4 Performance analysis

In this subsection we are going to analyze the performance of the modified CS control under the effect of a central force field in terms of the relevant parameters for the chosen setting: the control parameters (K, σ and β), the initial positions and velocities relative to the reference and the radius (more in general, the semi-major axis) of the reference orbit. As already mentioned (see equation (4.11) and Section 4.3.1) we will use an idealized low-thrust regime to better evaluate the feasibility of the proposed strategy. To this end, some considerations should be done.

First of all, there is the matter of the gravitational acceleration. As already mentioned, we analyze only the effectiveness of the control in the presence of a direct communication with the leader. Therefore, to try and evaluate fully the impact of this acceleration, we will consider three different leader-follower couples, all having in common the leader, the restrictions on the control listed before and the values of the simulation parameters listed in Table 4.1. However, the agents will be placed in different positions. The first one, displayed in dark blue in the plots, will be placed along the relative Z axis. This allows to evaluate completely the effect of the out of plane acceleration since, according to equations (4.13), it is actually independent from the in-plane one, and therefore its impact can be studied separately. The other two will instead be placed respectively on the relative X (red) and Y (dark green) axes. Do note that, while it is not possible to completely unravel the entanglement that characterizes the in-plane motion, this choice allows the evaluation of the difference in the control's performance for the best placed satellite and the worst one when their relative distances from the leader are the same. Of course, according to the keplerian geometry, the latter will be the one placed on the X axis (where the difference in acceleration is higher) and the former will be the one on the Y axis.

A second point comes from the radius of the leader's orbit. The baseline quantity chosen for this set of simulations corresponds to the geostationary ring around the Earth. Being a fairly high orbit, the effect of the acceleration is weak enough as to limit some expected instabilities in the control (like the ones corresponding to the parameters K and σ), both in the relative distances and in the integral of the thrust.

Finally, let us discuss a moment about the purpose behind the selected metrics. We have seen in the previous section that, by definition, the CS control takes some time to synchronize the spacecraft velocities. Thus, given a certain initial position for a follower relative to the leader, there may be some displacement from this initial state before the velocities synchronization, and the first metric that we are considering aims to catch the maximal value of this displacement. The thrust integral instead allows us to understand at a glance what are the most favourable configurations for the formation. This is because, again as we have seen in the previous subsection, after synchronization (which on average happens in a matter of seconds) the only relevant term remaining in the control is given by the natural acceleration felt by the follower, which in turn is determined by the leader's radius and the leader-follower relative distance. Thus, a lower value for the thrust integral indicates a more favourable set of conditions for the follower.

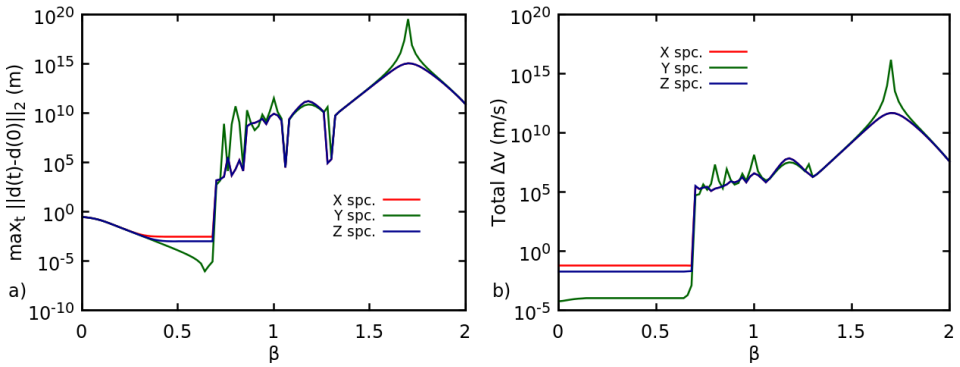

Figure 4.5: Variation with respect to β of the maximal deviation from the initial leader-follower distance (a) and total Δv (b).

For the simulations presented in this subsection, the total integration time has been set to 30 days. To facilitate the reading of the results, a logarithmic scale has been applied to the y axis of every plot. The results obtained, parameter by parameter, can be summarized as follows

- **Control parameter β:** in Figure 4.5 we have depicted the evolution of the two metrics with respect to the value of β. As it can be seen, the evolution of both is similar, but there are some notable differences. Let's look at the maximal variation of the initial relative distance first. The decaying character (present for all the satellites) for $\beta \leq 0.5$ derives from the fact that, being both $\sigma^2 << \|x_0 - x_1\| << 1$ (with the unit of length given by the equatorial radius of the Earth), the smaller is the value of β, the smaller is the value of the weights, which in turn slows down the convergence process. This decay is present also in the fuel expenditure. However, since the convergence process for this configuration values takes place in a matter of seconds, the CS term contribution in the modified control is very small when compared to the relative acceleration one that, therefore, constitutes be the major factor when determining the total fuel expenditure (thus, the seemingly flat plots).

  For $\beta > 0.5$ instead, a gradual growing instability is observed in both metrics. This happens because the initial maneuvers become increasingly large with a growing β and stabilization happens only at great relative distances. At this point the weights are so small that the method is no longer able to cancel the relative velocities, but only the relative dynamics. Of course, if we approximate further the continuous case by lowering the delay between maneuvers, this problem become less and less evident;

- **Control parameters K and σ:** in Figures 4.6 and 4.7 the evolution with respect to the parameters K and σ is considered. The first thing to note is that no significant instability is observed. This seems to be related to the weakness of the acceleration considered. In fact, lowering the altitude of the reference orbit shows up a strict relation between the two parameters. For small values of K and big values of σ (and therefore, overall small gains) instabilities can be observed in both plots. However, these are related to two other

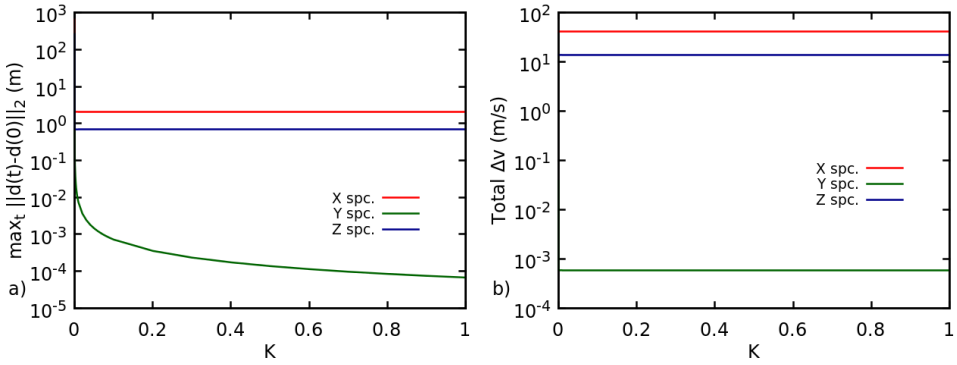

Figure 4.6: Variation with respect to K of the maximal deviation from the initial leader-follower distance (a) and total Δv (b).

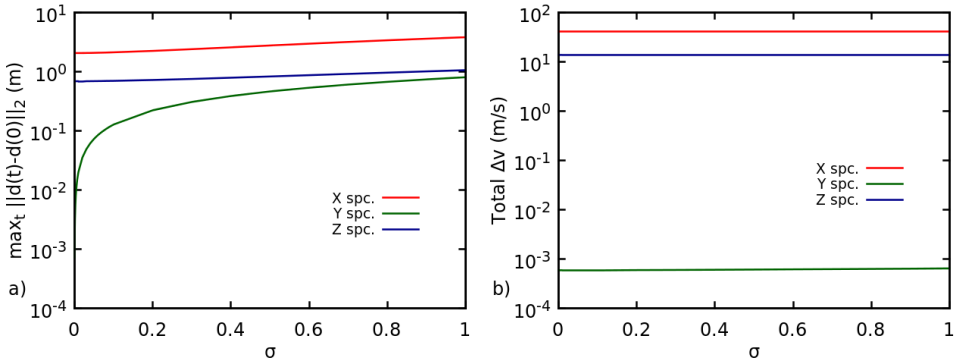

Figure 4.7: Variation with respect to σ of the maximal deviation from the initial leader-follower distance (a) and total Δv (b).

factors. First of all, relative distances must be small with respect to the value of σ, so the latter can define the denominator in the weights. Second, if the altitude is quite high (the geostationary ring is an example), these instabilities tend to not appear, since we are very close to a free space environment and the baseline value of β puts us in an unconditional convergence regime;

- **Initial relative distance (norm) $\|\Delta \mathbf{x}_0\|$:** the dependence of the two metrics from the initial relative distance is essentially linear for all the couples (Figure 4.8). This is easily explainable by looking at the equations (4.13). In fact, with a very high orbit, the variation of the relative acceleration tends to become linear with the relative distance (for all the three axis);

- **Leader's semimajor axis (radius) a:** a reasoning similar to the previous one can be applied for the variation of the metric with respect to the radius of the reference orbit (Figure 4.9), where the decay is actually cubic in shape. Note, however, that for very high orbits the shape for the satellites placed on the tangential direction tends to become flat due to the closeness of the follower and leader orbits;

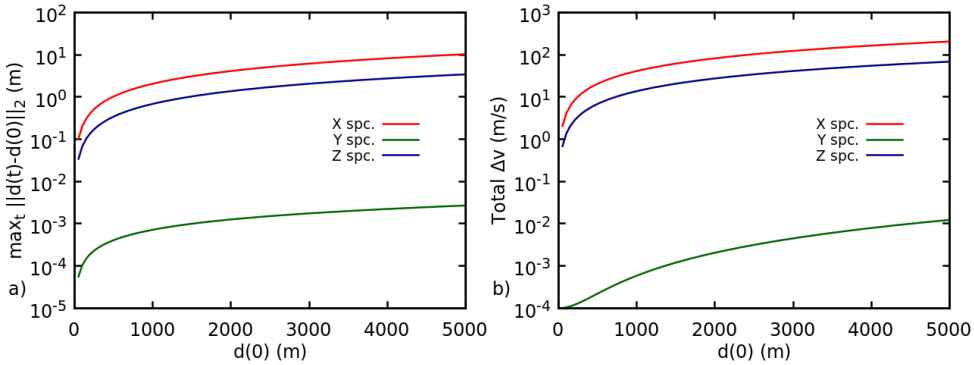

Figure 4.8: Variation with respect to initial relative distance Δx_0 of the maximal deviation from the initial leader-follower distance (a) and total Δv (b).

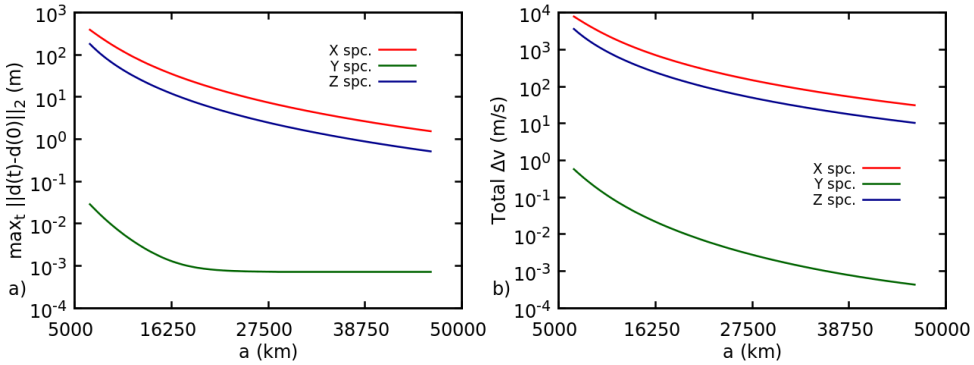

Figure 4.9: Variation with respect to radius of the leader's orbit of the maximal deviation from the initial leader-follower distance (a) and total Δv (b).

- **Initial relative velocity (norm) $\|\Delta \mathbf{v}_0\|$:** in Figure 4.10 we plot the variation of the metrics with respect to the initial magnitude of the relative velocities for three different sets of angles. The zero value for the angles is assigned to the positive X (θ) and Z (ϕ) semiaxes, with the increment for the first going counterclockwise and for the second going clockwise instead. The selected values for the plots ($(\theta, \phi) \in \left\{\left(0, \frac{\pi}{2}\right), \left(\frac{\pi}{2}, \frac{\pi}{2}\right), (0, 0)\right\}$) corresponds to the directions for increasing relative acceleration along the three axis. As could be expected, for every set of angles, the satellite that suffers more (in terms of variation from the initial distance) the increase in the initial relative velocity is the one placed on the axis corresponding to the direction of this variation. Still, despite the logarithmic scale, the difference with the other two is quite low and tend to reduce further as the magnitude of the initial relative velocity increases. It is interesting to note that the thrust integral variation is almost independent from the direction of the initial relative velocity. Again, this is due to the fast convergence of the control and the discretization adopted which assign a greater role to the relative dynamics for this kind of computation.

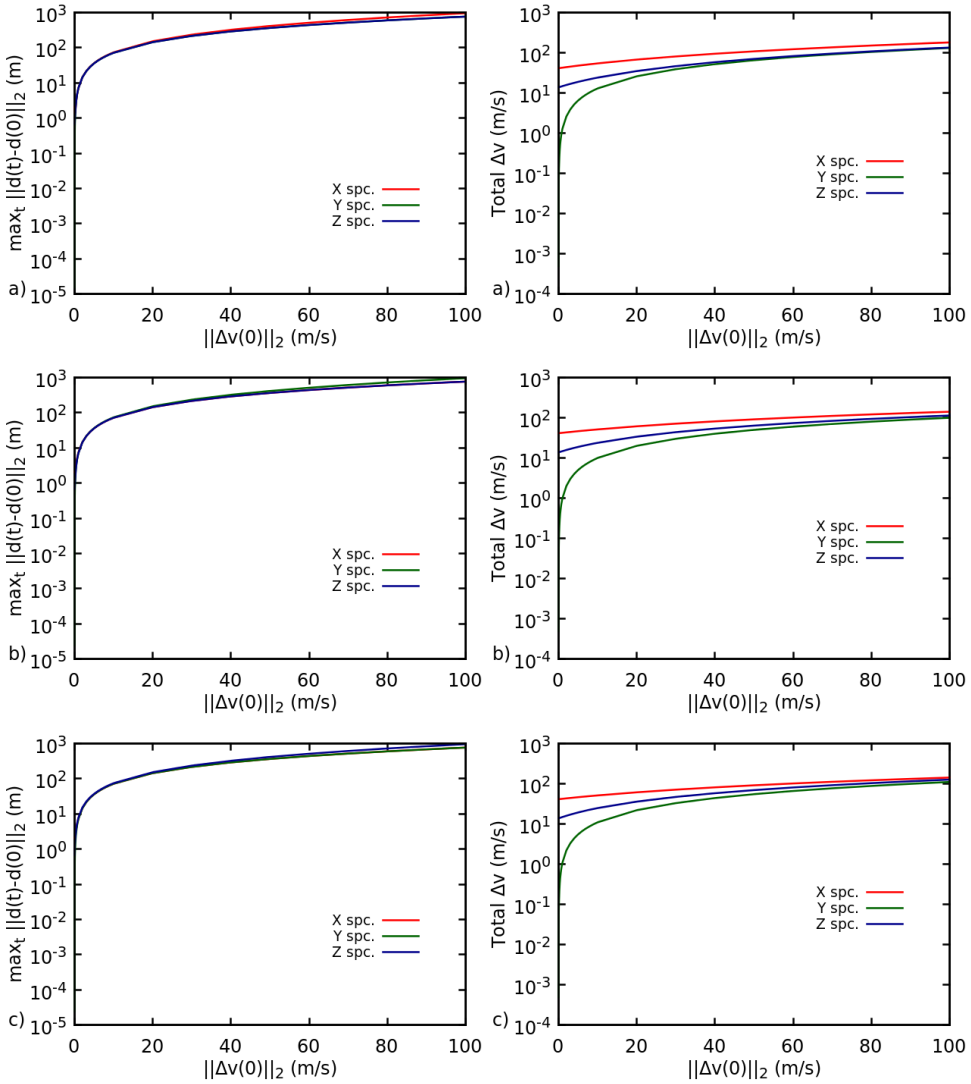

Figure 4.10: Variation with respect to the Euclidean norm of the initial follower velocity for the maximal deviation from the initial leader-follower distance (left) and total Δv (right). The values of (θ, ϕ) are: $\left(0, \frac{\pi}{2}\right)$ (a), $\left(\frac{\pi}{2}, \frac{\pi}{2}\right)$ (b) and $(0, 0)$ (c).

4.4 The planar bicircular problem

4.4.1 Introduction

In the previous sections we have first established how the Cucker-Smale dynamical model can be translated into a formation control, and then we have outlined its strengths and shortcomings by evaluating its performance for uncoupled pairs leader-follower orbiting around a central mass.

As we have seen, the efficacy of the method strongly depends on the magnitude of the leader-follower relative vector field, which in the previous context is expressed mainly through the leader's semi-major axis and the leader-follower relative distance.

Thus, in this section we want to evaluate the performance of the Cucker-Smale control when the magnitude of the relative vector field is low enough to not alter significantly the performance

of the control (particularly in terms of ΔV). To this end, we employ this control as part of a larger mission scenario, where, in light of the associated objectives and some methodology restrictions, "low magnitude" corresponds roughly to anything below $10^{-4}\ m/s^2$.

The scenario previously mentioned, along with the associated absolute equations of motion, is described in Section 4.4.2. This description is then expanded in Section 4.4.3, where the leader-follower relative motion for the scenario at hand is described through a generalization of the equations (4.13). Instead, in Section 4.4.4 we describe how the objectives of the scenario are reached, focusing mainly on an useful application of the Cucker-Smale control. The efficacy of the latter is subsequently evaluated in Section 4.4.5 through the use of metrics similar to those employed in the previous section. Finally, in Section 4.4.6 we present our conclusions and outline some future research directions associated with the scenario presented in this section.

4.4.2 Mission design and dynamical model

The scenario that we are considering in this section is that of periodical visits of the saddle point of the Earth-Moon-Sun system from a formation of spacecraft. Here the saddle point is defined as the zero of an appropriate inertial vector field describing the motion of a massless particle under the gravitational influences of Earth, Moon and Sun. The interest in this scenario builds upon some of the scientific objectives of the LISA Pathfinder extended mission, in particular the experimental test of Modified Newtonian Dynamics, which requires a gravitational acceleration below $10^{-10}\ m/s^2$ [152], thus making the SP an ideal location for this or a similar mission. In light of the results of the previous section, it is clear how the CS control can be employed in this to facilitate interferometric activities from the part of a formation.

To clarify the scenario above, let us first describe what is the model of reference and what is the dynamics of our target within this model. Since we are considering as primaries the Earth, Sun and Moon, we are actually working with a four body problem. The simplest model to describe this problem is given by the so called bicircular model, where the Earth and Moon are revolving in circular orbits around their center of mass, which in turn is moving along its own circular trajectory around the the Sun-Earth-Moon barycenter (as does the Sun itself). We remark that this model is not coherent, in the sense that the positions of Sun, Earth and Moon as computed below, do not satisfy Newton's equations [153]. Yet, due to its simplicity, it is functional for our goal, while still providing a good approximation of the dynamics. A further simplification comes from limiting ourselves to consider the planar case of this model (in the sense that the three main masses move on the same plane).

As we have said, the tree primaries move in circular orbits around specific points. In particular, under a standard normalization of the units of mass, let μ denote the mass of the Moon, $1-\mu$ the mass of the Earth and m_S the mass of the Sun. Furthermore, let us also normalize the unit of distance in such a way that the Earth-Moon distance is exactly 1. If we denote with (X, Y, Z) the coordinates of a point with respect to the Earth-Moon barycenter B, then the motions of the

primaries are described by the equations

$$\begin{aligned} X_E &= \mu\cos t, \quad X_M = (\mu-1)\cos t, \quad X_S = a_S\cos\left(n_S t\right), \\ Y_E &= \mu\sin t, \quad Y_M = (\mu-1)\sin t, \quad Y_S = a_S\sin\left(n_S t\right), \end{aligned} \tag{4.17}$$

where a_S and n_S denote respectively the distance between B and the Sun, and the mean motion of the latter around the system barycenter (with $a_S^3 n_S^2 = 1$). Of course, since we assumed the problem to be planar, it results $(Z_E, Z_M, Z_S) = (0,0,0)$. An extension taking into account aspects like the Moon's displacement with respect to the ecliptic is given in [154].

Due to the motion of the barycenter B, the coordinates (X, Y, Z) do not refer to an inertial frame. Yet, if we denote with (X_i, Y_i, Z_i) the coordinates referring to such a system (centered in the Sun-Earth-Moon barycenter), then the two sets are related by the equations

$$\begin{aligned} X_i &= X - \frac{m_S}{1+m_S} a_S\cos\left(n_S t\right) \\ Y_i &= Y - \frac{m_S}{1+m_S} a_S\sin\left(n_S t\right) \\ Z_i &= Z, \end{aligned} \tag{4.18}$$

which imply the dynamical relationship

$$\begin{aligned} \ddot{X}_i &= \ddot{X} - \frac{m_S}{a_S^2}\cos\left(n_S t\right) \\ \ddot{Y}_i &= \ddot{Y} - \frac{m_S}{a_S^2}\sin\left(n_S t\right) \\ \ddot{Z}_i &= \ddot{Z}. \end{aligned} \tag{4.19}$$

Note that in the previous equations we have implicitly used the equality

$$\frac{m_S a_S n_S^2}{1+m_S} = \frac{m_S}{a_S^2}. \tag{4.20}$$

To conclude the model's description, it remains only to state the standard equations of motion of a particle moving in the gravitational fields generated by multiple primaries. If we denote with $\left(\bar{X}_\star, \bar{Y}_\star, \bar{Z}_\star\right)$ the coordinates of the primaries in the inertial frame, the spacecraft's motion in the latter is governed by the equations

$$\begin{aligned} \ddot{X}_i &= -\frac{\left(X_i - \bar{X}_E\right)(1-\mu)}{r_{PE}^3} - \frac{\left(X_i - \bar{X}_M\right)\mu}{r_{PM}^3} - \frac{\left(X_i - \bar{X}_S\right)m_S}{r_{PS}^3} \\ \ddot{Y}_i &= -\frac{\left(Y_i - \bar{Y}_E\right)(1-\mu)}{r_{PE}^3} - \frac{\left(Y_i - \bar{Y}_M\right)\mu}{r_{PM}^3} - \frac{\left(Y_i - \bar{Y}_S\right)m_S}{r_{PS}^3} \\ \ddot{Z}_i &= -\frac{Z_i(1-\mu)}{r_{PE}^3} - \frac{Z_i\mu}{r_{PM}^3} - \frac{Z_i m_S}{r_{PS}^3}, \end{aligned} \tag{4.21}$$

where the denominators denote the distances of the particle from the the three primaries. In what follows we will limit ourselves to study the movement of a particle coplanar with the three main

masses (see Figure 4.11 for a visual representation of the problem's geometry). Thus, the last equation can be safely ignored. Finally, in the numerical implementation of the equations above, the following basic values have been used [155]

$$\mu = 0.012150298, \quad m_S = 328900.12, \quad n_S = 0.07480132816. \tag{4.22}$$

All the other values can be derived by exploiting the relations introduced before.

Besides the equations of motion presented above, in what follows we need also the first order variational equations associated to (4.21), since we make extensive use of shooting methods and root finding algorithms. These define the differential system

$$\dot{A} = DF \cdot A, \tag{4.23}$$

where

$$\begin{array}{c} A : \mathbb{R} \to \mathcal{L}\left(\mathbb{R}^4, \mathbb{R}^4\right) \\ t \to A\left(t\right) \end{array} \tag{4.24}$$

and $A\left(0\right) = I_4$. Do note that above we have implicitly exploited the fact that we are working with a planar problem, and thus we can uncouple the planar and vertical modes of the particle. As a consequence, the Jacobian matrix DF can be also reduced to

$$DF = \begin{pmatrix} 0 & 0 & 1 & 0 \\ 0 & 0 & 0 & 1 \\ g_{11} & g_{12} & 0 & 0 \\ g_{21} & g_{22} & 0 & 0 \end{pmatrix}, \tag{4.25}$$

where, noting that $g_{12} = g_{21}$, the components g_{ij} equal

$$\begin{aligned} g_{11} &= -\frac{(1-\mu)}{r_{PE}^3} - \frac{\mu}{r_{PM}^3} - \frac{m_S}{r_{PS}^3} + \frac{3\left(X_i - \bar{X}_E\right)^2(1-\mu)}{r_{PE}^5} + \frac{3\left(X_i - \bar{X}_M\right)^2\mu}{r_{PM}^5} + \frac{3\left(X_i - \bar{X}_S\right)^2 m_S}{r_{PS}^5}, \\ g_{12} &= \frac{3\left(X_i - \bar{X}_E\right)\left(Y_i - \bar{Y}_E\right)(1-\mu)}{r_{PE}^5} + \frac{3\left(X_i - \bar{X}_M\right)\left(Y_i - \bar{Y}_M\right)\mu}{r_{PM}^5} + \frac{3\left(X_i - \bar{X}_S\right)\left(Y_i - \bar{Y}_S\right)m_S}{r_{PS}^5}, \\ g_{22} &= -\frac{(1-\mu)}{r_{PE}^3} - \frac{\mu}{r_{PM}^3} - \frac{m_S}{r_{PS}^3} + \frac{3\left(Y_i - \bar{Y}_E\right)^2(1-\mu)}{r_{PE}^5} + \frac{3\left(Y_i - \bar{Y}_M\right)^2\mu}{r_{PM}^5} + \frac{3\left(Y_i - \bar{Y}_S\right)^2 m_S}{r_{PS}^5}. \end{aligned} \tag{4.26}$$

With the reference equations laid down, we can define our target within the model they describe. In particular the saddle point of the Earth-Moon-Sun system is defined as the point where the gravitational contributions of the primaries cancel each other. Thus, it can be easily located

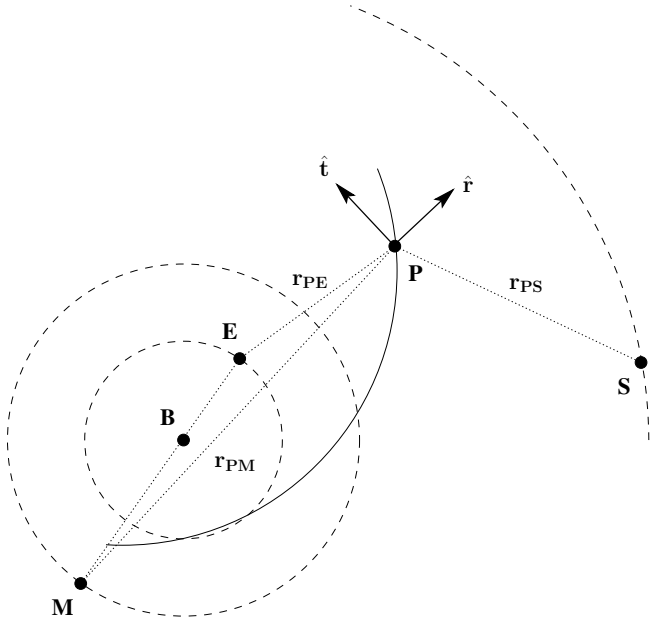

Figure 4.11: Geometry of the planar bicircular problem and leader's relative motion. The unitary vector $\hat{\boldsymbol{r}}$ points along the radial direction of particle P (with respect to the Earth-Moon barycenter), while $\hat{\boldsymbol{t}}$ remains perpendicular to $\hat{\boldsymbol{r}}$.

numerically (for example via a Newton method) as a zero of the equations (4.21), and its (partial) trajectory can be found in Figure 4.12, given in dark green in the plot on the left. One can notice that, albeit circular in shape, its trajectory is quite bumped. This is actually due to the sharp influence of the Moon, as it can be seen in the plot on the right where the saddle point distance from the Earth is plotted against time.

4.4.3 Equations of relative motion

Similarly to what done in the case of an Earth orbiting formation, it is convenient to introduce relative equations of motion to perform part of the necessary computations and, eventually, search for invariant structures useful to improve on the strategy adopted.

In light of the fact that we want both a precise estimate of the fuel consumed in our strategy and flexible equations that may be adapted in the future to different reference orbits, we consider the most general formulation for the relative equations of motion. It can be shown (see for example [156]) that they can be reduced to more recent approximate formulations, like the Hill-Clohessy-Wiltshire for circular reference orbits [157, 158], linearization of the equations used in the previous section, or the de Vries/Tschauner-Hempel for elliptical ones [159, 160].

In particular, if we consider the orbit drawn by the formation's leader in the non-inertial frame centered in the Earth-Moon barycenter, we can define a rotating reference frame with origin corresponding to the leader's position and instantaneously described by the unitary vectors

$$\hat{\mathbf{r}} = \frac{\mathbf{r}}{r}, \quad \hat{\mathbf{t}} = \hat{\mathbf{n}} \wedge \hat{\mathbf{r}}, \quad \hat{\mathbf{n}} = \frac{\mathbf{r} \wedge \dot{\mathbf{r}}}{\|\mathbf{r} \wedge \dot{\mathbf{r}}\|}, \tag{4.27}$$

where the versors $\left(\hat{\mathbf{r}}, \hat{\mathbf{t}}, \hat{\mathbf{n}}\right)$ indicate respectively the radial, transversal and normal direction, $\mathbf{r}$ and $\dot{\mathbf{r}}$ denote the leader's position and velocity in the Earth-Moon frame, and finally a variable is not bolded when its Euclidean norm is considered. Do note that, since the reference orbit is no longer necessarily circular, the transversal direction may not be the one indicated by $\dot{\mathbf{r}}$.

Since the frame defined before is rotating not necessarily in an uniform manner, we need expressions for both the angular velocity and acceleration, which, if $\mathbf{h}$ denotes the leader's angular momentum, read respectively as

$$\boldsymbol{\omega} = \frac{r}{h}\left(\ddot{\mathbf{r}} \cdot \hat{\mathbf{n}}\right)\hat{\mathbf{r}} + \frac{\dot{\mathbf{r}} \cdot \hat{\mathbf{t}}}{r}\hat{\mathbf{n}} \tag{4.28}$$

and

$$\dot{\boldsymbol{\omega}} = \frac{r}{h}\left[\frac{\dot{r}}{r}\left(\mathbf{r} \cdot \hat{\mathbf{n}}\right) - 2\frac{r}{h}\left(\ddot{\mathbf{r}} \cdot \hat{\mathbf{t}}\right)\left(\ddot{\mathbf{r}} \cdot \hat{\mathbf{n}}\right) + \left(\dddot{\mathbf{r}} \cdot \hat{\mathbf{n}}\right)\right]\hat{\mathbf{r}} + \frac{1}{r}\left[\left(\ddot{\mathbf{r}} \cdot \hat{\mathbf{t}}\right) - 2\frac{\|\dot{\mathbf{r}}\|}{r}\left(\dot{\mathbf{r}} \cdot \hat{\mathbf{t}}\right)\right]\hat{\mathbf{n}}. \tag{4.29}$$

With the previous expressions in tow, we can derive the last term relevant for a description of the dynamics in our non-inertial frame, that is the centripetal acceleration. If we denote with $\boldsymbol{\rho}$ the vector difference $\Delta\boldsymbol{r} = \boldsymbol{r}_1 - \boldsymbol{r}$ as seen in the rotating frame, where $\boldsymbol{r}_1$ indicates the follower's vector distance from the Earth-Moon barycenter, then we can write the previous acceleration as

$$\begin{aligned}\boldsymbol{\omega} \times \left(\boldsymbol{\omega} \times \boldsymbol{\rho}\right) = &\left[\frac{\left(\dot{\boldsymbol{r}} \cdot \hat{\boldsymbol{t}}\right)\left(\hat{\boldsymbol{n}} \cdot \boldsymbol{\rho}\right)}{h} + \left(\frac{r}{h}\right)^2\left(\ddot{\boldsymbol{r}} \cdot \hat{\boldsymbol{n}}\right)\left(\hat{\boldsymbol{r}} \cdot \boldsymbol{\rho}\right)\right]\left(\ddot{\boldsymbol{r}} \cdot \hat{\boldsymbol{n}}\right)\hat{\boldsymbol{r}} \\ + &\left[\frac{\left(\dot{\boldsymbol{r}} \cdot \hat{\boldsymbol{t}}\right)\left(\hat{\boldsymbol{n}} \cdot \boldsymbol{\rho}\right)}{r^2} + \frac{\left(\ddot{\boldsymbol{r}} \cdot \hat{\boldsymbol{n}}\right)\left(\hat{\boldsymbol{r}} \cdot \boldsymbol{\rho}\right)}{h}\right]\left(\dot{\boldsymbol{r}} \cdot \hat{\boldsymbol{t}}\right)\hat{\boldsymbol{n}} - \left[\left(\frac{\dot{\boldsymbol{r}} \cdot \hat{\boldsymbol{t}}}{r}\right)^2 + \left(\frac{r}{h}\right)^2\left(\ddot{\boldsymbol{r}} \cdot \hat{\boldsymbol{n}}\right)^2\right]\boldsymbol{\rho}.\end{aligned} \tag{4.30}$$

As well known, the follower's acceleration $\ddot{\boldsymbol{r}}_1$ can be expressed in a rotating frame as

$$\ddot{\boldsymbol{r}}_1 = \ddot{\boldsymbol{r}} + \ddot{\boldsymbol{\rho}} + 2\boldsymbol{\omega} \times \dot{\boldsymbol{\rho}} + \dot{\boldsymbol{\omega}} \times \boldsymbol{\rho} + \boldsymbol{\omega} \times \left(\boldsymbol{\omega} \times \boldsymbol{\rho}\right), \tag{4.31}$$

where, following the notation in [156], we use the expedient of denoting the derivatives of the relative position with two different symbols depending on the frame in which they are taken. Thus, since we have imposed $\Delta\boldsymbol{r}$ as $\boldsymbol{\rho}$ in the rotating frame, in the previous equation (and in the rest of the subsection) we have $\Delta\dot{\boldsymbol{r}} \neq \dot{\boldsymbol{\rho}}$ and $\Delta\ddot{\boldsymbol{r}} \neq \ddot{\boldsymbol{\rho}}$, since the derivatives on the left hand sides are taken in the frame of the Earth-Moon barycenter, while those on the right hand sides are taken in the leader-centered rotating frame.

If we now substitute equations (4.28), (4.29) and (4.30) in (4.31), we obtain the expression

$$\begin{aligned}\Delta\ddot{\boldsymbol{r}} = \ddot{\boldsymbol{\rho}} - \left(A + B\right)\boldsymbol{\rho} + D\left(\hat{\boldsymbol{r}} \times \boldsymbol{\rho}\right) + E\left(\hat{\boldsymbol{n}} \times \boldsymbol{\rho}\right) + L\left(\hat{\boldsymbol{n}} \times \dot{\boldsymbol{\rho}}\right) + M\left(\hat{\boldsymbol{r}} \times \dot{\boldsymbol{\rho}}\right) \\ + \left[C\left(\hat{\boldsymbol{n}} \cdot \boldsymbol{\rho}\right) + B\left(\hat{\boldsymbol{r}} \cdot \boldsymbol{\rho}\right)\right]\hat{\boldsymbol{r}} + \left[A\left(\hat{\boldsymbol{n}} \cdot \boldsymbol{\rho}\right) + C\left(\hat{\boldsymbol{r}} \cdot \boldsymbol{\rho}\right)\right],\end{aligned} \tag{4.32}$$

where the capital letters stand for the scalar coefficients

$$
\begin{aligned}
&A = \frac{\left(\dot{\mathbf{r}} \cdot \hat{\mathbf{t}}\right)^2}{r^2}, \quad B = \left(\frac{r}{h}\right)^2 \left(\ddot{\mathbf{r}} \cdot \hat{\mathbf{n}}\right)^2, \quad C = \frac{\left(\dot{\mathbf{r}} \cdot \hat{\mathbf{t}}\right)\left(\ddot{\mathbf{r}} \cdot \hat{\mathbf{n}}\right)}{h}, \\
&D = \left[\frac{\dot{\mathbf{r}} \cdot \hat{\mathbf{r}}}{h} - 2\left(\frac{r}{h}\right)^2 \left(\dot{\mathbf{r}} \cdot \hat{\mathbf{t}}\right)\right]\left(\ddot{\mathbf{r}} \cdot \hat{\mathbf{n}}\right) + \frac{r}{h}\left[\hat{\mathbf{n}}^T \left(\nabla \ddot{\mathbf{r}}\right) \dot{\mathbf{r}}\right], \\
&E = -\frac{2}{r^2}\left(\dot{\mathbf{r}} \cdot \hat{\mathbf{r}}\right)\left(\dot{\mathbf{r}} \cdot \hat{\mathbf{t}}\right) + \frac{\ddot{\mathbf{r}} \cdot \hat{\mathbf{t}}}{r}, \quad L = \frac{2}{r}\left(\dot{\mathbf{r}} \cdot \hat{\mathbf{t}}\right), \quad M = 2\frac{r}{h}\left(\ddot{\mathbf{r}} \cdot \hat{\mathbf{n}}\right).
\end{aligned}
\tag{4.33}
$$

If we indicate with $\Delta\mathbf{N}$ and $\Delta\mathbf{P}$ the differential gravitational acceleration and perturbation experienced by the follower with respect to the leader, then we can write the relative equations of motion as

$$
\Delta\ddot{\boldsymbol{r}} = \ddot{\boldsymbol{r}}_1 - \ddot{\boldsymbol{r}} = \Delta\mathbf{N} + \Delta\mathbf{P}. \tag{4.34}
$$

Of course, in our case one can derive the difference $\Delta\mathbf{N}$ ($\Delta\mathbf{P}$ is not present) from equation (4.21) by evaluating it for the leader and the follower, and then taking the difference.

If we now denote with (x, y, z) the coordinates of the follower in the rotating frame, we obtain

$$
\begin{aligned}
\boldsymbol{\rho} &= x\hat{\boldsymbol{r}} + y\hat{\boldsymbol{t}} + z\hat{\boldsymbol{n}} \\
\dot{\boldsymbol{\rho}} &= \dot{x}\hat{\boldsymbol{r}} + \dot{y}\hat{\boldsymbol{t}} + \dot{z}\hat{\boldsymbol{n}} \\
\ddot{\boldsymbol{\rho}} &= \ddot{x}\hat{\boldsymbol{r}} + \ddot{y}\hat{\boldsymbol{t}} + \ddot{z}\hat{\boldsymbol{n}},
\end{aligned}
\tag{4.35}
$$

and therefore the expressions

$$
\begin{aligned}
\hat{\boldsymbol{r}} \times \boldsymbol{\rho} &= y\hat{\boldsymbol{n}} - z\hat{\boldsymbol{t}} \\
\hat{\boldsymbol{r}} \times \dot{\boldsymbol{\rho}} &= \dot{y}\hat{\boldsymbol{n}} - \dot{z}\hat{\boldsymbol{t}} \\
\hat{\boldsymbol{n}} \times \boldsymbol{\rho} &= x\hat{\boldsymbol{t}} - y\hat{\boldsymbol{r}} \\
\hat{\boldsymbol{n}} \times \dot{\boldsymbol{\rho}} &= \dot{x}\hat{\boldsymbol{t}} - \dot{y}\hat{\boldsymbol{r}}.
\end{aligned}
\tag{4.36}
$$

Finally, by first substituting the previous terms in (4.32) and then the latter in (4.34), we obtain the relative equations of motion in the rotating frame, which read componentwise as

$$
\begin{aligned}
\ddot{x} &= Ax + Ey - Cz + L\dot{y} + \left(\Delta\mathbf{N}\right)_x + \left(\Delta\mathbf{P}\right)_x + \mathbf{T}_x \\
\ddot{y} &= -Ex + (A + B)y + Dz - L\dot{x} + M\dot{z} + \left(\Delta\mathbf{N}\right)_y + \left(\Delta\mathbf{P}\right)_y + \mathbf{T}_y \\
\ddot{z} &= -Cx - Dy + Bz - M\dot{y} + \left(\Delta\mathbf{N}\right)_z + \left(\Delta\mathbf{P}\right)_z + \mathbf{T}_z.
\end{aligned}
\tag{4.37}
$$

Do note that in the equations above the additional term $\mathbf{T}$ accounts for any control thrust that one may want to apply to the follower.

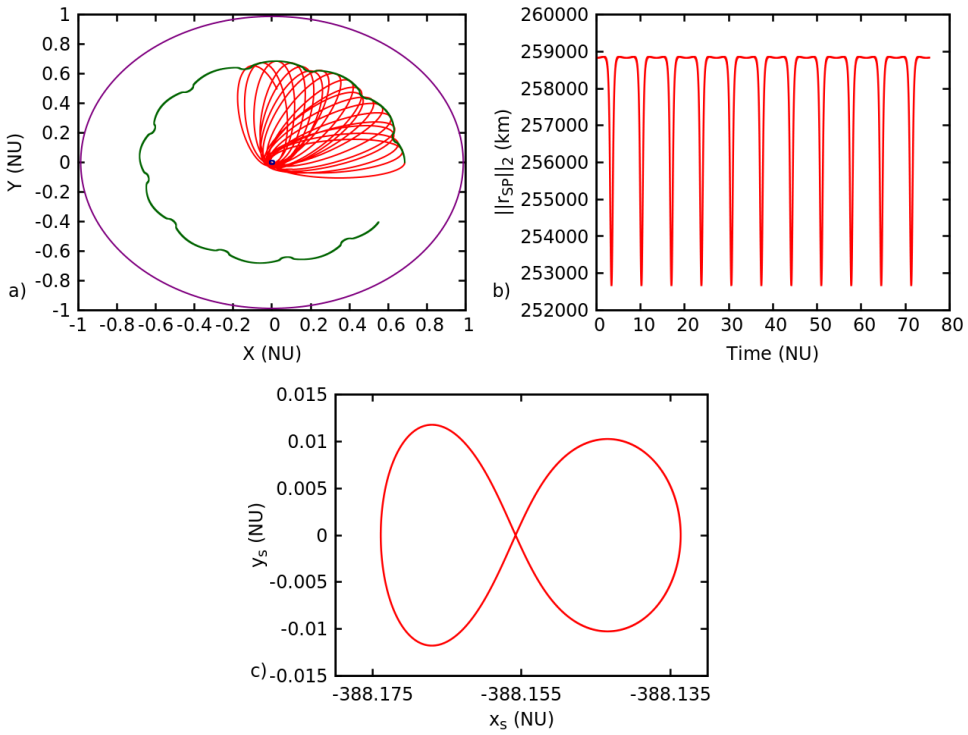

Figure 4.12: Mission scenario considered within the bicircular model (a). The orbits are drawn in the Earth-Moon barycenter frame and they are: the leader's one (red), the saddle point's one (green), Earth (blue) and the Moon (purple). The latter's sharp effect on the SP trajectory is visible in the time evolution of its distance from the Earth (b). Finally, the SP trajectory is drawn in a Sun-synchronous rotating frame centered in the Sun-Earth-Moon barycenter (c).

4.4.4 Spacecraft orbits and control application

As we have said before, our objective is to periodically visit the Earth-Moon-Sun saddle point and, in a neighborhood of this point, apply the Cucker-Smale control in order to keep a rigid formation. This is achieved by exploiting eccentric elliptic orbits having Earth as one of the foci and with apogee located exactly at the saddle point. Suitable maneuvers are performed at the corresponding perigees in order to meet again the saddle point at a subsequent time. It is important to note that the one employed is only a baseline strategy aimed to show the potential and low cost of the Cucker-Smale control (thus, the encounter with the saddle point after every revolution). Later on we will discuss future research directions aimed to better flesh out the overall approach.

For what concerns exclusively the design of the spacecraft orbits in the Earth-Moon barycenter frame, the overall strategy can be summarized as follows

- We consider as initial position for the leader the Sun-Earth-Moon saddle point location at a certain epoch ($t = 0$ in the plots), and we take its velocity in order to achieve an elliptical, bounded orbit. For the plots at hand, we have derived this velocity from the vis-viva equation, starting with osculating semi-major axis $a \approx 0.685$ (in normalized units).

- We determine the perigee corresponding to the previous orbit as the intersection between the latter and the line joining the leader's initial position and the origin of the non-rotating, non-inertial frame, subsequently propagating the spacecraft's orbits until the leader reaches this point.

- If we denote with T the period of the leader's osculating orbit and t_p its arrival at perigee, then we compute via a shooting method the maneuver bringing the leader to encounter the saddle point at time $t_p + \frac{T}{2}$ (of course, starting from its conditions at t_p).

- In parallel, at time t_p we compute the maneuvers bringing each follower into achieving a specified relative position at a given time t_1. The latter corresponds to the instant in which the magnitude of the inertial vector field associated with the leader goes below a threshold selected a priori. Let t_2 denote the instant where this threshold is passed again.

- Finally, the spacecraft's orbits are propagated from t_p after the previous maneuvers are performed. At t_1 the followers start applying the Cucker-Smale strategy, and they interrupt it at t_2. Furthermore, at $t_p + \frac{T}{2}$ the new perigee is computed and the procedure is repeated starting from the second step.

As for the aspects pertaining to the Cucker-Smale control, we have already determined, for every encounter with the SP, the initial and final time of application. In light of the results obtained in the previous section, we can safely apply it in its discrete form, since the relative vector field remains weak thanks to the choices that we made when designing the leader's orbit.

Similarly to the analysis already performed, we consider only a single couple leader-follower for the simulations of this section, since this allows us to extrapolate a basic level of efficiency for the control when applied in a favourable situation. Of course, given how we have designed our orbits, small variations in the performance of the control follow from considering different relative positions at the times t_1 (here we consider only the transversal direction, with a baseline distance of 100 meters).

For the same reason, instead of using the Cucker-Smale design for the control gains, we limit ourselves to consider constant ones. This choice is motivated by the fact that the variations in the relative distance born while the algorithm converges are minimal and that determining the optimal regime for the control becomes much easier with only one parameter to define. However, with a slight abuse of nomenclature, we refer to this new control again as Cucker-Smale control.

In conclusion, we want to remark that the previous observations imply the possibility of employing formations like the one used in Figure 4.4, that is formations where every follower communicates directly with the leader. As we are going to point out in the conclusions, in the future we will consider more layered formations.

4.4.5 Numerical results

In the context of an Earth-bound circular reference orbit we have seen that the major factor that affect the cost of the (hierarchical) Cucker-Smale method is given by the magnitude of the leader-follower relative vector field. In turn this express itself in the dependencies of the total cost from the leader-follower relative distance and the leader's orbit semi major axis (see Figure 4.8 and 4.9 respectively).

In the case of the bicircular problem instead, the magnitude above is set a priori, in the sense that, as already said before, we enter in a Cucker-Smale application regime when the inertial vector field experienced by the leader of the formation is below a certain threshold. Analogously, we exit from this regime when the same threshold is surpassed again. Of course, this is possible because our orbits have as apogee the saddle point, that is a point where the inertial vector field vanishes.

Together with the relative distance that we impose the follower to recover, this allows us to determine almost completely the cost of the Cucker-Smale application. We will see later that the latter is also a matter of the number of maneuvers and gains that we use during the Cucker-Smale phase. Yet, if we fix the number of maneuvers and scale the gains accordingly, it is possible to describe the cost of the Cucker-Smale method when in an optimal regime.

In Figure 4.13, we plot on the left the total Δv expended to apply the CS method over 18 encounters with the SP with respect to the magnitude of the leader's vector field and the relative distance leader-follower, with the former ranging from 10^{-9} to $10^{-7}\ m/s^2$ and the latter going from 10 meters to 1 kilometer. As it can be seen, the plot is quite uniform in the threshold direction, with only the relative distance causing a linear increase in the expenditure (see relative equations). Of course, this depends on the fact that we are very close to the SP and the application interval is very small (see plot in the middle), thus the cubic terms at the denominators impose very small acceleration coefficients.

Do note that, for what concerns the evolution of the application interval amplitude with respect to the entrance threshold, the value of this interval is not constant in a single threshold, and this seems to be due to the dynamics of the problem (with minimum and maximum appearing always at the same encounter). However, it is not completely clear what is the source of this behaviour.

Finally, on the right of Figure 4.13 we plot the time evolution, in the CS application intervals, of relative velocity and position for an entrance threshold of $10^{-7}\ m/s^2$ and a relative distance of $1\ km$, that is the worst possible situation within the ranges considered. On one side, we can see the quick recovery of a null relative velocity, which in turn leads to a variation in the relative distance (with respect to the one imposed at entrance) which is well below the meter.

Similar plots have been done for the interval $[10^{-6}, 10^{-4}]\ m/s^2$ in order to evaluate a scenario with a more useful time span for exploiting the benefits of a rigid formation. Of course, in this case also the magnitude of the threshold selected for the vector field plays a role, and this can be

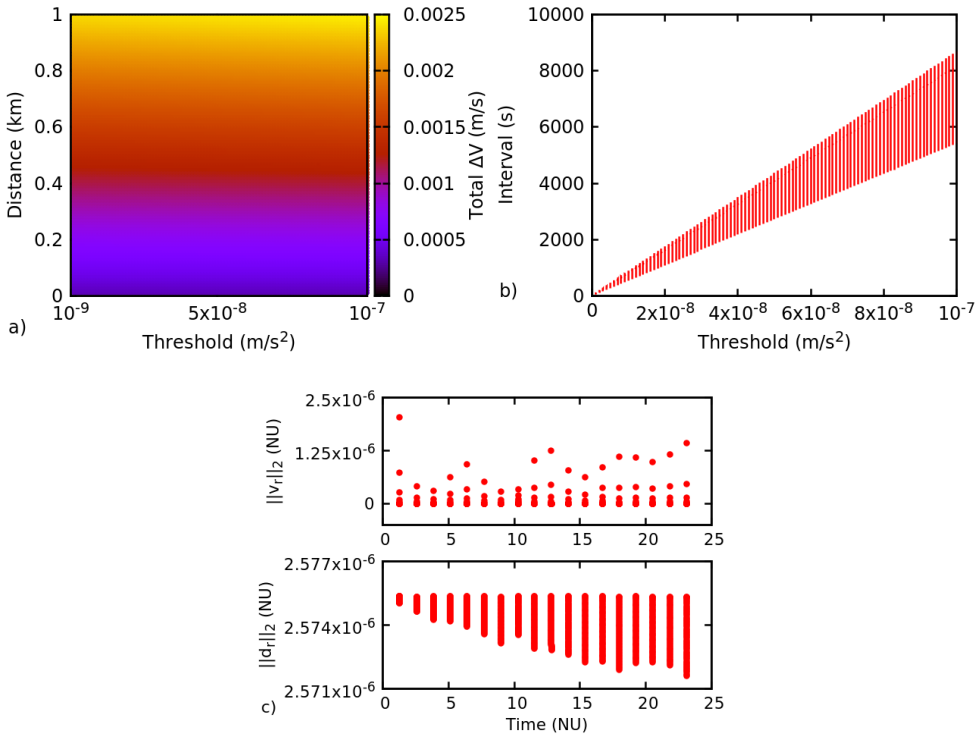

Figure 4.13: Metrics values for the CS starting threshold interval $[10^{-9}, 10^{-7}]\ m/s^2$: total Δv expended for the CS method as a function of the leader's vector field magnitude and the follower relative distance (expressed over a 100×100 uniformly spaced grid) (a), corresponding evolution of the CS application interval amplitude with respect to the threshold value (b) and example of time evolution of the relative velocity and distance norms in the CS application areas (threshold $10^{-7}\ m/s^2$, relative distance $1\ km$) (c).

observed in the heat map at the right side of Figure 4.14.

In fact, the main difference with the the interval $[10^{-9}, 10^{-7}]\ m/s^2$ lies in the fact that, for high relative distances, we can observe that on the rightmost part of the heat map the cost of application of the CS control starts to become significant (albeit still viable). This is related to the fact that, with the values of the gain and number of maneuvers selected, the control manages to adjust the relative velocity of the follower only up to a certain degree. In turn, this causes the spacecraft to arrive to the new starting point for the CS application with a velocity greater in magnitude, and this process is exacerbated further the more encounters one does with the SP. Consequently, the expended Δv gets higher due to the higher entry velocity, and furthermore it becomes increasingly more difficult to asymptotically recover a zero relative velocity and thus fix a relative distance (rightmost plot in Figure 4.14).

We remark that, in the plots above the value of the gain employed for the follower varies according to a law of the form $10^6/x$ or $10^3/x$, where x varies from 1 to 100, with 1 corresponding to the minimum threshold (respectively 10^{-9} and 10^{-6}) and 100 to the maximum (10^{-7} and 10^{-4}). This scaling is actually necessary, since for every value of the threshold magnitude (and thus every value of the Δt determined by the discretization process (4.11)) there is only a

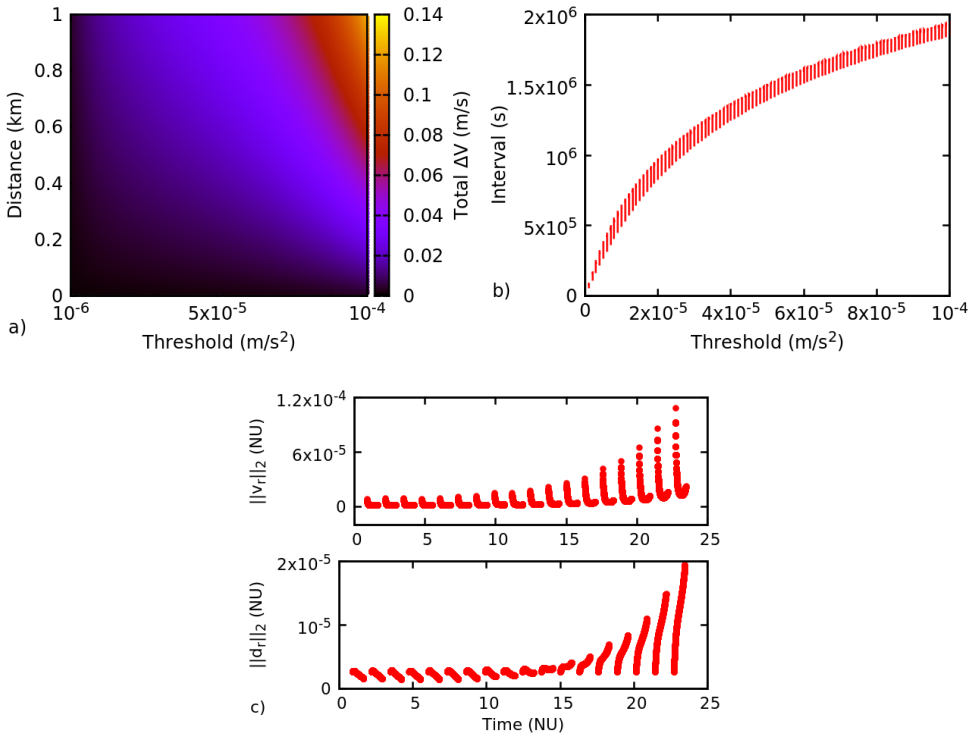

Figure 4.14: Metrics values for the CS starting threshold interval $[10^{-6}, 10^{-4}]\ m/s^2$: total Δv expended for the CS method as a function of the leader's vector field magnitude and the follower relative distance (expressed over a 100×100 uniformly spaced grid) (a), corresponding evolution of the CS application interval amplitude with respect to the threshold value (b) and example of time evolution of the relative velocity and distance norms in the CS application areas (threshold $10^{-4}\ m/s^2$, relative distance $1\ km$) (c).

bounded set of gains that will actually bring the two spacecraft to consensus.

As an example, in Figure 4.15 (a), we consider an entrance threshold of $10^{-4}\ m/s^2$ and an entrance relative distance of 100 meters, and we plot the value of the total Δv expended as a function of the number of maneuvers and the gain employed for the follower. The actual range for the latter goes up to 10^3, but only a small amount of gains actually bring leader and follower to consensus. In fact, the points not plotted cause problems to the procedure that can be classified in one of two ways. Either the value of the gain is too high, thus leading to a cumulative increase of the norm of the relative velocity and therefore a similar variation for the relative distance (see plot (b) where these two values are plotted in the areas of application of the CS method), or it is too low, thus causing the same phenomena but in a manner similar to Figure 4.14 (c).

4.4.6 Expansion of the overall strategy

The previous results show that the performance of the Cucker-Smale control (with constant gains) employed in this Section is quite remarkable, although one has to be smart in the ways he applies it. Of course, in light of what discussed in Section 4.4.4, the same conclusion can be drawn for the more general Cucker-Smale control that we have employed in the rest of the chapter (albeit

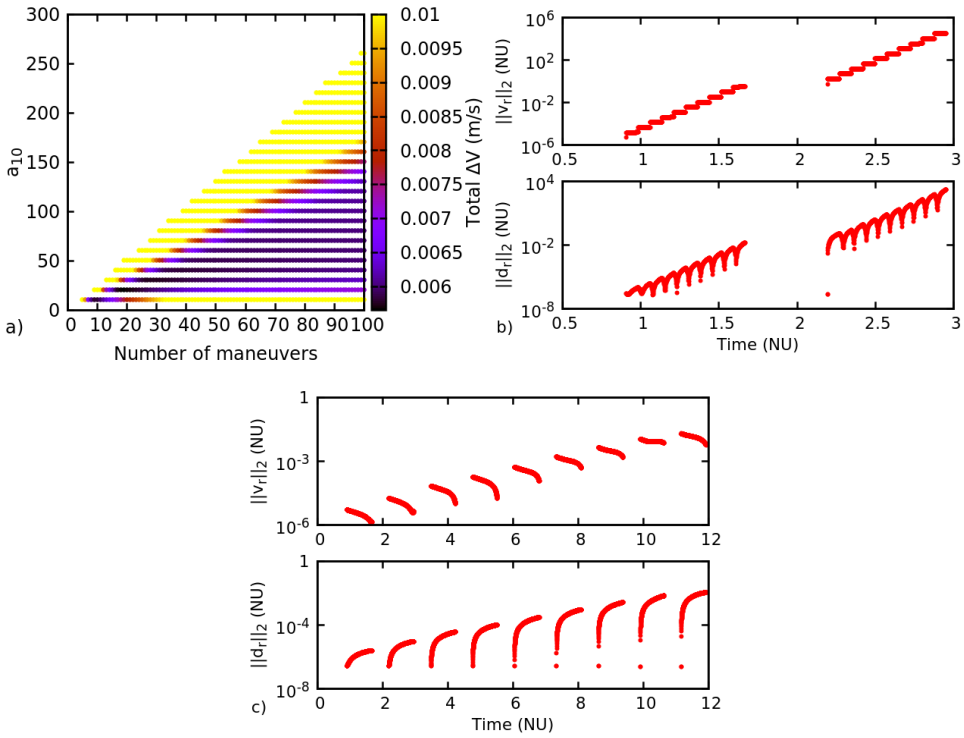

Figure 4.15: Value of the total Δv expended for the CS application with a threshold of 10^{-4} m/s^2 and a relative distance of 100 m, taken as a function of the number of maneuvers and the value of the gain (a). Time evolution of the follower's relative velocity and position for $K = 51$ (b) and $K = 1$ (c).

the specific numbers may vary slightly). Furthermore, among the places of application one can naturally find equilibrium points of different systems, which are natural locations for employing formations to achieve different scientific objectives.

As for the strategy that we have used in the bicircular problem, it has been designed to show the potential of the CS control, but in its current state needs some improvement. In order to better understand where we can make it better, the computations and observations provided in this subsection have been done by approximating the bicircular model with a Kepler problem (Earth as focus). In this way all the calculations under scrutiny can be done analytically, and some preliminary estimates and observations can be provided.

The main aspect in need of improvement is the total cost of the maneuvers done around the perigees by the leader and follower both, which is greater than 10^3 m/s. This is mainly a consequence of keeping a relatively low perigee for the orbits considered. In fact, let us suppose of having fixed the distances of both apogee and perigee for our leader's orbits (we'll see in a moment about the validity of this choice, particularly for the apogee). If we evaluate the total cost of the maneuvers done around the perigee for this reference orbit, we can see (left of Figure 4.16) that this cost decreases dramatically with the increase of the perigee altitude.

In the previous plot the apogee distance is fixed at 258850 km, while the apses lines of the various orbits are rotated with respect to one another by an angle $\eta = \frac{2\pi}{365}T$, where T denotes the

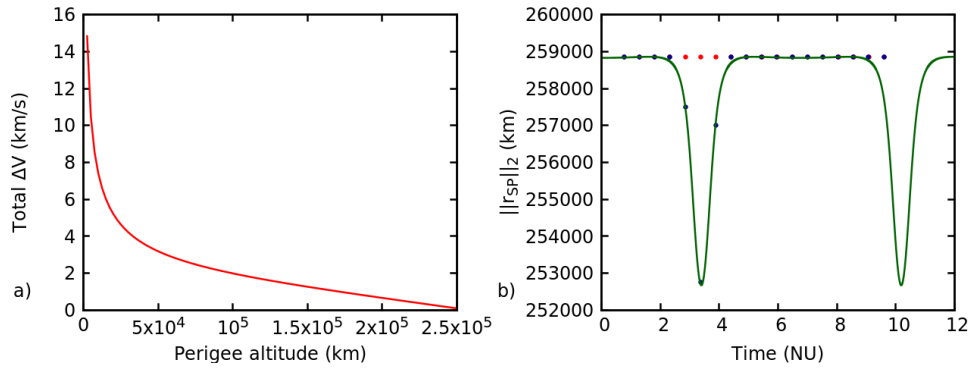

Figure 4.16: Total ΔV expended by a spacecraft to sequentially switch among 18 mutually inclined orbits within a Kepler problem as a function of the orbits perigee. The orbits apogees are all located at a $258850\ km$ altitude and their apses lines are inclined with an angle $\eta = \frac{2\pi}{365}T$, where T denotes the period of the orbits (a). Said apogees (for a $250000\ km$ perigee altitude) time evolution superimposed on the Earth-saddle point distance within the bicircular model (red dots). Dots in blue represent a similar sequence of apogees, but with three of them having a different altitude (by the definition of η, the subsequent are slightly shifted in time) (b).

period of the orbits. The latter is of course always the same, since apogee and perigee distances are kept fixed. Furthermore, for this same reason, our procedure (and therefore the associated results) remains independent of the phase of the initial orbit.

As shown on the right of Figure 4.16, where, on top of the time evolution of the Earth-saddle point distance, we plot in red the apogees corresponding to a $250000\ km$ perigee altitude, the previous observation allows us to shift the initial phase in order to maximize the number of encounters with the saddle point (as long as the apogee distance is correctly chosen). Of course, regardless of the shift applied, some of the apogees will end up in the "valleys" caused by the Moon's passage. This appears not to be a problem, since in these instances one can simply vary the apogee distance, as done for example with the blue dots of Figure 4.16 (which represent a corrected version of the red ones). As long as the perigee distance remains high enough the variation in the ΔV remains minimal (although this observation requires further analysis in order to be properly quantified).

We also observe that the previous strategy covers the needed cost reduction only for the leader's orbit (although is has to be integrated within the complete bicircular model). However, for a single follower at close distance and with similar apogee and perigee altitudes, we have seen in the previous section that the relative dynamics becomes quite mild. Thus, while this has not yet been verified, we expect that it is possible to continue employing the shooting strategy associated to the Cucker-Smale control and achieve a ΔV similar to the one in Figure 4.16.

Do note however that it is by applying this control at every encounter with the saddle point that we are able to achieve "small" relative distances for the shooting phase. Thus, depending on mission requirements, it may be worth to better explore the dynamics of the relative motion in such a way to cover for the eventual lack of the CS control and/or to facilitate the insertion of additional spacecraft within the formation (while the orbits are elliptical, and thus the relative

motion is naturally bounded, the amplitudes of the relative orbits are of the order of tens or hundreds of kilometers).

4.5 Conclusion

In the present chapter we have expanded on the study of a novel translational control built to allow a formation of autonomous agents to achieve and maintain a structure characterized by zero relative velocities, and therefore asymptotically fixed relative distances.

In order to evaluate the efficacy of the control and the dynamical aspects affecting it, we have first employed the algorithm in the presence of a central force field determined by the gravitational pull of a primary (Earth for the simulations considered here). Putting aside the effect of the control parameters, which follows the behaviour outlined by the theorems of Chapter 2, by studying the relative motion of different couples leader-follower, we have shown that the applicability and the cost of the proposed control depend strongly on the magnitude of the spacecraft differential field. In our case, this is determined mainly by the semi-major axis of the leader's orbit and the distance leader-follower, which in turn affect the relative acceleration between the spacecraft that the control is designed to cancel and replace with appropriate terms.

In light of these conclusions, we have designed a more favourable instance for the application of our control. In particular, starting from the scientific objectives of the LISA Pathfinder mission, we have considered the scenario of a spacecraft formation visiting periodically the saddle point of the Earth-Moon-Sun system, with the spacecraft travelling along Earth-bound elliptical orbits. The control defined has been then employed to maintain a rigid configuration for the formation in a neighborhood of the saddle point, where the differential field is naturally low in magnitude thanks to the gravitational contributions balancing out. Thus, we have managed to evaluate the dependence on the inherent parameters of the control, that is number of maneuvers done in the application interval and gains employed, showing how the control designed offers a reliable a cheap strategy to maintain a spacecraft formation in a rigid configuration.

Chapter 5

On attitude synchronization for formation flying

5.1 Introduction

In the present chapter we consider the problem of attitude synchronization for a group of autonomous or semi-autonomous agents. This means that we want them to asymptotically achieve the same attitude and the same spin rate, and eventually maintain this synchronized state indefinitely. While the underlying theory is valid for every kind of synchronizing formation, the assumptions made in this chapter strictly refer to the limitations encountered when performing these operations with spacecraft.

That said, two are the main goals of this chapter. On one side, we aim to complete the analysis of the factors that affect the performance of the consensus strategies considered in this thesis. In Chapter 4 we have seen how, in a translational, orbital context, the geometry and magnitude of the vector field under which a formation is operating characterize a consensus control up to the point of practical inapplicability. As we are going to see, for several reasons these factors are not a problem in a rotational context. Therefore, we can focus on understanding the dependence of the controlled dynamics from the parameters inherent in a formation: dimension, initial relative conditions and communication graph structure.

On the other side, since we are no longer burdened by a heavily characterizing vector field, we consider again the adaptive design of Cucker and Smale introduced in Chapter 3 and we transpose it to the attitude synchronization context in order to evaluate its effectiveness over existing control laws, and thus its suitability as an adaptive synchronization control. Of course, this approach is motivated by the will of investigating if elements of the consensus dynamics can be exploited in the control design to improve on the consensus process.

After laying down some necessary theoretical notions at the beginning of Section 5.2, in the same section we present a baseline control law, flexible enough to accommodate for all the features that we want, and we modify it in an adaptive sense following the same idea of Cucker

and Smale. Furthermore, we derive analytical sufficient conditions over the graph structure and the control gains in order for the spacecraft to achieve attitude synchronization under the effect of these control laws.

In Section 5.3 we first extend numerically the previous discussion in order to outline aspects that are not treated in depth in this thesis or that lack a complete analytical support. Then, in order to compare the controls previously introduced, we present a numerical and statistical approach aimed to quantify the dependencies outlined in the second paragraph. Furthermore, we show how the numerical complexity of this approach can be cut down significantly by exploiting a hierarchical communication graph, and how the latter provides at the same time analytical informations on the convergence speed of consensus algorithms. Finally, we employ the previous tools to study the dynamics of a formation synchronizing in free space under the direction of a three-axis stabilized leader.

The previous analysis is extended in Section 5.4, where the leader's attitude is now changing with time. First we consider the case of a spin stabilized leader, which is therefore rotating with a constant angular velocity, where we obtain results similar to those presented in the previous Section. Secondly, we consider formations trying to synchronize with a leader subject to a non-vanishing acceleration. In particular, the latter is considered travelling along an elliptical keplerian orbit and rotating with the corresponding angular rate, so that we are effectively simulating the synchronization of an interferometric array orbiting around a primary.

Finally, in Section 5.5 we summarize the results shown in this Chapter and present our conclusions.

5.2 Attitude dynamics and control

5.2.1 Formalism and dynamics

In this subsection we introduce some minimal concepts and notations regarding attitude dynamics to be used in the rest of the chapter. In order to present this concepts in an geometrically understandable way, we omit the algebraic considerations needed to wrap up everything in a formal fashion. For the interested reader, a classical review of the formalism can be found in any book of spacecraft control theory (like [161]) and it can be extended with some of its applications in the context of orbital dynamics [162].

According to Euler's rotation theorem, any rotation or sequence of rotations of a rigid body (equivalently, a reference frame) about a fixed point is equivalent to a single rotation by a given angle θ about a fixed axis running through this point (commonly known as *Euler axis*), which we suppose individuated by a certain versor $\hat{u}$. A simple way to work with this axis-angle representation is to encode it within an unitary *quaternion*, that is a versor of four components that we can use to apply the corresponding rotation to any vector in $\mathbb{R}^3$ and thus to the point of the rigid body that this vector individuates.

If we denote with $(\mathbf{i}, \mathbf{j}, \mathbf{k})$ the basis for our fixed frame, then we can write our versor $\hat{u}$ in components as

$$\hat{u} = (u_x, u_y, u_z) = u_x\mathbf{i} + u_y\mathbf{j} + \mathbf{k}u_k. \tag{5.1}$$

This allows us, through an extension of the Euler's formula, to define the quaternion associated to the $(\theta, \hat{u})$ rotation as

$$q = e^{\frac{\theta}{2}(u_x\mathbf{i}+u_y\mathbf{j}+\mathbf{k}u_k)} = \cos\frac{\theta}{2} + (u_x\mathbf{i} + u_y\mathbf{j} + \mathbf{k}u_k)\sin\frac{\theta}{2}, \tag{5.2}$$

or equivalently by denoting it as $q = (\bar{q}, \hat{q})$, where $\bar{q} = \cos\left(\frac{\theta}{2}\right)$ denotes its scalar part and $\hat{q} = \hat{u}\sin\left(\frac{\theta}{2}\right)$ the vectorial part.

If we indicate with $r = (r_x, r_y, r_z)$ the vector that we want to rotate, then it can be proved that this rotation can be obtained by evaluating the *conjugation* of r by q

$$r' = qrq^{-1}, \tag{5.3}$$

where r' denotes the rotated vector. In the previous expression, after extending r to a quaternion with a null scalar part, we have implicitly employed the *Hamilton product* among quaternions, which, if p and q denote two unitary quaternions, reads as

$$\overline{qp} = \bar{q}\bar{p} - \hat{q}\cdot\hat{p}, \quad \widehat{qp} = \bar{q}\hat{p} + \bar{p}\hat{q} + \hat{q}\times\hat{p}, \tag{5.4}$$

and it describes the composition of two rotations (abiding to standard rules of associativity, but not commutativity).

It is important to note that the same rotation can be obtained in two different ways. Intuitively, let's say that if our line of sight points along the direction individuated by $\hat{u}$, then we have to rotate by an angle θ. This is the same of looking in the same direction of $-\hat{u}$ and rotating with angle $2\pi - \theta$. In terms of quaternions, this means that the rotation described by the quaternion q is individuated also by its opposite $\tilde{q}$, defined as

$$\tilde{q} = (-\bar{q}, -\hat{q}) = \left(\cos\left(\pi - \frac{\theta}{2}\right), (-\hat{u})\sin\left(\pi - \frac{\theta}{2}\right)\right). \tag{5.5}$$

This duality gives birth to unwanted phenomena like unwinding [163]. Still, to establish uniqueness, one can simply restrict θ to the interval $0 \leq \theta \leq \pi$ so that $\bar{q} \geq 0$ [164].

Finally, to describe the inverse rotation of the one individuated by the quaternion q, it is enough to consider the *conjugate* of q, that is the quaternion $q^\star = (\bar{q}, -\hat{q})$. It is easy to convince oneself that the previous statement is true by looking at the product of q and $q^\star$, which actually gives $q^\star q = qq^\star = \mathbf{q}_I$, where $\mathbf{q}_I = (1, 0, 0, 0)$ identifies the identity rotation. Furthermore, given two quaternions q and p, one can consider the conjugate of their Hamilton product, thus ending up with $(qp)^\star = p^\star q^\star$.

As a concluding remark for quaternions kinematics (and more in general for attitude), it should be noted that there exists another duality that one should be aware of, although it does not really enter in what we are going to discuss in the chapter. This duality sprouts from considering either a vector *rotation*, that is an operation that changes the orientation of the vector within the same reference frame, or a vector *transformation*, that is an operation which represents the vector in a different reference frame without actually changing its orientation. These two operations can be seen as inverse operations, in the sense that, given a vector in a certain frame, if we rotate it by a given angle and then transform it with the same angle, the new vector will have, within the rotated frame, the same coordinates than the original one has within the starting frame. While this is something that one should be aware of when actually reading the values of a quaternion, in abstract terms it is of no concern since the associated kinematics remains the same.

The latter, when the dynamics of the body is also included, can be described by the equations [164]

$$\begin{gathered}\dot{\bar{q}} = -\frac{1}{2}\omega \cdot \hat{q}, \quad \dot{\hat{q}} = -\frac{1}{2}\omega \times \hat{q} + \frac{1}{2}\bar{q}\omega, \\ I\dot{\omega} + \omega \times I\omega = \tau,\end{gathered} \tag{5.6}$$

where I denotes the tensor of inertia of the spacecraft, ω its angular velocity and τ the torque due to external and control forces. The dynamical equations are the so called Euler's equations, which describe the dynamics of the spacecraft in its own principal frame, a rotating frame centered on the center of mass of the spacecraft and with axes parallel to its principal axes of inertia. In what follows, we assume that, where appropriate, all the vectors have been transformed and represented in the same coordinate frame.

5.2.2 Controls and synchronization under an undirected connected graph

We present here the distributed attitude control laws adopted and the conditions required for a group of spacecraft to asymptotically achieve attitude synchronization under these laws.

Our starting point is given by the PD-like control law [165] defined via the i-th control torque

$$\tau_i = \omega_i \times I_i\omega_i - I_i \sum_{j=0}^{N} g_{ij}\left[a_{ij}\widehat{q_j^\star q_i} + b_{ij}\left(\omega_i - \omega_j\right)\right], \tag{5.7}$$

where the weights a_{ij} and b_{ij} are real positive constants, while $g_{ij} = 1$ if agents i and j are connected by an edge and $g_{ij} = 0$ otherwise. The control above is model dependent (i.e., depends from the I_j's) and, given different control objectives and circumstances, can be easily replaced with other laws (see [165] for an example list). However, it is also the "minimal" control achieving attitude synchronization which is flexible enough to accommodate for all the features that we need (in particular, numerical evidence shows that it is still viable for a spin-stabilized or

mildly accelerating leader). Therefore, it allows us to develop our analysis framework without having to change the baseline control law. Furthermore, the induced closed-loop dynamics is as structurally close as possible to the Cucker-Smale model, so to make easier to bridge the gap between the two.

Now, following the idea of Cucker and Smale of adjusting the gains by scaling them with respect to some metric, we can define our adaptive design by imposing

$$b_{ij} = b_{ij}(t) = K_\omega \left(\sigma^2 + \phi^2(q_i, q_j)\right)^\beta \tag{5.8}$$

where $K_\omega > 0$, $\sigma^2 > 0$ and $\beta \in \mathbb{R}$ are constants, while $\phi(q_i, q_j) = 2\arccos(|q_i \cdot q_j|)$ denotes the geodesic distance between spacecraft i and j [166]. As shown in the previous reference, this is not the only metric on $\mathrm{SO}(3)$ that one can use, but it is certainly the most natural. It is possible that slightly different results may be obtained for different metrics, but such a study is outside the scope of this thesis.

Given this appropriate alternate concept of relative distance, for $\beta < 0$ one can recognize the same structure of the Cucker-Smale gains. But one can also see that we have chosen to extend the range of this parameter to the entire real line. This choice stems from the fact that when we think of a formation we think of it as comprised of simple spacecraft, which are limited in the magnitude of the control torque that they can apply in every direction. Thus, for a positive β, the gains b_{ij} grow bigger for larger distances. This should help offset the oscillatory behaviours related to torque accumulation by simply slowing down the motion for large angle maneuvers (in place of taking large swings, which are difficult to recover due to the threshold on the magnitude of the applicable torque).

Of course, a formation acting under one of the controls defined before achieves synchronization (as long as some other conditions are satisfied). Before stating the related theorem however, we need a preliminary lemma [165] in order to justify some of the computations. The proof of the theorem relies on the construction of a Lyapunov function, and this lemma is useful for this construction.

Lemma 9. *If* (q_i, ω_i) *and* (q_j, ω_j) *satisfy the quaternion kinematics defined in* (5.6)*, then also* $(q_i^\star q_j, \omega_i - \omega_j)$ *satisfies it. In addition, consider* $V_q = \|q_i^\star q_j - \mathbf{q}_I\|^2$*. Then* $\dot{V}_q = (\omega_i - \omega_j) \cdot \widehat{q_j^\star q_i}$*.*

With this lemma in tow, we are ready to prove asymptotic convergence for our controls. We want to point out that the following theorem, albeit only for constant gains, has been stated already in [165]. Here we just observe how it allows to prove asymptotic convergence also for certain adaptive controls, thus eliminating the need to modify the baseline law. Of course, also the proof can be found in [165], but we repeat it here for the sake of completeness. Assuming $q = q(t) = (q_0, \ldots, q_N)$ and $\omega = \omega(t) = (\omega_0, \ldots, \omega_N)$, the theorem states

Theorem 20. *Consider the equations of motion* (5.6)*, with the control torque defined by equation* (5.7)*. For every couple* (i, j)*, let* a_{ij} *be a positive constant and* $b_{ij} = b_{ij}(q, \omega) > 0$*. Furthermore,*

assume that the underlying communication graph is undirected and connected. Then, there exist $\tilde{q}$ *and* $\tilde{\omega}$ *such that* $q_i \to \tilde{q}$ *and* $\omega_i \to \tilde{\omega}$, $\forall i \in \{0, \ldots, N\}$.

Proof. The proof rests on the LaSalle's invariance principle. Consider the Lyapunov function candidate

$$V = \frac{1}{2} \sum_{i,j=0}^{N} g_{ij} a_{ij} \|q_j^\star q_i - \mathbf{q}_I\|^2 + \frac{1}{2} \sum_{i=0}^{N} \|\omega_i\|^2. \tag{5.9}$$

By keeping in mind Lemma 1 and the equations of motion (5.6), the derivation of the function above yields

$$\dot{V} = \frac{1}{2} \sum_{i,j=0}^{N} g_{ij} a_{ij} \left(\omega_i - \omega_j\right)^T \cdot \widehat{q_j^\star q_i} + \sum_{i=0}^{N} I_i^{-1} \left[\omega_i^T \cdot \left(\tau_i - \omega_i \times I_i \omega_i\right)\right]. \tag{5.10}$$

If we now substitute in the previous equation the expression of the control torque (5.7), we obtain

$$\dot{V} = \frac{1}{2} \sum_{i,j=0}^{N} g_{ij} a_{ij} \left(\omega_i - \omega_j\right)^T \cdot \widehat{q_j^\star q_i} - \sum_{i=0}^{N} \omega_i^T \cdot \left[\sum_{j=0}^{N} g_{ij} a_{ij} \widehat{q_j^\star q_i} + b_{ij} \left(\omega_i - \omega_j\right)\right]. \tag{5.11}$$

Do note that, given the definition of the control torque τ_i, the terms $\omega_i \times I_i \omega_i$ cancel each other. Still, it is also true that $\omega_i^T \cdot (\omega_i \times I_i \omega_i) = 0$. Thus, we do not strictly need the term $-\omega_i \times I_i \omega_i$ in (5.7). However, we prefer to keep it in order to have the closed-loop dynamics be as similar as possible to the Cucker-Smale model. Now, since we have

$$\begin{aligned}
&\frac{1}{2} \sum_{i,j=0}^{N} g_{ij} a_{ij} \left(\omega_i - \omega_j\right)^T \cdot \widehat{q_j^\star q_i} = \frac{1}{2} \sum_{i=0}^{N} \omega_i^T \left(\sum_{j=0}^{N} g_{ij} a_{ij} \widehat{q_j^\star q_i}\right) - \\
&\frac{1}{2} \sum_{j=0}^{N} \omega_j^T \left(\sum_{i=0}^{N} g_{ij} a_{ij} \widehat{q_j^\star q_i}\right) = \frac{1}{2} \sum_{i=0}^{N} \omega_i^T \left(\sum_{j=0}^{N} g_{ij} a_{ij} \widehat{q_j^\star q_i}\right) + \\
&\frac{1}{2} \sum_{j=0}^{N} \omega_j^T \left(\sum_{i=0}^{N} g_{ji} a_{ji} \widehat{q_i^\star q_j}\right) = \sum_{i=0}^{N} \omega_i^T \left(\sum_{j=0}^{N} g_{ij} a_{ij} \widehat{q_j^\star q_i}\right),
\end{aligned} \tag{5.12}$$

due to the fact that $\widehat{q_j^\star q_i} = -\widehat{q_i^\star q_j}$ and both $a_{ij} = a_{ji}$ and $g_{ij} = g_{ji}$ (since the graph is undirected), it results

$$\dot{V} = -\frac{1}{2} \sum_{i,j=0}^{N} g_{ij} b_{ij} \|\omega_i - \omega_j\|^2 \leq 0. \tag{5.13}$$

Let $\Gamma = \left\{(q_i, \omega_i)_{i=0,\ldots,N} \,|\dot{V} = 0\right\}$. Also, let $\bar{\Gamma}$ be the largest invariant set contained in Γ. On $\bar{\Gamma}$ it results $\dot{V} = 0$, which in turn implies $\omega_i = \omega_j$, $\forall i, j$. This follows from the weights b_{ij} being strictly positive and the connection hypothesis that we made. As a consequence, we see that $\dot{\omega}_i = \dot{\omega}_j$, and therefore the vector $\dot{\omega} = (\dot{\omega}_0, \ldots, \dot{\omega}_N)$ must belong to $span\,\{\mathbf{1} \otimes \eta\}$, for some $\eta \in \mathbb{R}^3$.

Since $\omega_i = \omega_j$, it follows from the controlled equations of motion that

$$\dot{\omega}_i = -\sum_{j=0}^{N} g_{ij} a_{ij} \widehat{q_j^\star q_i}, \quad i = 0, \dots, N. \tag{5.14}$$

We also know that

$$\sum_{i=0}^{N} \eta^T \cdot \dot{\omega}_i = -\sum_{i=0}^{N} \eta^T \cdot \left(\sum_{j=0}^{N} g_{ij} a_{ij} \widehat{q_j^\star q_i} \right) = 0, \tag{5.15}$$

since the graph is connected and $\widehat{q_j^\star q_i} = -\widehat{q_i^\star q_j}$. Therefore, since $\dot{\omega}$ is orthogonal to $\mathbf{1} \otimes \eta$, it results that $\dot{\omega}_i = 0, \forall i$.

As a consequence we can state that

$$\sum_{j=0}^{N} g_{ij} a_{ij} \widehat{q_j^\star q_i} = 0, \quad i = 0, \dots, N. \tag{5.16}$$

It is easy to see [167] that the previous expression can be rewritten in matrix form as

$$(L \otimes I_3)\, \hat{q}_l = 0, \tag{5.17}$$

with $\hat{q}_l = (\hat{q}_0, \dots, \hat{q}_N)$ and $L = (l_{ij})$ denoting the Laplacian with diagonal entries $l_{ii} = \sum_{j=0}^{N} g_{ij} a_{ij} \bar{q}_i$ and out of diagonal ones $l_{ij} = -g_{ij} a_{ij} \bar{q}_i$. From our hypotheses (and the unitarity of the quaternion) follows directly $q_i = q_j, \forall i, j$. Finally, the thesis follows by applying the LaSalle's invariance principle. □

The previous proof rests heavily on the Laplacian L being a symmetric positive-semidefinite matrix, which is a consequence of the graph being undirected and connected. Similarly to what seen in Chapter 3 for the CS model, these characteristics can also be exploited to derive some informations on the convergence rate towards the consensus state. In particular, the derivative $\dot{V}$ of the Lyapunov function considered satisfies

$$\dot{V} = -\frac{1}{2} \sum_{i,j=0}^{N} g_{ij} b_{ij} \|\omega_i - \omega_j\|^2 = -\langle L_\omega \omega, \omega \rangle, \tag{5.18}$$

where L_ω denotes the Laplacian associated to the Adjacency matrix defined by the gains b_{ij} and a proof of the equality can be found in [99]. Following the idea of Cucker and Smale described in Chapter 3, we reduce ourselves to consider the agents angular velocities in the space

$$X = \left(\mathbb{R}^3\right)^{N+1} / \Delta = \Delta^\perp, \tag{5.19}$$

where $\Delta = \{(\bar{\omega}, \dots, \bar{\omega}) \,|\bar{\omega} \in \mathbb{R}^3\}$ defines the diagonal of $(\mathbb{R}^3)^{N+1}$ (of course, being in Δ brings us back to the situation described in the proof). Furthermore, we consider this space as equipped

with the standard norm induced by the modulo structure (note that Δ is closed in $(\mathbb{R}^3)^{N+1}$), that is

$$\| [\omega] \|_{(\mathbb{R}^3)^{N+1}/\Delta} = \inf_{\bar{\omega} \in \Delta} \|\omega - \bar{\omega}\|, \tag{5.20}$$

and, with an abuse of notation, continue to indicate the previous norm as $\|\|$.

Since L_ω is a positive definite matrix in $\Delta^\perp$, it follows [98]

$$\dot{V} = -\langle L_\omega \omega, \omega \rangle \leq -\lambda_{min}\left(L_\omega\right) \|\omega\|_2^2, \tag{5.21}$$

where $\lambda_{min}\left(L_\omega\right)$ denotes the smallest eigenvalue of the Laplacian L_ω.

Therefore, for any $t \in \mathbb{R}^+$, we can state that

$$\ln\left[V\left(\tau\right)\right]|_0^t = \int_0^t \frac{\dot{V}}{V} d\tau \leq -\int_0^t \frac{\lambda_{min}\left(L_\omega\right)\|\omega\|_2^2}{V} d\tau = -\int_0^t \frac{2\lambda_{min}\left(L_\omega\right)\left(V - f\left(q\right)\right)}{V} d\tau, \tag{5.22}$$

where $f\left(q\right) = \frac{1}{2}\sum_{i,j=0}^{N} g_{ij} a_{ij} \|q_j^\star q_i - \mathbf{q}_I\|^2$. By continuity of V and from the fact that we are in $\Delta^\perp$ (and therefore at least one of the $\|\omega_i\|_2$ must be different from zero), $\frac{V - f(q)}{V}$ is bounded from below in $[0, t]$ by some positive constant $C_t = \min_{[0,t]} \frac{V - f(q)}{V}$. Thus, we can say that

$$\ln\left[V\left(\tau\right)\right]|_0^t \leq -\int_0^t \frac{2\lambda_{min}\left(L_\omega\right)\left(V - f\left(q\right)\right)}{V} d\tau \leq -2C_t \mathbf{\Phi}_t t, \tag{5.23}$$

where $\mathbf{\Phi}_t = \min_{[0,t]} \lambda_{min}\left(L_\omega\right)$. As a consequence, for any $t \in \mathbb{R}^+$, we have

$$V\left(t\right) \leq V\left(0\right) e^{-2C_t \mathbf{\Phi}_t t}. \tag{5.24}$$

Now, $C_t \neq 0$ for all $t \in \mathbb{R}^+$ and it asymptotically goes to 1. Considering that $\frac{V - f(q)}{V} = 1 - \frac{f(q)}{V}$, this follows from the fact that

$$0 < 1 - \frac{f\left(q\right)}{V\left(0\right)} < 1 - \frac{f\left(q\right)}{V} \leq 1, \tag{5.25}$$

which in turn concludes the argument, since in $\Delta^\perp$ it results $\lim_{t\to\infty} V\left(t\right) = 0$, and therefore the same happens to $f\left(q\right)$. This is because the induced norm of ω is zero when $\omega \in \Delta$, and therefore at consensus the term $\|\omega\|^2$ in $V\left(t\right)$ equals zero. Additionally, the chain of inequalities (5.25) stands thanks to the fact that $\dot{V} < 0$ in $\Delta^\perp$, which in turn implies both $V\left(t\right) < V\left(0\right)$ for all $t \in \mathbb{R}^+$ (thus the second inequality) and $0 \leq \frac{f(q)}{V(0)} < 1$ (thus the first inequality), with the latter a consequence of the former if one decomposes $V\left(t\right)$ in $f\left(q\right) + \|\omega\|^2$ and brings the second addendum to the right hand side in the rightmost inequality.

In conclusion, C_t can be globally bounded from below by some other constant $\bar{C} \in (0, 1]$, and therefore, from Proposition 2 in Chapter 2, we know that

$$\lambda_{min}\left(L_\omega\right) \geq \frac{1}{2}\nu\mu_t, \tag{5.26}$$

with $\mu_t = min_{i \neq j} b_{ij}$ in $[0, t]$ and $\nu = \frac{N}{2}$ (see [92]). If the gains b_{ij} are constant this leads us to the final inequality

$$V(t) \leq V(0) e^{-\frac{\bar{C} N \mu}{2} t}, \tag{5.27}$$

since $\mu_t = \mu$ and $\lambda_{min}(L_\omega)$ are constant in time. Of course, the previous inequality holds also if the gains b_{ij} vary with some time-dependent quantity. In particular, for the gains design (5.8), one can trivially observe that

$$\mu_t = \min_{i \neq j} K_\omega \left(\sigma^2 + \phi^2(q_i, q_j)\right)^\beta \geq K_\omega \sigma^{2\beta}. \tag{5.28}$$

Of course, the previous is just a trivial estimate and a deeper analysis is needed in order to understand how the geodesic distance affects the exponential estimate.

The previous arguments allow us to completely describe consensus under control (5.7) in the undirected connected case. However, in Chapters 2 and 3 we have seen that asymptotic convergence can be proved also for non-symmetric Laplacian matrices. In the next Sections, we discuss what happens when a particular instance of this kind of Laplacian is considered for the problem at hand.

5.3 Hierarchical synchronization: three-axis stabilized leader

5.3.1 Introduction

In the present subsection we lay down some notions necessary to understand the simulations performed in this Section and in the next one. As previously stated, these are aimed to understand the closed-loop dynamics of a formation of spacecraft acting in free space or in other environments under the control law (5.7), with and without the adaptive modification given by equation (5.8), in such a way that a comparison as global as possible can be drawn between the two. Additionally, we restrict the analysis of the controlled dynamics to the case in which the spacecraft are subjected to a limitation in the magnitude of the applicable torque.

In particular, the formations considered are comprised of standard 3U-cubesats ($10 \times 10 \times 30$ cm, 4 kg) equipped with "ideal" reaction wheels. That is, we suppose them unbreakable and capable of applying in every direction a maximal torque of 10^{-3} Nm.

The initial conditions for the spacecraft are generated in the same manner for every plot. Specifically, the associated quaternions are selected randomly on the rotation group $\mathrm{SO}(3)$ according to a uniform distribution. To do so, first we choose three independent values u_1, u_2 and u_3 uniformly generated in the interval $[0, 1]$; then, we define the quaternion as [168]

$$q = \left(\sqrt{u_1}\cos 2\pi u_3, \sqrt{1-u_1}\sin 2\pi u_2, \sqrt{1-u_1}\cos 2\pi u_2, \sqrt{u_1}\sin 2\pi u_3\right).$$

Additionally, in order to respect the antipodal identification for rotations, given a quaternion q such that $\bar{q} < 0$, we substitute it with its opposite $-q$. As for the angular velocities, we impose them all to zero (of course, non-zero velocities act only as perturbations on the plots that we are going to show). For every plot, the only exception is given by the first spacecraft of the formation, which is supposed to be three-axis stabilized, that is again with zero initial angular velocity but also aligned with the inertial frame of reference. For the analysis conducted in the next subsection, some dispensations to these rules will be necessary. Where appropriate, we will point them out.

Finally, we assume that the spacecraft have reached a synchronized state when, for every i, it results $\phi(q_i, q_0) < 10^{-4}\ rad$ and $\|\omega_i - \omega_0\|_\infty < 5 \times 10^{-5}\ rad/s$. Do note that this ensures that we are truly close to the wanted state, and not in some oscillatory one where we are still moving with a significant angular velocity.

In what follows, as a first step we are going to expand numerically the discussion started in the previous section regarding the graph structures needed for a formation to synchronize under the proposed control laws. In particular, we are going to show how there is strong evidence that consensus for the closed-loop dynamics is reached also when a hierarchical graph is considered.

Secondly, we are going to analyze, under certain assumptions, the parameter spaces of the proposed controls in search for their optimal regimes. Once this is done, we are going to compare how the respective closed-loop dynamics in these regimes behave with respect to the dimension of the formation, the relative conditions of the spacecraft and the structure of the communication graph. Finally, following some results of this analysis, we are going to see what happens in the case of two spacecraft.

Before concluding, we want to remark that, while this study is conducted in the context of attitude synchronization, it is easy to extend to similar control laws for translational dynamics. However, as shown in the previous chapter, particular attention must be paid to the vector field acting on the spacecraft, since a strong gravitational pull may very well render impossible the application of certain control techniques.

5.3.2 Preliminary remarks

In this subsection we briefly expand the discussion on the conditions required over the communication graph for a formation to synchronize under the control law (5.7) and its adaptive modification (5.8). Additional details will be given in the next section.

Previously, we have seen that synchronization can be obtained if the graph is undirected and connected. Although we do not have an analytical proof, we believe that there is enough material to claim that synchronization can be obtained also for a hierarchical graph, as defined for the Cucker-Smale model, and therefore to employ these graphs in the study of the consensus processes. Of course, as already stated, we could have just modified the baseline control law in order to fit such an hypothesis, but that would have contrasted with the objective of defining a

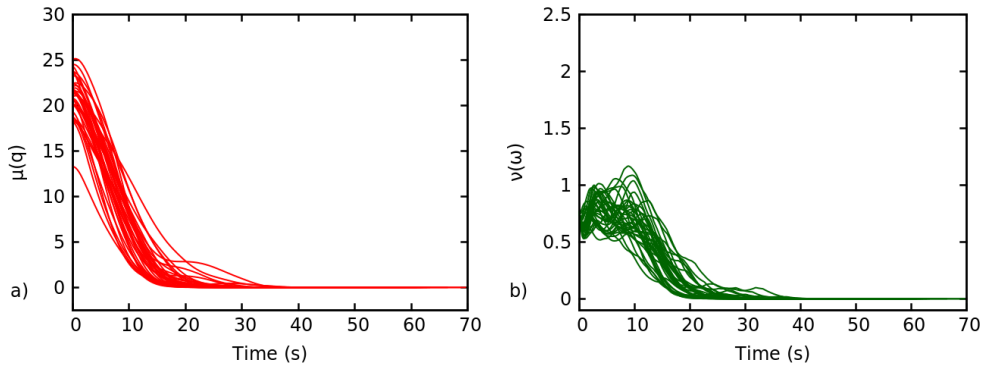

Figure 5.1: Time evolution (up to synchronization time) of functions $\mu(q)$ (a) and $\nu(\omega)$ (b) for 35 sets of initial conditions associated to a 20 spacecraft formation acting under a hierarchical graph (Figure 5.3, $5P$) and with a three-axis stabilized leader. Control (5.7) is the one employed and the gains are selected as $a_{ij} = 0.5$ and $b_{ij} = 1$ for every couple (i, j).

rotational equivalent of the Cucker-Smale model.

From a numerical point of view, it is easy to convince oneself of the goodness of the previous claim. In fact, let's define the two non-negative functions $\mu(q) = \sum_{i=1}^{N} \|q_i - q_0\|^2$ and $\nu(\omega) = \sum_{i=1}^{N} \|\omega_i - \omega_0\|^2$, where the variables have the same meaning that they have in Theorem 20. Since these functions are non-negative, if they become zero the spacecraft have respectively the same attitude and the same angular velocity, which correspond to those of the root.

These allow us to do plots like those of Figure 5.1, where the time evolution of these functions (for control (5.7)) is considered up to the threshold defined in the previous subsection. This is done for 35 different sets of initial conditions associated to a 20 spacecraft formation, with the leader three-axis stabilized and the angular velocities of the follower generated uniformly over a sphere of radius $0.2\ rad/s$. The spacecraft are allowed to communicate with the first 5 preceding them in the indexation or with the maximal number of spacecraft available. As it can be seen, both functions go asymptotically to zero with a minimum amount of oscillations. Of course, this happens also by employing control (5.8) and, as far as we know, for different initial conditions and different hierarchical graphs.

From an analytical point of view instead, some guidelines can be derived from the approach adopted by Shen in [137]. In particular, if we limit ourselves to the baseline control (5.7), one can observe that the latter reduces to a standard quaternion feedback control in the case $N = 2$. Then, assuming a proof by induction over the dimension, since in a N spacecraft formation the last agent only receives informations (due to the hierarchy), the first $N - 1$ will asymptotically achieve attitude synchronization for the inductive hypothesis. So, in a sense, the last spacecraft will end up again in the case $N = 2$, tracking approximately the same state, with gains obtained from the sum of those associated with the different edges. Therefore, it is a matter of proving that, under a suitable metric, the last agent gets asymptotically closer and closer to the rest of the formation. Of course, as done for the Cucker-Smale model, in the case of an adaptive control there may be need of establishing some preliminary properties in order to make the proof valid.

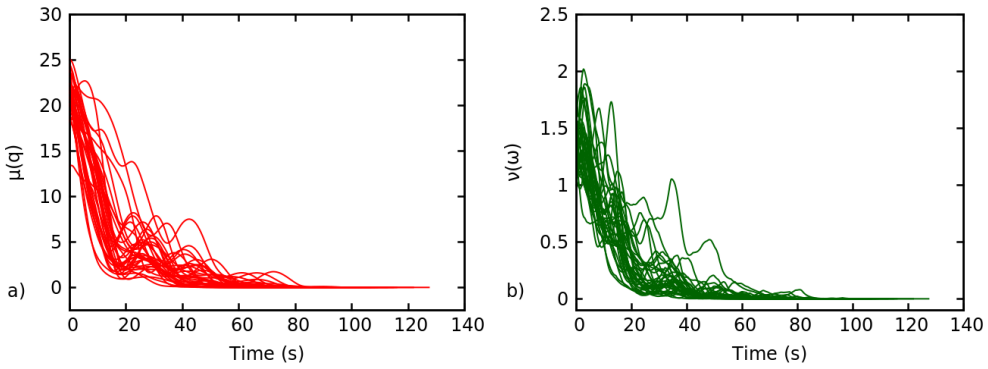

Figure 5.2: Time evolution (up to synchronization time) of functions $\mu(q)$ (a) and $\nu(\omega)$ (b) for the same situation of Figure 5.1, with the exception that the formation leader is spinning with angular velocity $\omega_0 = (0, 0, 0.2)$.

A natural follow-up of the previous analysis lies in asking what is the applicability range of the control with respect to the leader's dynamics. That is, if we assume as true synchronization under hierarchical graphs and with a three-axis stabilized (or anyway fixed) leader, then we can ask if, similarly to what has been proved by Shen, synchronization can still be obtained with a spin-stabilized or accelerating one.

Do note that, as we have formalized it, the leader is always applying a braking term $-\omega_0 \times I\omega_0$. For practical uses however, one may want to understand what happens with an uncontrolled leader (real or virtual), so that the formation is able to reach autonomously as many states as possible with the same control law. As far as we are aware, as long as the angular velocity of the leader is mild in magnitude, there is no problem in achieving a spin-stabilized state (which corresponds to a leader moving with a constant angular velocity). For example, in Figure 5.2 we consider the same situation of Figure 5.1, but we make the leader rotate around its axis of minimum inertia with a velocity of $0.2\ rad/s$. As you can see, albeit it obviously takes more time, control (5.7) is still able to achieve attitude synchronization (at least given the threshold that we imposed). Similar results can be obtained with its adaptive modification (5.8).

The discussion for the case of a free-spinning leader is naturally a little bit more complicated, due to the fact that in principle several accelerating signals can be defined. However, this number can be easily cut down by sticking to real mission scenarios. We will see how, along with a more in depth treatment of the spin-stabilized case, in the next section, after developing in this one the necessary framework to discuss these cases.

5.3.3 Optimal control regimes

In this subsection we analyze, under certain assumptions, the parameter spaces associated with the control (5.7) and its adaptive modification (5.8). This is done with the goal of individuating the optimal parametrical regimes for both controls in order to be able to compare them when they are at their best.

For this analysis we limit ourselves to consider hierarchical graphs as defined for the Cucker-Smale model. Besides being an example of a digraph with a spanning tree, and therefore inherently more interesting since the presence of a leader ensures that we can define a priori the asymptotical state for the formation, there are several other reasons to consider this particular graph. Where appropriate, they will be discussed more in depth.

For the moment we can say that hierarchical graphs are useful to simulate formations that are stretched over long distances and that therefore see their own agents unable to communicate with every single one of their neighbours. As an example, consider a group of spacecraft that are trying to synchronize in order to build an interferometer. To precisely determine the synchronized state, one could consider a leader at the center of the formation with different unconnected hierarchical structures sprouting from it. This would give rise to several anular levels, each one corresponding to different levels of the hierarchies considered. With this arrangement, the aperture of the interferometer would be as large as one would want, but with the advantage of reducing the synchronization problem to several formations smaller than the entire one. This offers not only a reduced computational load for every spacecraft but also, as we are going to see in the next subsection, a reduced synchronization time for the entire formation.

Of course, we have to keep in mind that we are relying on the well functioning of a leader. For a single hierarchical structure, the failure of a leader can be compensated by simply noticing that this brings along a reduced formation dimension. Thus, given a certain graph structure, one can pass down the leadership along the hierarchy and consider the same graph restricted to the lower dimension. More in general, one may define a multi-leader formation, with the different hierarchies attached to one and only one leader. Thus, if one of the latter fails, the associated hierarchy can be attached to one of the surviving leaders, which for the latter translates to passing information to an additional spacecraft.

Coming back to the analysis mentioned at the beginning, as a first step, for a given baseline configuration of the formation and certain communication graphs, in Figure 5.3 we plot the average synchronization time for a 20 spacecraft formation, acting under control (5.7), as a function of the gains a_{ij} and b_{ij}. The average is done on 500 different sets of initial conditions and a maximum of 50 sets are allowed to surpass a time threshold of 600 seconds (i.e., if more than 50 sets fail to synchronize within this threshold, the average is not computed). Obviously, this is done to catch extreme conditions that float around our time threshold.

Before continuing with the study of the results, let us clarify some points. First, the gains are assumed equal for all the agents and thus we can refer to them in a general manner as a_{ij} and b_{ij}. Also, we said that we work with particular examples of hierarchical graphs. Specifically, they are constructed in such a way that each spacecraft receives information from a fixed number of agents preceding it in the indexation (7, 5, 3 or 1; correspondingly referred to as $7P$, $5P$, $3P$ and $1P$ in the figure) or from the maximal number available if this fixed quantity cannot be reached. Finally, in order to construct our baseline configuration, every set of initial conditions is arranged in ascending order with respect to the geodesic distances of the spacecraft from the leader.

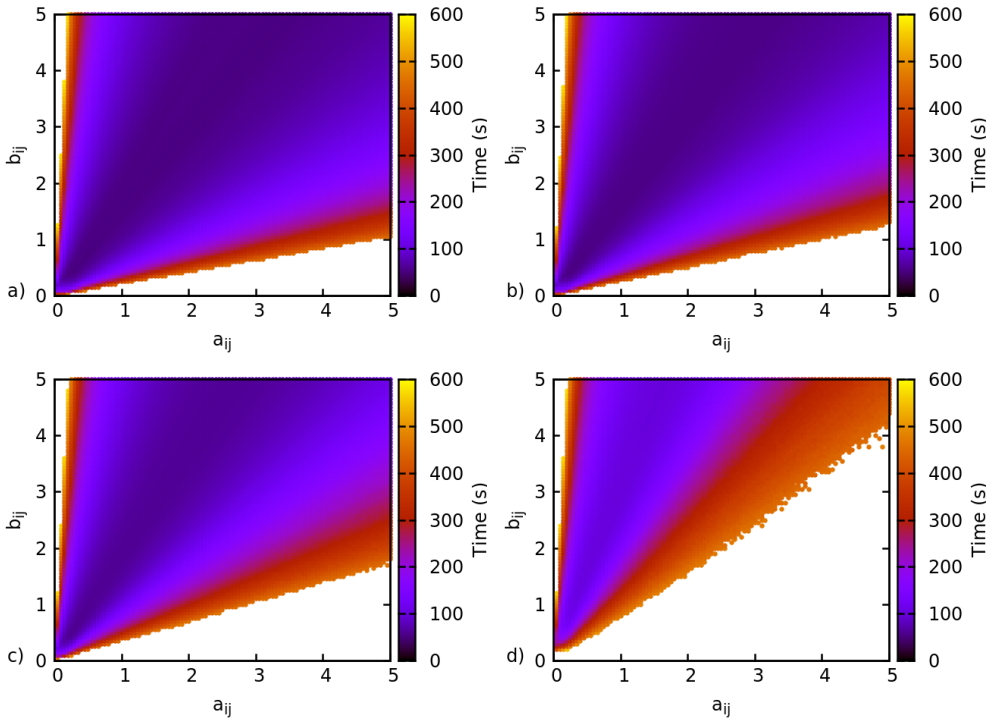

Figure 5.3: Average synchronization time for a 20 spacecraft formation as a function of the gains a_{ij} and b_{ij} (equal for all the agents) via control (5.7), with a 100×100 uniformly spaced grid (from 10^{-1} to 5 in both directions). The graph structures are $7P$ (a), $5P$ (b), $3P$ (c) and $1P$ (d).

We can now look at the plots themselves. In particular, for all the graph structures considered, we can observe that both an excessive acceleration (high a_{ij}) and an excessive braking (high b_{ij}) are cause of a very long synchronization time, which instead tends to take the lowest values in the lower left corner of the plots. Furthermore, we can also observe that the synchronization time gets higher seemingly the more sparse the communication graph becomes where, from now on, for sparseness of a graph we roughly intend the number of edges. This apparent behaviour is obviously not good, since a more sparse graph, which means less communication links per spacecraft, means also a reduced computational load for the agents. Do note that, while in what follows we will refer to this concept in an independent fashion, other authors have shown that it can be codified in the behaviour of appropriate matrices eigenvalues (like what seen with the Laplacian of the Cucker-Smale model).

Before going onward, we give the first additional reason to work with hierarchical graphs, which is related to the following remark

Remark 1. *Let ϵ_1 and ϵ_2 denote the numerical thresholds determining consensus according to what said in Section 5.3.1 (respectively, $\phi(q_i, q_0) < \epsilon_1$ and $\|\omega_i - \omega_0\|_\infty < \epsilon_2$ for every agent of the formation). Furthermore, let T_1 denote the convergence time associated to these thresholds for a formation of N spacecraft synchronizing under a hierarchical graph. Then, if we extend this formation by adding further spacecraft to the tail of the hierarchy (and leaving the other as they were), the time T_2 of this extended formation satisfies $T_1 < T_2$.*

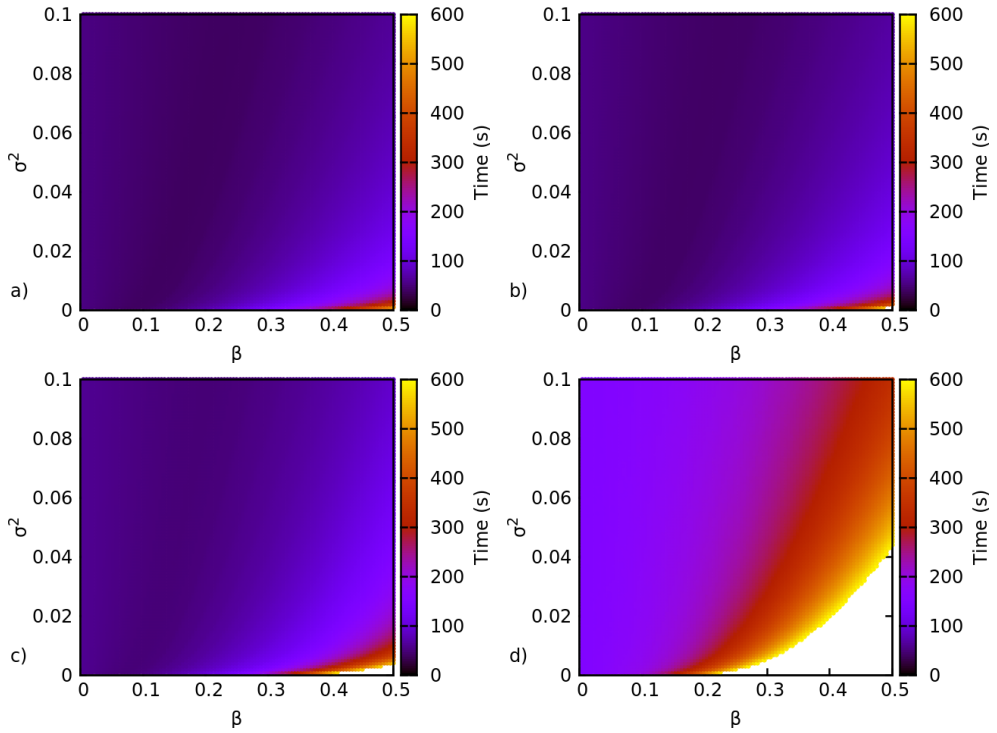

Figure 5.4: Average synchronization time for a 20 spacecraft formation as a function of the parameters β and σ^2 (equal for all the agents) via control (5.8), with a 100×100 uniformly spaced grid (with $\beta \in [10^{-2}, 0.5]$ and $\sigma^2 \in [0.005, 10^{-1}]$) and baseline values $K_q = 0.5$ and $K_\omega = 1$. The graph structures are $7P$ (a), $5P$ (b), $3P$ (c) and $1P$ (d). Initial conditions correspond to those of Figure 5.3.

The previous statement stands true thanks to the fact that, due to the hierarchy, the torque applied by the first N spacecraft remains the same, whether they act independently or embedded in a larger formation. Thus, since in both cases we are going towards the same equilibrium point, the synchronization time of the extended formation has to be greater or equal to that of the restricted one. Furthermore, it is clear that the statement continues to hold if we consider the average synchronization times over multiple sets of initial conditions.

In practice, the remark above tells us that the values plotted in Figure 5.3 actually constitute an upper bound for the average synchronization times of formations of dimension less than the plotted one (20 in this case) and that are comprised of the same initial conditions in the same indexation spots (e.g., the average synchronization time for a formation of 10 spacecraft is computed on the sets corresponding to the first 10 agents of the 20 spacecraft formation).

We remark that the previous argument is not valid for an undirected connected graph, since a larger dimension means additional data for at least one of the torques (due to the connection) and more generally a different equilibrium altogether. In a similar fashion, the argument cannot be extended as it is to a general digraph with a spanning tree, since in this case a new spacecraft may also pass information; therefore, the closed-loop dynamics of some of the previous spacecraft may be different due to the additional data.

Now, starting from the pictures above, which give us an idea of the maximum capability of

control (5.7), we can perform an analysis similar to the previous one for the proposed adaptive modification, and for which the same considerations apply. If we define $a_{ij} = K_q$ we can search, at parity of K_q and K_ω (see (5.8)) with respect to control (5.7), for values of β and σ^2 which improve the synchronization times obtained for that control. Again, the constants are assumed equal for all the agents. Do note however that, due to the term $\phi^2(q_i, q_j)$, in this case the final gains will obviously result being different from agent to agent.

In Figure 5.4 we plot the results of this analysis conducted with the baseline values $K_q = 0.5$ and $K_\omega = 1$, which of course lie in the optimal parametric zone of control (5.7), and the same surrounding conditions of Figure 5.3. Similarly to that Figure we can see how the results tend to get worse as the communication graph grows more sparse. However, for every graph, we can always find a set of (β, σ^2) combinations which improve on the synchronization time obtained with constant gains, although the number of combinations and the advantage that they offer shrink down with the sparseness of the graph, seemingly indicating that not much can be done if there is not a sufficient number of links. These are the regions that we were searching for, and we analyze them in greater detail in the next subsection.

5.3.4 Formation configuration effects

Through the previous two analyses we have managed to obtain, at parity of surrounding conditions, a set of "optimal" gains which we can use to derive some information on the dependence of the controlled dynamics from the dimension of the formation and the initial relative conditions. However, a remark on this analysis is necessary. As already stated, some relevant parameters are equal for all the agents. Therefore, we may not be working in a real optimal region for the controls defined. While this is not a problem for the adaptive control (after all, for the purpose of the next analysis, we just need a couple (β, σ^2) that fastens the synchronization time definitely with respect to the dimension, and not necessarily the best in absolute terms), it may very well be for control (5.7) since, by considering gains equal across the agents, we may be preventing a better choice of parameters to arise. Thus, in a similar manner to what happens with the denseness of the graph, starting from an optimum parametrical situation for control (5.7) may very well weaken the improvement of our adaptive modification.

Furthermore, we have to remember that the analysis of the parameter spaces is conducted with a particular baseline formation configuration. Obviously, optimal parameters tied to this configuration may not be so if initial conditions are arranged in another way.

With these considerations in mind we can proceed to Figure 5.5, where, for each of the graphs considered before, we plot the average synchronization time against the dimension of the formation. In particular, starting from the exact 20 spacecraft formation considered in the previous subsection, to study lower dimensions we simply remove the conditions associated to the spacecraft that are no longer there. Additionally, for every dimension, we consider 400 shuffles of the baseline formations determined in this way (or the maximal number of permutations

allowed by the dimension), but we keep the leader fixed. Then, for every permutation, we compute again the average synchronization time. In the plots we indicate the results for the baseline configuration in black (for both controls), while the differently colored error bars denote the largest interval containing the synchronization times associated with the shuffles.

Before discussing the results contained in these plots, we remark that the simulations generating them are computationally quite heavy. This is because, given a general graph structure, one has to propagate the controlled equations of motion for every dimension under analysis, thus ending up integrating $N!$ equations (with N denoting the highest dimension). However, besides the fact that the propagations can be easily parallelized, the cost of the simulations can be lowered significantly by exploiting the hierarchical graph structure that we are giving to our formations. The starting point is given by the following lemma

Lemma 10. *Let G_1 and G_2 denote the hierarchical communication graphs associated to two formations of dimensions $N_1 + 1$ and $N_2 + 1$, with $N_1 < N_2$ and G_1 being a subgraph of G_2 having the same first N_1+1 nodes. Furthermore, if $\{q_i^0, \omega_i^0\}_{i=0,\dots,N_1}$ and $\left\{q_j^0, \omega_j^0\right\}_{i=0,\dots,N_2}$ denote the rotational initial conditions of the spacecraft for the formations G_1 and G_2, assume that $q_i^0 = q_j^0$ and $\omega_i^0 = \omega_j^0$ for all $i = j$, with $i = 0, \dots, N_1$. Then, if we indicate with $\phi\left(q_\star^0, \omega_\star^0; t\right)$ the flow associated with the equations* (5.6) *(subject to the control* (5.7)*) and derived from the initial conditions $(q_\star^0, \omega_\star^0)$, it results*

$$\phi\left(q_i^0, \omega_i^0; t\right) = \phi\left(q_j^0, \omega_j^0; t\right), \quad \forall i = j,\ i \in \{0, \dots, N_1\}, \tag{5.29}$$

and for all $t \in \mathbb{R}$.

Proof. It is enough to observe that, due to the hierarchical structure of the graph G_2, the flows $\phi\left(q_{j_1}^0, \omega_{j_1}^0; t\right)$ (with $j_1 \in \{0, \dots, N_1\}$) do not depend in any way from the states (q_{j_2}, ω_{j_2}), with $j_2 \in \{N_1 + 1, \dots, N_2\}$. The thesis then follows from G_1 being a subgraph of G_2 having the same first $N_1 + 1$ nodes. □

In essence, the previous result is saying that, due to the hierarchy and the way in which we expand the initial conditions with respect to the formation dimension, the torque applied by every spacecraft depends only on the data received by the agents preceding it in the indexation. Thus, the synchronization time obtained at a certain dimension will stay the same when the same group of spacecraft is embedded in a formation of higher dimension. This allows to integrate only the maximal number of equations N and check when the single dimensions have reached consensus. Of course, disparities in the synchronization times among dimensions are no problem, since the spacecraft are being driven towards a (supposedly) asymptotically stable equilibrium. This means that when lower dimensions have reached consensus and we continue integrating in order to synchronize the higher ones, the spacecraft already under the consensus threshold cannot do anything else than getting even closer to the equilibrium (as long as the threshold is sufficiently strict). Also, do note that this lemma is at the base of the remark in the previous section. Finally,

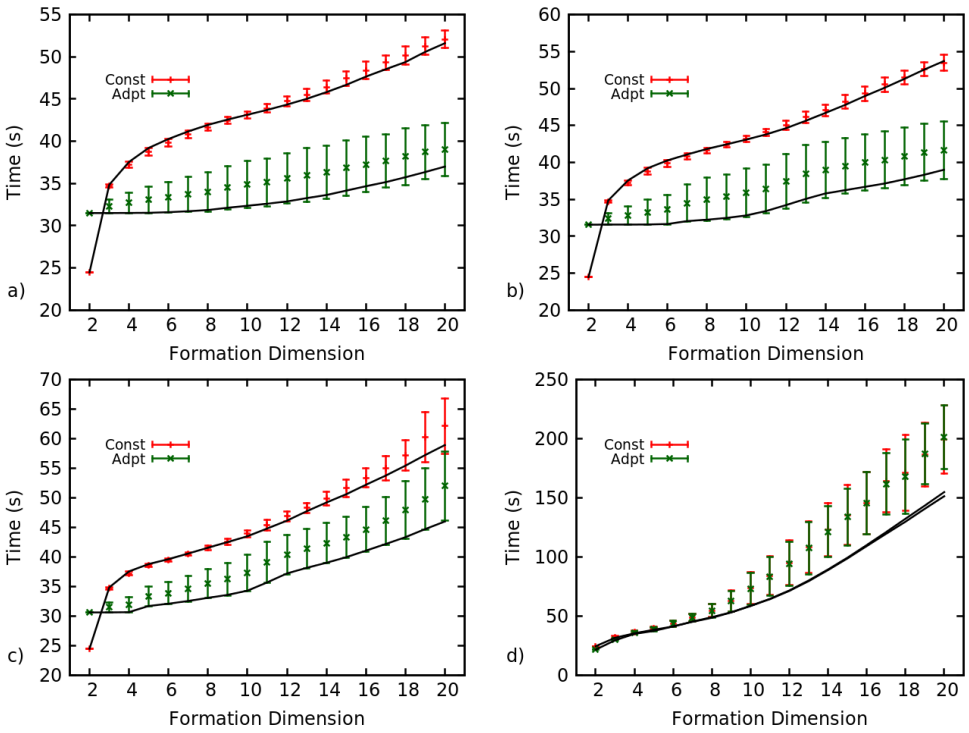

Figure 5.5: Synchronization time against formation dimension for 400 permutations of the baseline configurations considered in the plots of the previous subsection. For every picture, we plot in red the results obtained with control (5.7), in green those given by the adaptive design (5.8) while in black we indicate the corresponding results obtained with the baseline configuration. As for the gains parameters, we have $K_q = 0.5$ and $K_\omega = 1$. Instead, β and σ^2 are different for every graph: $\beta = 0.18$ and $\sigma^2 = 0.051$ ($7P$, a), $\beta = 0.225$ and $\sigma^2 = 0.088$ ($5P$, b), $\beta = 0.205$ and $\sigma^2 = 0.097$ ($3P$, c), $\beta = 0.015$ and $\sigma^2 = 0.096$ ($1P$, d).

it is easy to observe how the previous lemma is valid for any controlled dynamics (not just rotational), as long as one employs the correct distributed consensus algorithms.

Obviously, the previous argument cannot be applied to an undirected graph since new spacecraft mean new contributions to the torque of the preceding ones and thus a different equilibrium altogether. Similarly, it cannot be extended directly to a general digraph with a spanning tree, since the lack of a hierarchy may imply the addition of the same contributions of the undirected connected case.

Now, if we look at Figure 5.5, we can immediately see that, regardless of the permutation, our adaptive design performs definitely better than control (5.7). In particular, for the first two communication graphs, not only the average synchronization time is lower, but also the increasing rate seems to be much smaller. However, in line with what has been observed in the previous plots, the advantage tends to disappear the more sparse the graph becomes. It is also interesting to note that, with the exception of $1P$ and $3P$ for the adaptive control, the selected baseline configuration is not exactly the best performing permutation, despite the fact that the "good" parameters have been chosen with regard to this indexation. We remark however that, since strictly speaking they are not optimal parameters (being extracted from a discrete set), this

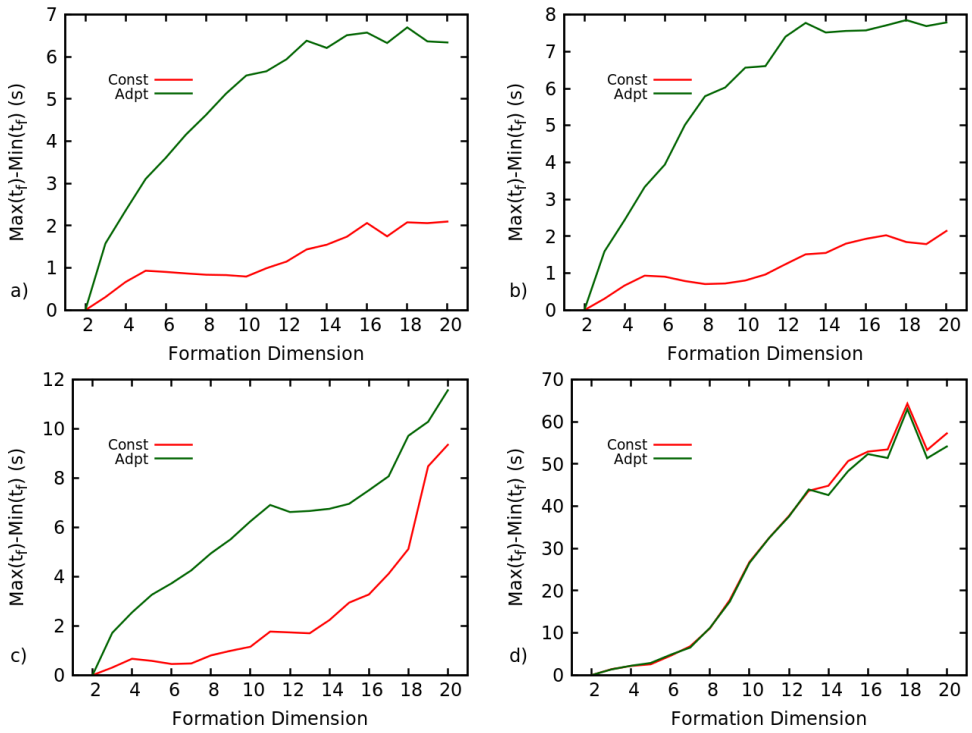

Figure 5.6: Difference between the maximal and minimal synchronization times of Figure 5.5 plotted against the dimension of the formation. Every relevant data corresponds to the equivalent of Figure 5.5.

may cause some differences in the plots.

While the previous discussion may not appear important at first glance, in Figure 5.6 we plot the difference between the maximum and minimum synchronization times achieved for a certain dimension. We can see that these differences, particularly for the adaptive case, tend to grow with the dimension N. This seems a reasonable behaviour, since on one side the number of possible permutations, with fixed leader, increases as $(N-1)!$ and on the other, when we increase the formation dimension, we just add the missing initial conditions instead of replacing the entire set. Still, with the exception of $1P$, the increments are not that dramatic. Of course, the number of permutations considered are just a minimal part of the possible ones, particularly for the highest dimensions. Therefore, one may wonder if the real increment is far greater than the plotted one.

In order to check this, in Figure 5.7 we plot the average synchronization times for some of the permutations of Figure 5.5 against the number associated to these permutations. This is done for $N = 13$ and, from left to right, for the graphs $7P$, $3P$ and $1P$ ($5P$ is excluded from this analysis, since the corresponding results are very similar to those associated to $7P$). Additionally, these plots and those that follow are done only for control (5.8). In fact, the behaviour that we are going to describe seems associated only to this control.

What we can see is that for the most dense graph, the computed average times distribute themselves along different lines. However these lines first crack ($3P$) and then seems to disappear

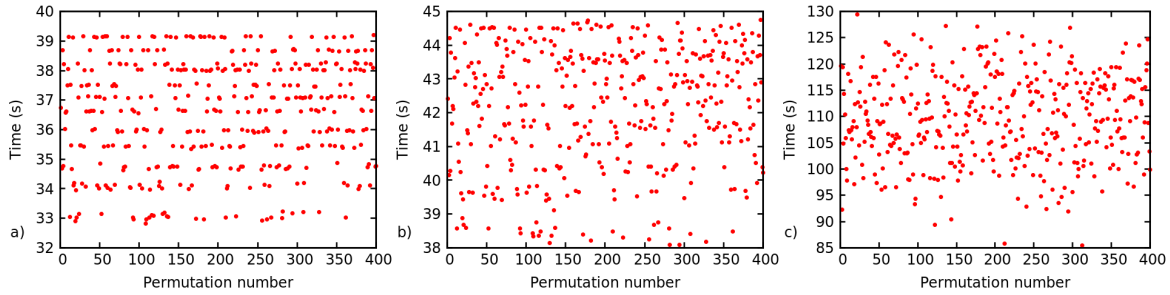

Figure 5.7: Average synchronization times corresponding to the various permutations of Figure 5.5. The dimension considered is $N = 13$, while the graphs are $7P$ (a), $3P$ (b) and $1P$ (c).

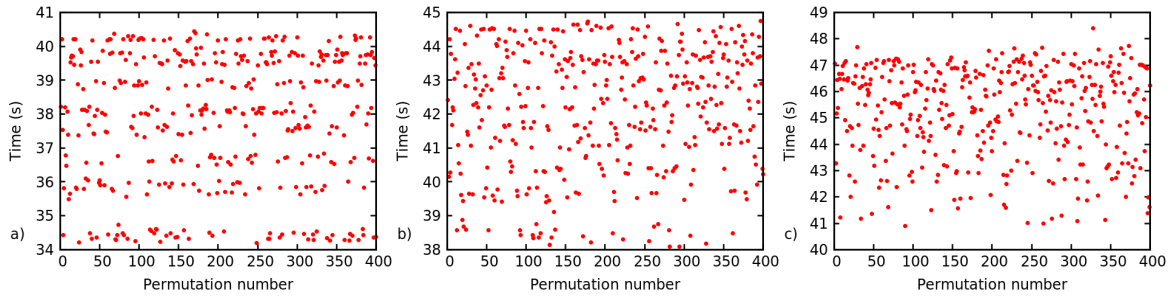

Figure 5.8: Average synchronization times corresponding to the various permutations of Figure 5.5. The graph considered is $3P$, while the dimensions are $N = 10$ (a), $N = 13$ (b) and $N = 16$ (c).

($1P$) the sparser the graph becomes. What's interesting about this result is that if we check the configurations adopted for the times which can be said to belong to the same line (say, they are within a time strip of the order of 10^{-1} seconds), then we can see that the second agent is always the same. Of course, this statement is quite clear for the graph $7P$ where these "lines" are well drawn. However, for the sparser graphs, these strip tend to stretch and intermingle, thus this behaviour results much less clear.

Furthermore, it seems to depend not only from the sparseness of the graph, but also on how the latter relates to the dimension of the formation considered. For example, if we look at Figure 5.8 (where the same kind of plot of Figure 5.7 is done for the $3P$ graph and, from left to right, $N = 10$, $N = 13$ and $N = 16$), we can see similar results to those of Fig 5.7. These and the previous plots seem to expose a sort of asymptotic behaviour, that is, for a given dimension, the closer a hierarchical graph is to a full triangular inferior matrix, the more solid these lines appear. Of course, this is just a possible conclusion and further study is needed to unravel this behaviour.

As a final comment, we only want to remark that this kind of disposition (with the number of lines equal to the number of agents) actually imbue our statistical analysis with some deterministic value, in the sense that the plots of Figure 5.5 and Figure 5.6 are practically exact approximations of the initial relative conditions effect, at least for the more dense graphs and control (5.8), since every agent can be found indexed as second at least in one of the permutations.

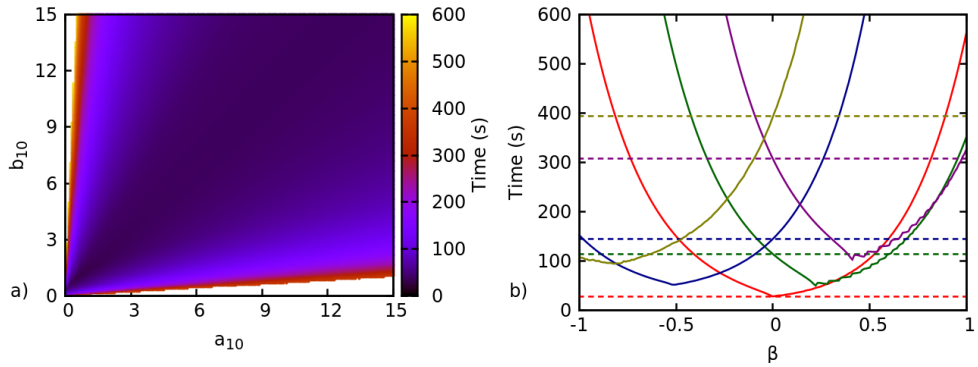

Figure 5.9: (a) Average synchronization time for a leader-follower formation as a function of the gains a_{10} and b_{10} via control (5.7), with a 200×200 uniformly spaced grid on the interval $[10^{-1}, 15]$. (b) Corresponding average synchronization time for control (5.8) as a function of β, with $\sigma^2 = 3.9 \times 10^{-2}$ and different values of (K_q, K_ω) associated to the different colors: $(0.5492462311558, 0.9984924623116)$ [red], $(0.2, 1.2)$ [dark green], $(0.6, 0.2)$ [dark blue], $(0.1, 1.55)$ [purple] and $(1, 10^{-1})$ [olive green]. The dashed lines correspond to the times achieved by control (5.7) with the same baseline values.

5.3.5 The case $N = 2$

The analysis that we have conducted in the previous subsections has given us a global view on the dependence of our control strategies from the parameters affecting the formation synchronization dynamics and it has shown how the adaptive design that we have introduced performs definitely better than an isoparametrized PD-like control law. Furthermore, despite being statistical in nature, it has provided us with a certain measure of deterministic results (seemingly related with the class of graphs analyzed). However, not only it rests on some assumptions that weaken its globality, but it has also shown how the improvement previously mentioned seems not to be true for the case $N = 2$. Thus, in the present subsection we analyze what happens in the latter case, where we are not burdened by the assumptions made and we can therefore obtain a more precise description of the controls behaviour.

Following the guidelines introduced earlier, in Figure 5.9 (left) we do a plot similar to those of Figure 5.3, but for a two spacecraft formation in a leader-follower situation. What we find is a behaviour similar to that of Figure 5.3, but with better times. Due to the reduced number of spacecraft to synchronize, this seems to be a reasonable behaviour.

Now, starting from this plot, we perform the same search for improving parameters (β, σ^2) that we have done in subsection 5.3.3. The search is done on a 200×200 uniformly space grid (with $\beta \in [-10^{-1}, 10^{-1}]$ and $\sigma^2 \in [5 \times 10^{-4}, 10^{-1}]$) and it is limited to the baseline parameters K_q and K_ω (rounded up to the twelfth digit) corresponding to the minimal average synchronization time. Since our main goals here are to see if there is any reason to employ our adaptive design for a two spacecraft formation and at the same time to understand its behaviour a little bit more, we do not plot the results here.

Instead, given the couple (β, σ^2) which offers the best performance, we plot (Figure 5.9,

right) the average synchronization time given by our adaptive control as a function of β, for σ^2 fixed as the optimal one. The result is then compared with the average synchronization time obtained with the baseline K_q and K_ω. Finally, by keeping the same σ^2, the plot is repeated for four other couples (K_q, K_ω) hand-picked to represent the different colored zones.

The first thing that we see is that on average our adaptive design has a parabolic behaviour with respect to the parameter β. Secondly, while for couples (K_q, K_ω) which are far from the optimal zone of control (5.7), our adaptive design offers always some sort of increasing, for a couple which is in the optimal region, the minimum synchronization time achieved by the control (5.8) is so close to the one given by control (5.7) to be practically the same (the difference is of the order of 10^{-3} seconds).

Thus, as a final remark, from the previous analysis one can infer that in the tracking case, if we look only at the average synchronization time, employing the adaptive design is not advisable unless the gains are for some reason chosen very badly.

5.4 Hierarchical synchronization: rotating leader

5.4.1 Spin-stabilized leader

In the previous section we have established a numerical approach aimed to derive quantitative informations over the synchronization of a formation. In particular, we have considered formations acting under a hierarchical leadership and with the leader being three-axis stabilized. But we have also seen in Chapter 3 that a consensus process is characterized by the dynamics of the leader, when it is present. Therefore, in this Section we consider the closed loop dynamics of the previous one under a leader subject to a time-changing rotational trajectory. As a first step, in this subsection we consider it as a spin-stabilized agent, that is one that is rotating with constant angular velocity about one of its principal axes of inertia.

The main goal is to understand if and in what magnitude a non-zero angular velocity affects the average synchronization time for controls (5.7) and (5.8), thus also discussing whether the latter improves on the former also in this instance (with the assumptions outlined in Section 5.3.1 still standing).

To simplify things, for the formations considered in this subsection, we impose that the leader is spinning around its z-body axis. Since the rotational energy is conserved and we are spinning around the axis of minimum inertia, this represents a stable configuration (albeit, as the case of the Explorer-1 teaches, it can become unstable in the presence of dissipation).

Following the methodology introduced in the previous section, we begin our analysis by studying the parameters spaces of control (5.7) corresponding to the graphs that we have introduced in the previous section. This investigation is conducted for multiple values of the initial angular velocity of the leader (in particular, we have $\omega_0(0) \in \{0.05, 1, 1.5, 2\}$, where the unit is always rad/s) and with the maps corresponding to the different graphs computed on a set

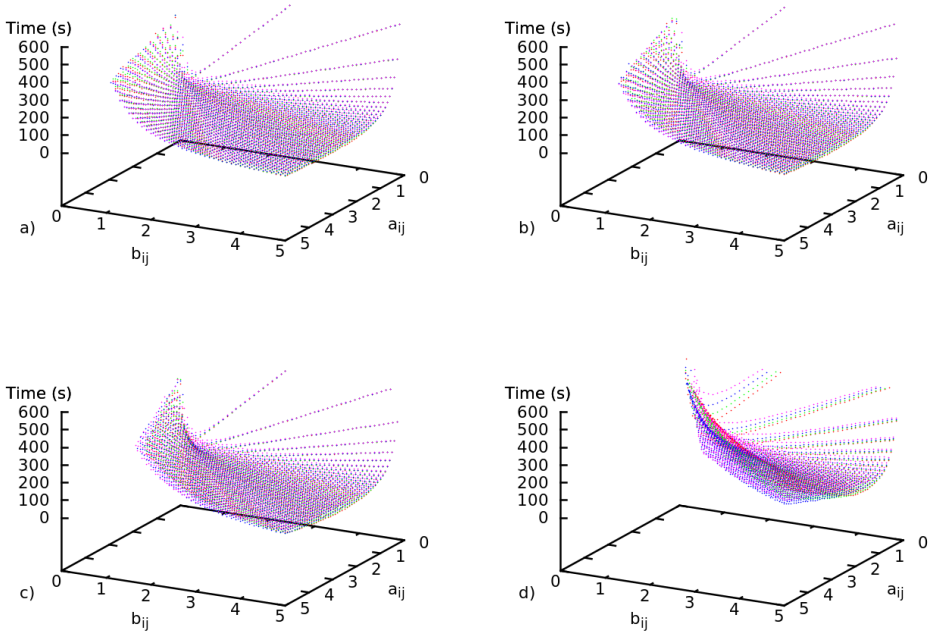

Figure 5.10: Average synchronization time for a 20 spacecraft formation as a function of the gains a_{ij} and b_{ij} (equal for all the agents) via control (5.7), with a 50×50 uniformly spaced grid (from 10^{-1} to 5 in both directions) and the different graphs indicated in red ($7P$), green ($5P$), blue ($3P$) and purple ($1P$). The values of the leader's angular velocity $\omega_0\,(0)$ (in rad/s) are respectively 0.05 (a), 1 (b), 1.5 (c) and 2 (d).

of 50×50 uniformly spaced values of the gains a_{ij} and b_{ij}. The intervals, as well as the other conditions are the same of Figure 5.3. We also remark that the reduction in the number of values considered has been necessary due to computational time reasons.

Similarly to the plots shown in Figure 5.3, in Figure 5.10 we can see that when one of the gains is much greater than the other the average synchronization time tends to get higher, and this remains true for every one of the graphs considered. Furthermore, as the graph becomes more sparse, the different surfaces tend to "fold" towards high values of b_{ij} and low ones of a_{ij}, while concurrently their differences in the average synchronization time remain pretty much bounded. Finally, it is interesting to note that in pictures (d) and (c), when the gains values are far from the optimal region, a more sparse graph offers better synchronization times.

From the previous plots, for every graph and every value of $\omega_0\,(0)$, we extract the couples (K_q, K_ω) that give us the minimum value of the respective average synchronization times and we employ them as baseline values to explore the (β, σ^2) parameters spaces of control (5.8), in a similar fashion to what has been done for Figure 5.4. Again, for computational reasons, the exploration is limited to a 50×50 version of the uniformly spaced grid of Figure 5.4.

The results are plotted in Figure 5.11, where again we can observe that the average synchronization time gets higher for higher values of β. Furthermore, with the exception of the last picture, we find that for these values of β the smallest synchronization time is obtained for the

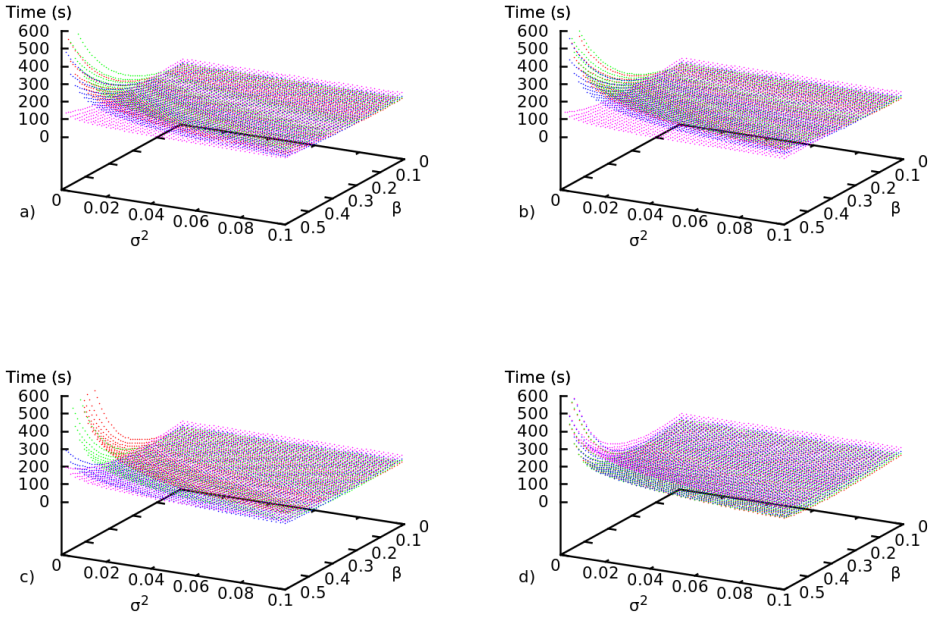

Figure 5.11: Average synchronization time for a 20 spacecraft formation as a function of the parameters β and σ^2 (equal for all the agents) via control (5.8), with a 50×50 uniformly spaced grid (with $\beta \in [10^{-2}, 0.05]$ and $\sigma^2 \in [0.005, 10^{-1}]$) and the different graphs indicated in red ($7P$), green ($5P$), blue ($3P$) and purple ($1P$). The values of the leader's angular velocity $\omega_0\,(0)$ (in rad/s) are respectively 0.05 (a), 1 (b), 1.5 (c) and 2 (d). Initial conditions correspond to those of Figure 5.10, while the values of (K_q, K_ω) can be looked upon in Figure 5.12.

sparsest graph, while the behaviour is reversed in the more optimal zones. Still, similarly to what happens in Figure 5.4, we always find a couple (β, σ^2) that improves on the corresponding synchronization time obtained in Figure 5.10 (albeit in this case the gain seems to be pretty minimal).

Starting from the optimal values of the previous plots, in Figure 5.12 we plot the evolution of the average synchronization time with respect to the magnitude of the initial angular velocity, both for control (5.7) (left) and (5.8) (right). Every plot corresponds to a different graph, going from $7P$ in the upper part to $1P$ in the lower one, and it contains this evolution as computed for the previously mentioned optimal values. Here we can clearly notice two facts that we have already mentioned: on one side the minimal improvement in time that we obtained with our adaptive control (remember that the advantage offered by every couple of gains must be evaluated at specific values of the initial angular velocity), while on the other the fact that for higher values of $\omega_0\,(0)$ (and more sparse graphs) one must also steadily increase the values of the gains.

To conclude this subsection, in the same fashion of Figure 5.5, in Figure 5.13 we consider again the evolution of the average synchronization time with respect to the dimension of the formation and for different permutations of the baseline configurations considered in the other plots of this section. In this case, the plots bear differences both in the communication graph

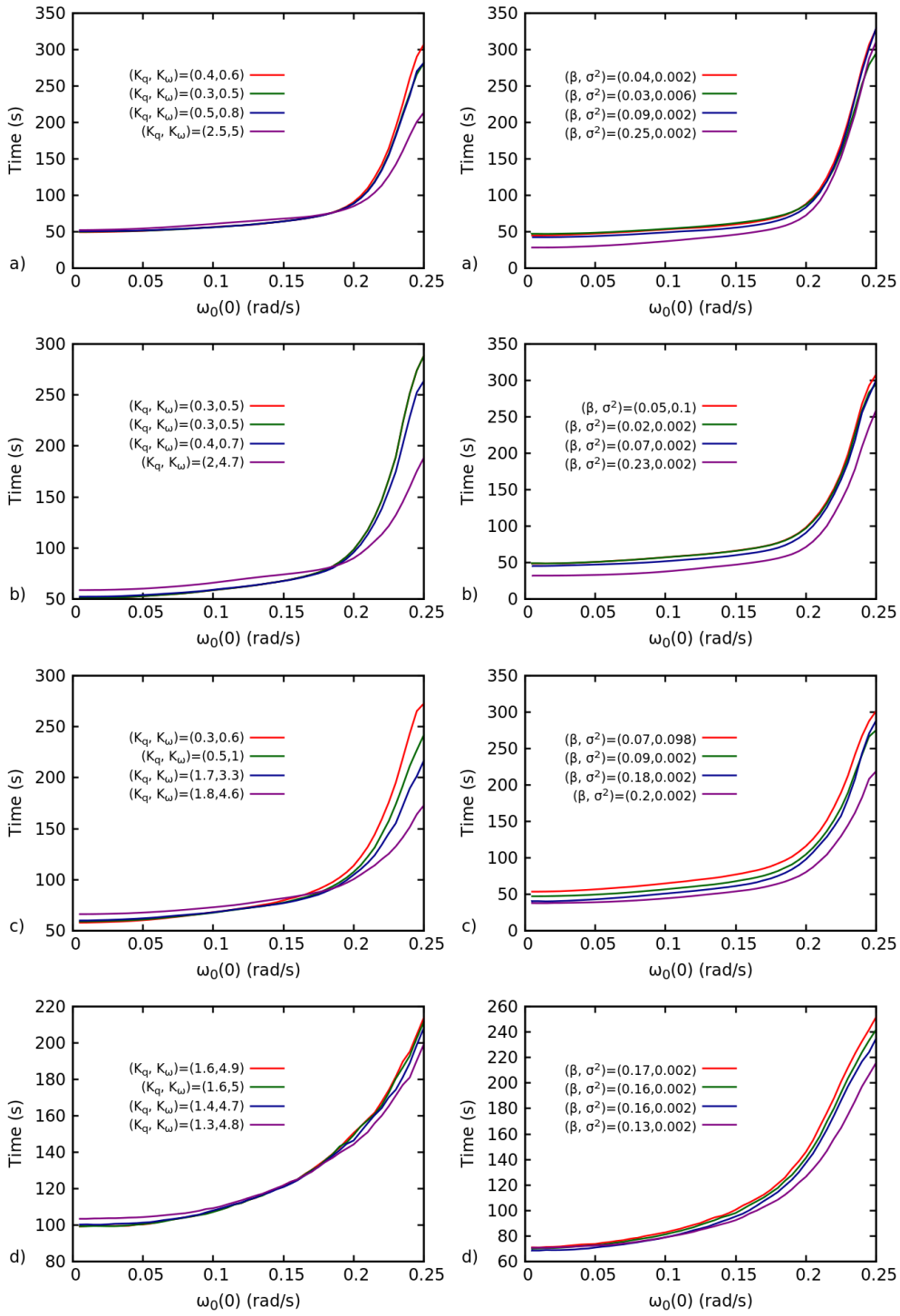

Figure 5.12: Average synchronization time for a 20 spacecraft formation as a function of the initial angular velocity of the formation's leader, both for control (5.7) (left) and (5.8) (right). The graphs are ordered from top to bottom as $7P$ (a), $5P$ (b), $3P$ (c) and $1P$ (d). For every plot, the optimal gains associated to the different values of $\omega_0\left(0\right)$ are indicated by the different colors: red (0.05), dark green (0.1), dark blue (0.15) and purple (0.2).

structure (indicated by different letters) and in the value of $\omega_0\left(0\right)$ (denoted by the different colors in the single plots). Again, we can see an advantage in employing the proposed adaptive design

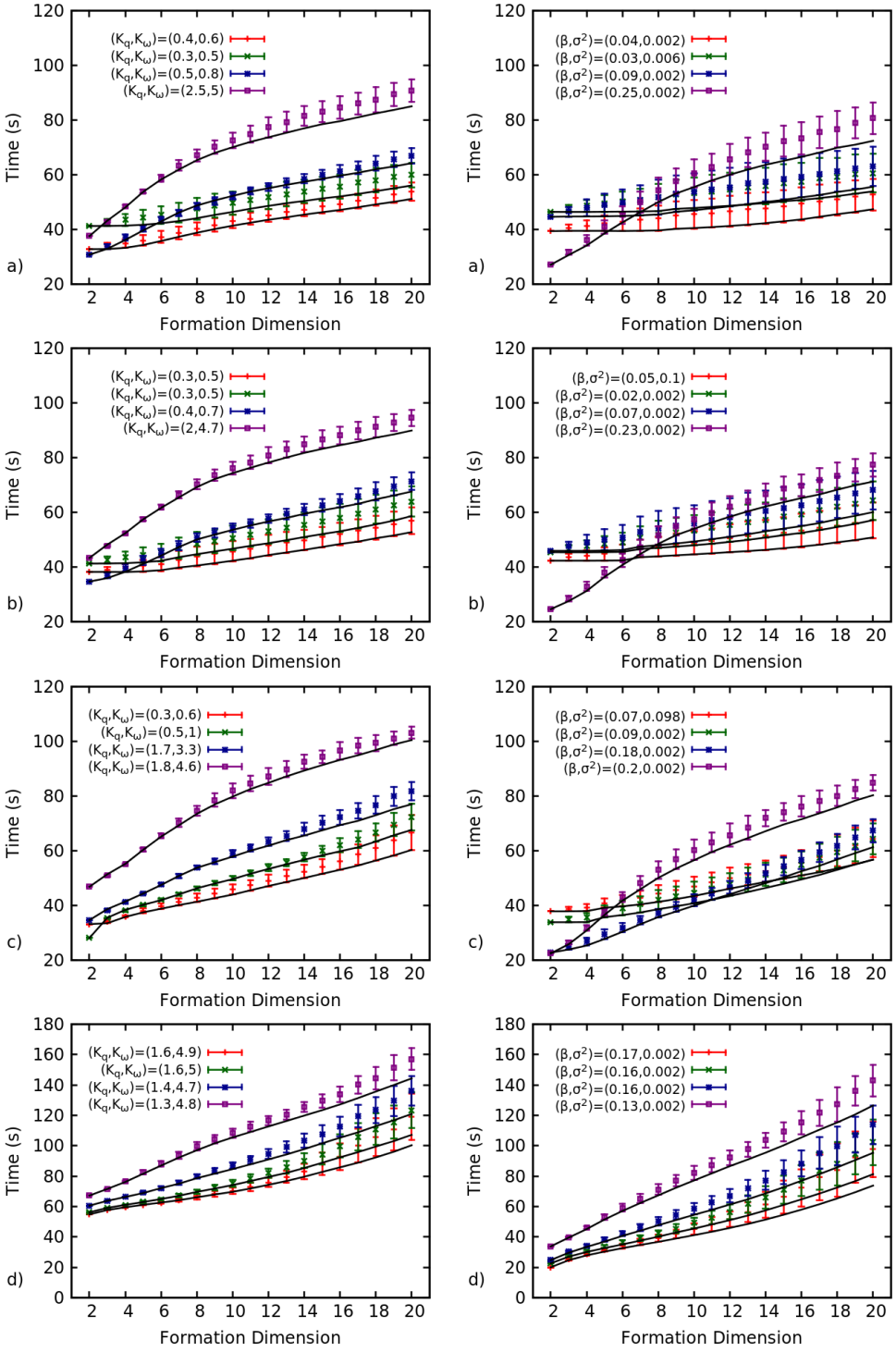

Figure 5.13: Synchronization time against formation dimension for 400 permutations of the baseline configurations considered in Figures 5.10 and 5.11, both for control (5.7) (left) and (5.8) (right). For every picture, different colors correspond to different leader's initial angular velocities: 0.05 (red), 0.1 (dark green), 0.15 (dark blue) and 0.2 (purple). The graph considered are, going from (a) to (d), $7P$, $5P$, $3P$ and $1P$, while the gains are indicated in the plots. For the adaptive case, the baseline K_q and K_ω are equal to those of the constant one.

(particularly in the rate of increase of the plots). Still, unless the value of $\omega_0\,(0)$ gets very high

or the graph becomes sparser, the gain obtained is not that significant. Of course, the latter is welcome news, since this may indicate the possibility of effective usage of less computationally expensive graph topologies.

5.4.2 Time varying spinning rate

In the present subsection we go a step further with respect to the previous one and we consider the closed loop dynamics induced by controls (5.7) and (5.8) for formations acting under a hierarchical leadership with a leader spinning at a time varying rate. The primary reason to conduct such an analysis is to understand if the controls that we have considered can effectively be applied in a real life scenario without the need of adding terms to compensate for the leader's dynamics. Of course, this is only a first step, since a rotating leader is not the only thing to take into account and its effect must be coupled with those generated by different perturbations acting on the formation.

On a very general level, one can define whatever acceleration signal one desires. In order to bring this work closer to reality, the reference scenario considered in this subsection is a keplerian one, where the formation orbiting a given primary is also trying to synchronize in order to form and maintain an interferometric array. What we want for this array is to rotate (in terms of attitude) with the same magnitude of the angular velocity of a reference keplerian orbit, in such a way that a strip defined by the array dimension and composition can be continuously observed either on the primary or on the surrounding space (depending whether we are looking inside or outside).

Since in this chapter we are considering only the attitude dynamics of the spacecraft, some hypotheses have to be made in order for the previous scenario to make sense:

- Assuming that we place the formation's leader on the (natural) reference orbit, it has to be possible to control it in such a way that it spins according to the previous requirements, so that the rest of the formation can track its motion via the controls defined in Section 5.2;

- It has to be possible to control the orbital motion of the other spacecraft in such a way that, in a frame relative to the leader and rotating with the angular velocity of the reference orbit, their velocities are zero, so that the interferometer structure is kept in time.

While the first hypothesis can be achieved with any attitude tracking control law, the second requires more specialized controls. As an example, in the proper time interval, one can exploit the Cucker-Smale control defined in Chapter 4.

To better describe the situation, we need to define some reference frames. In light of planned future expansions for this work, the model that we are going to introduce is taken from the work of Misra and Panchenko [169] and it takes into account elements that we do not need here, but that will be useful in the future. Therefore we describe it in its most encompassing case, pointing

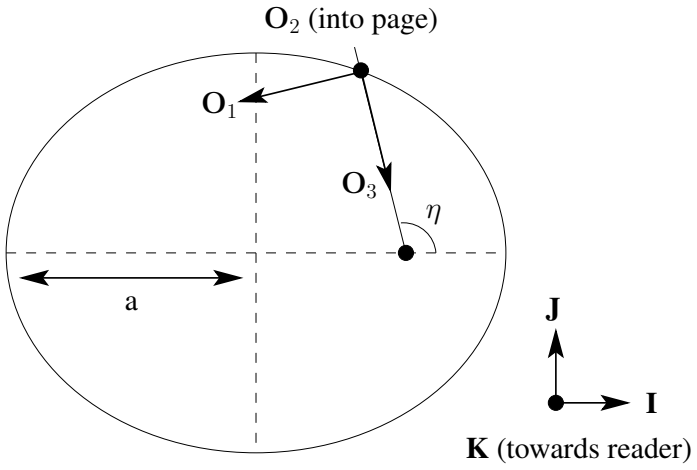

Figure 5.14: Reference frames adopted for the scenario of Sections 5.4.2 and 5.4.3.

out where appropriate how it restricts to the situation considered in this subsection. A graphical depiction of the situation can be found in Figure 5.14.

First, let us assume that the primary is rotating around one of its axis of inertia with angular speed Ω and let us fix as inertial a frame $(\mathbf{I}, \mathbf{J}, \mathbf{K})$ with axes parallel to the body's axes of inertia as given at a certain epoch (aligned respectively with the smallest, intermediate and largest one). Then, let us define a rotating frame $(\mathbf{I}', \mathbf{J}', \mathbf{K}')$ attached to the body, and therefore rotating with angular velocity $\Omega\mathbf{K}$ with respect to the inertial system. Of course, since in this subsection we are considering keplerian motion, this implies that $\Omega = 0$ and that the two frames coincide.

Now, along the reference orbit in the orbital plane (the equatorial one in our case), let us define a rotating frame $(\mathbf{O}_1, \mathbf{O}_2, \mathbf{O}_3)$ with the axes defined similarly to the Hill's frame of Chapter 3: $\mathbf{O}_3$ points towards the center of mass of the primary, $\mathbf{O}_1$ in the direction tangent to the orbit while $\mathbf{O}_2$ is defined as $\mathbf{O}_2 = \mathbf{O}_3 \times \mathbf{O}_1$ according to the right hand rule. In particular this frame is rotating with respect to the inertial one with an angular speed equal to the derivative $\dot{\eta}$ of the true anomaly.

Finally, for the leader of the formation, which is travelling along the reference orbit by hypothesis, we define a body fixed frame $(\mathbf{b}_1, \mathbf{b}_2, \mathbf{b}_3)$ to describe its attitude with respect to the inertial one (similar frames are defined implicitly for the other spacecraft). In particular, throughout this subsection, we assume that the leader is spinning around its $\mathbf{b}_2$ body axis with the same angular velocity of the orbital frame (in accordance with the second hypothesis mentioned before).

It is well known that in the keplerian motion the main factors that determine the instantaneous orbital velocity are the mass M of the primary, the semi-major axis a of the orbit and its eccentricity e. Thus, in line with what we have discussed in the previous subsection, it is only natural to ask in what amount these quantities affect the synchronization process of a formation defined as before.

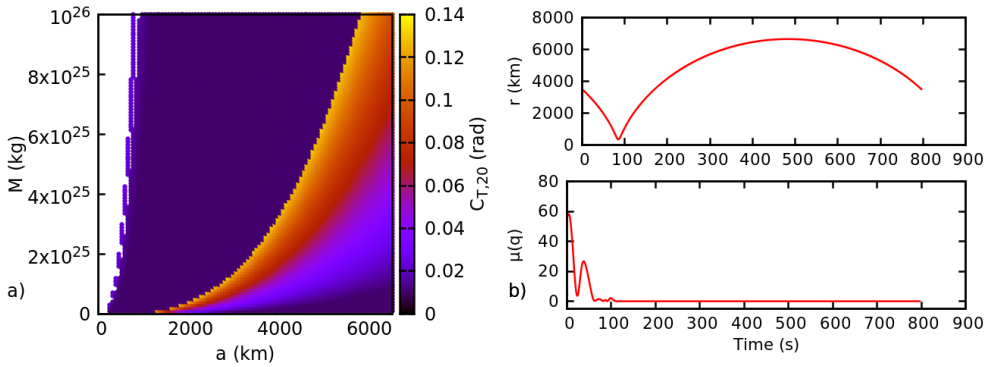

Figure 5.15: (a) Value of $C_{T,20}$ for a 20 spacecraft formation (under the dynamics induced by (5.7)) considered as a function of the reference orbit's semi-major axis a and the primary mass M, for an eccentricity of $e = 0.9$ and an integration time of one orbital period. (b) Time evolution of the reference radius r (top) and metric $\mu\left(q\right)$ (bottom) for the point $(a, M) = (3500, 4 \times 10^{25})$ up to one orbital period T. The formation is always inserted at $\eta = \frac{3}{2}\pi$ while the gains are defined as $K_q = 0.5$ and $K_\omega = 1$.

To check this, in Figure 5.15 (a) we plot the maximal geodesic distance

$$C_{T,N} = \max_{t\in[0,T]} \left(\max_{i=1,\dots,N} \phi\left(q_0, q_i\right) \right), \tag{5.30}$$

where T denotes the orbital period of the reference orbit. The latter is supposed having an eccentricity of 0.9, while the formation considered is the same 20 spacecraft one used as baseline in the previous subsections, with the leader inserted at $\eta = \frac{3}{2}\pi$ with inertial angular speed equal to $\dot{\eta}\mathbf{K}$. The graph considered for the formation is $7P$.

As you can see on the right of Figure 5.15, where we plot the time evolution of the reference orbit radius r and the metric $\mu\left(q\right)$ defined in Section 5.3.2 for the point $(a, M) = (3500, 4 \times 10^{25})$, the only problem that the formation is having is in the passage at the periaxis, where the angular speed may increase so much that the formation breaks and subsequently recovers synchronization.

Leaving aside for the moment the intervals of a and M employed, in the heat map we can distinguish areas with different behaviours. Points that are not plotted (white region) correspond of course to situations where the formation has not synchronized within the requested thresholds (which, differently from Section 5.3.1, have been relaxed to $10^{-2}\ rad$ and $5 \times 10^{-3}\ rad/s$ respectively) for the entire orbit. Points in the dark purple region correspond instead to situations where the synchronization happens roughly after the passage at the periaxis, so that the maximal value computed is exactly that of the threshold (after that consensus is just refined further). Finally, the rest of the points synchronize roughly before the arrival at periaxis but, depending on the level of synchronization achieved, suffer this passage with different degrees.

Of course, we can have border situations that depend on the spacecraft initial conditions. For example, if we look at Figure 5.16 (a), where we plot the time evolution of the $\mu\left(q\right)$ and $\nu\left(\omega\right)$ metrics for 35 sets of initial conditions corresponding to the point (a, M) of Figure 5.15 (b), we can see that the different orbits, although starting relatively clustered, may end up oscillating

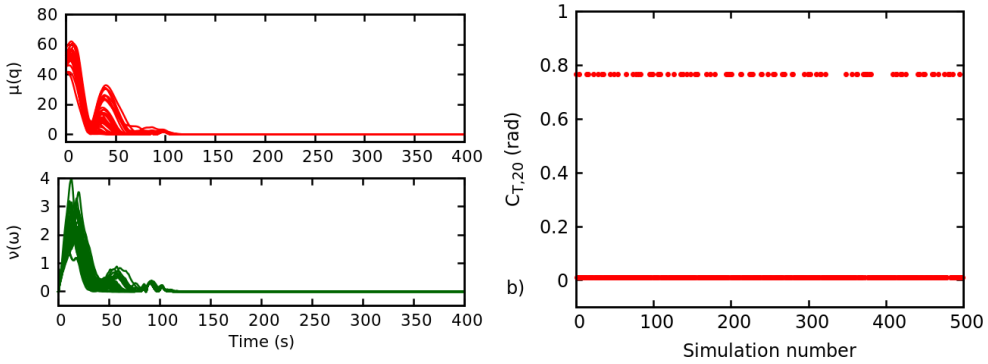

Figure 5.16: (a) Time evolution up to one orbital period of the metrics $\mu\,(q)$ and $\nu\,(\omega)$ for 35 sets of initial conditions associated to a 20 spacecraft formation in an orbit defined by $(a, M) = (3500, 4 \times 10^{25})$. (b) $C_{T,20}$ as a function of the simulation number for 500 sets of initial conditions associated to the previous formation. Other conditions are the same of Figure 5.15.

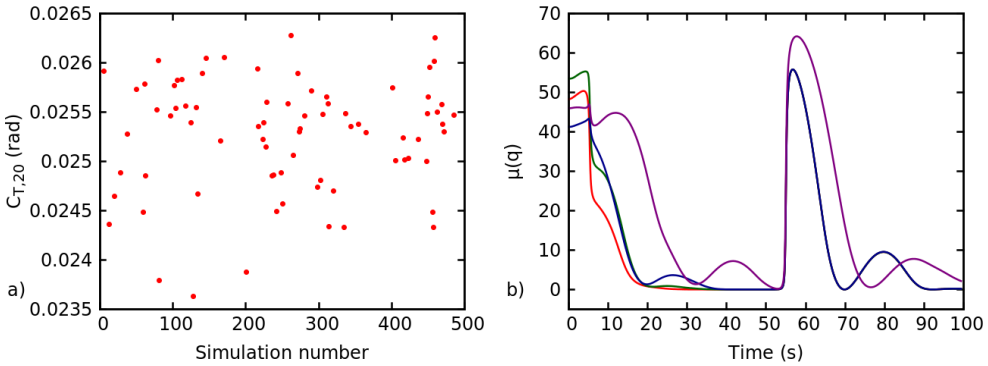

Figure 5.17: (a) $C_{T,20}$ as a function of the simulation number for 500 sets of initial conditions associated to a 20 spacecraft formation in an orbit defined by $(a, M) = (500, 3 \times 10^{25})$. (b) Time evolution up to two orbital periods of the metric $\mu\,(q)$ for 4 sets of initial conditions associated to the previous formation. Other conditions are the same of Figure 5.15.

with different amplitudes. Thus, due to the way in which we distinguish them, some of them may be recognized as in a synchronization status after the passage at periaxis. This can be observed clearly on the right of Figure 5.16, where the value of $C_{T,20}$ for each set is plotted against the number of this same set and where the quantity of this sets has been increased to 500. In this plot we can see that the orbits synchronizing before the passage achieve more or less the same maximal displacement, while the rest have a value of $C_{T,20}$ in the proximity of the threshold.

The previous describes what happens in grey area defined by the purple zone. The other type of border conditions can be found in the transition between the previous zone and the white one. This, as shown in Figure 5.17, represents points for which most of the sets of initial conditions (a) need more than one orbital period to synchronize (b).

Now, what is important to note about this map lies in the values considered for a and M. What these are apparently saying is that, unless the primary is extremely small and massive, the passage at the periaxis does not cause any significant synchronization loss in the formation.

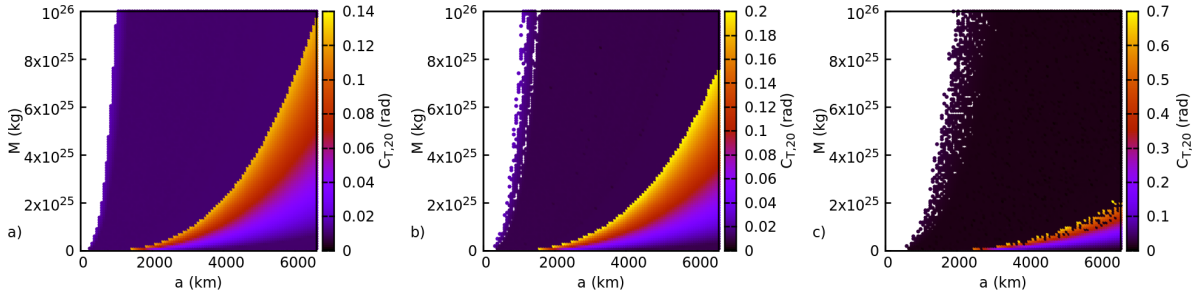

Figure 5.18: Value of $C_{T,20}$ for a 20 spacecraft formation (under the dynamics induced by (5.7)) considered as a function of the reference semi-major axis a and the primary mass M, for an eccentricity of $e = 0.9$ and an integration time of one orbital period. The graphs considered are $5P$ (a), $3P$ (b) and $1P$ (c).

However, we have seen in the previous section how the dimension of the formation and the graph structure may change significantly the closed-loop dynamics. In the present scenario, the latter does not seem to give too many problems in the sense that, if we look at Figure 5.18, where we have plotted the same heat map of Figure 5.15 for the graphs $5P$ (a), $3P$ (b) and $1P$ (c), even if the values of $C_{T,20}$ for the same points are increasing, it can be guessed that no real primary is going to lie in the problematic zones (for example, an Earth low altitude orbit consistently gives values below $10^{-2}\ rad$, as can be seen in the lower right corner of the plots).

The same happens with the dimension of the formation. To clarify, let's look at Figure 5.19 (a), where we have plotted the value of $C_{T,N}$ against the dimension of the formation (considered with only one set of initial conditions) for $(a, M) = (6478.14, 5.97237 \times 10^{24})$ (top) and $(a, M) = (2017.72, 1.52971 \times 10^{25})$ (bottom). In both cases, the formation is inserted at the apoaxis, so that we can be assured of its synchronization in rapid times (due to the low angular velocity), and with a $7P$ communication graph.

The plot on the bottom, taken with clearly unrealistic values, shows us what happens eventually to every formation considered. For low dimensions, we can observe a steady increase in the maximal geodesic distance related with the fact that the graph structure is not changing to compensate for the growing dimension. Sometimes, this can be preceded by a small plateau at the selected threshold height, given by the fact that no significant desynchronization is observed during the passage at periaxis. Another plateau is found at height π, which is of course the absolute maximal geodesic distance (since the rotation direction does not count). Finally, we observe again a drop at the threshold height, where formations are now synchronizing after the periaxis, followed by an empty region signalling formations that are not able to synchronize within one orbital period.

While theoretically this behaviour should be observed wherever we put our formation, we can see in the top of Figure 5.19 that in a realistic scenario the growth rate with respect to the dimension is so small to require extremely large formations (in the case of cubesats) for the value of $C_{T,N}$ to become significant. Furthermore, as we can see on the right of the same figure, where the value of $C_{T,N}$ for the formation on the left is considered for different initial conditions and

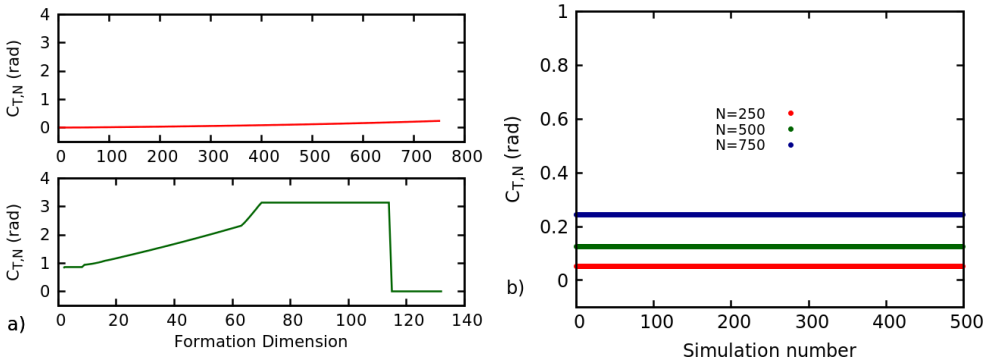

Figure 5.19: (a) Value of $C_{T,N}$ as a function of the dimension of the formation, with the latter considered at $(a, M) = (6478.14, 5.97237 \times 10^{24})$ (top) and $(a, M) = (2017.72, 1.52971 \times 10^{25})$ (bottom), inserted at the apoaxis and evolved up to one orbital period. (b) Value of $C_{T,N}$ as a function of the sets of initial conditions considered for different values of N.

different dimensions, these results appear to be independent of the initial conditions (at least at relatively low dimensions), and therefore define a strict behaviour of the formations.

5.5 Conclusion

In this chapter we have studied the problem of attitude synchronization in spacecraft formation flying, with the double goal of understanding some aspects of the dynamics and exploit the latter in order to improve the performance of common control laws used for this purpose. In particular, for this analysis we have considered a standard PD-like control law alongside a possible adaptive modification of it. Starting from the study of the average parameters spaces of the two control laws, with a formation moving in free space, we have derived " optimal " parameters for both controls, in the sense of best performance in terms of average synchronization time, for a given configuration of the formation. By employing these parameters, we have compared the evolution of the synchronization time with respect to the dimension of the formation for both controls and for different arrangements of the initial conditions within the same graph structures, included the configuration used to derive the parameters. Finally, driven by some of the results obtained, we have reduced the problem to the tracking case (leader-follower configuration), where we have shaped the previous analysis in order to obtain additional informations on the behaviour of the controls considered.

Subsequently, we have extended the previous study to the case of formations synchronizing under a leader with a time changing trajectory. As a first step, we have considered the case of a leader moving with constant angular velocity, where, by direct application of the method developed before, we have managed to describe quantitavely the dependence of the average synchronization time with respect to the magnitude of the leader's spin rate. Secondly, we have generalized the previous scenario by considering a leader rotating with a time-varying rate. In particular, by considering a formation synchronizing in order to build and maintain an

interferometer in a keplerian context, we have shown, similarly to what done in Chapter 4, the strong dependence from the leader's orbit semi-major axis and the mass of the primary.

The main result of this chapter lies in the numerical evidence showing the advantage, given a hierarchical graph structure, of using the proposed adaptive design over a standard quaternion feedback control, both for a three-axis stabilized leader and for a spin-stabilized one. At the same time, we have established a mixed numerical and analytical approach, relying on a particular graph structure, which has allowed us to obtain an almost global description of the closed-loop dynamics induced by the proposed controls.

Chapter 6

Conclusion and open problems

This Ph. D. thesis has addressed the problem of designing distributed control algorithms for spacecraft formation flying, that is control laws where the spacecraft exchange data between themselves in order to achieve the desired formation state. In particular, we have focused on linear algorithms, where the spacecraft define their accelerations through linear combinations of the states that they want to bring to consensus, that is to the same numerical value. Finally, out of all the possible formation dynamics where these algorithms can be employed, we have considered only those of formation acquisition and maintenance on the translational side, and attitude synchronization on the rotational one.

In regard to the first dynamics, in Chapter 4 we have expanded on the development of a novel distributed, adaptive control strategy (indicated as the Cucker-Smale control) aimed to asymptotically cancel the spacecraft relative velocities, so that the relative positions may remain fixed in time. This strategy, as it was originally introduced, was used to maintain a three spacecraft formation travelling along a transfer orbit to the L_2 Sun-Earth libration point. In order to conserve the triangular shape selected, the control was applied under an undirected connected communication graph.

As we observed in Section 4.3.3, employing an undirected graph with the control's chosen design requires a careful placement of the reference orbit around which the formation is travelling. In particular, the velocity vector of an imaginary particle travelling along this orbit should correspond to the sum of the spacecraft velocities normalized by the formation's dimension, which is exactly the velocity reached at consensus by the spacecraft. Failing to do so still allows the spacecraft to achieve consensus, but the formation will end up in a different region of the phase space.

Thus, our first contribution lies in observing that this problem can be easily overcome if it is possible for the spacecraft to automatically reach the velocity of the reference by applying the Cucker-Smale control. In light of the literature presented in Section 3.1, this is possible if the control is applied under a hierarchical graph, that is a directed graph with spanning tree where, assuming a natural indexation of the formation as $[1, \dots, N]$, each numbered spacecraft receives

informations only from those associated to smaller numbers. This means that, for the formation to achieve both consensus and trailing of the reference, it is sufficient to define as root of the graph a particle (real or imaginary) travelling along this same reference orbit. It is important to note that using a hierarchical graph is only a sufficient condition for achieving the previous objective. Consequently, as seen in Chapter 2 for different consensus models, it is possible that the same result can be obtained for a general digraph with a spanning tree, without requiring any hierarchy in the formation. While such generalization was beyond the goals of the thesis, it may be readily addressed in the future in conjuction with the other issues that we mention below.

Our second improvement has a more general scope, and lies in a deeper analysis on how the relative dynamics of the spacecraft affects the control's performance. This was motivated by the fact that, over long periods of application, the main cost of the Cucker-Smale control comes exactly from compensating for the relative dynamics and not from bringing the spacecraft to consensus (see Figure 4.4). Thus, taking a step back from the transfer orbits mentioned before, we have considered the simplest possible situation of a formation travelling around a primary and applying the Cucker-Smale control in order to achieve and maintain a definite shape for the entire operational time. By studying the dynamics in the Hill's frame relative to a circular, keplerian reference orbit we have observed that the in-plane and out of plane motions can be separated, and that for the former it is trivial to define, at parity of distance from the reference, the positions of minimal and maximal relative acceleration. Thus, we have exploited independent and aptly placed couples leader-follower (with the leader travelling on the reference) to study the effects of the relative accelerations in these extremal situations. This study have been conducted by observing the time variation of two metrics (maximal variation of the intervehicle distance and total thrust integral) with respect to control and dynamical parameters. The first metric told us how much the relative dynamics affects the speed of consensus achievement, while the second indicated how much the control's cost is affected by it. The results have shown that in the dynamical situation considered, applying the Cucker-Smale control in the suggested form is not feasible even for moderate periods of time, due to the fact that reasonable application costs can be reached only with the follower in the along-track direction (minimal relative acceleration), and even then a large semi-major axis for the reference orbit and moderate relative distances are required to achieve a low cost. Do note that the effects of these quantities are not equally important, since a lower semi-major axis must always be compensated by a lower relative distance, up to the point of risking collisions.

The previous conclusions seems to indicate (more on that in the next paragraph) that the Cucker-Smale control, in its current form, can be applied under the effects of gravitation for reasonable amounts of time only when the dominant term of the relative acceleration becomes the relative distance (which has a linear growth) instead of the distance from the main mass (which is cubic). Thus, in order to confirm the previous conclusions and show the potential of the proposed control in a favourable condition, we have considered a different mission objective, which builds upon the proposed scientific goals for the extended LISA Pathfinder mission. In particular, we

have taken a formation travelling on elliptical orbits around the Earth and periodically visiting the Sun-Earth-Moon saddle point (within the context of a planar bicircular model), a location deemed suitable to perform relativity experiments with the previous mission. Furthermore, we have supposed that, in order to perform interferometric operations, the formation's spacecraft apply a simplified Cucker-Smale control (constant gains instead of adaptive) in a neighborood of the saddle point (characterized as apogee of the previous orbits) at each successive visit, with shooting maneuvers performed at the orbits perigees in order to encounter again the saddle point at a successive time. Limiting ourselves to consider again only couples leader-follower moving coplanarly with the main masses, we have first analyzed the performance of the Cucker-Smale control in terms of the neighborood "dimension", that is the magnitude of the gravitational acceleration of the leader, and the interveichle distance, showing that in this case the cost of the control remains of the order of mm/s even for an operational time of roughly two years with multiple windows of control application each spanning tens of days. Futhermore, by fixing a value for the threshold and one for the relative distance, we have discussed the limitations of the control in terms of number of maneuvers and magnitude of the gains, showing that too strong or too weak a thrust causes the intervehicle distance to grow excessively, thus destroying the formation over the course of a few orbits. Finally, we have focused on the shooting maneuvers, showing on one side that, for the their cost to be of the same order of the control, the perigee of the orbits should be chosen to be sufficiently high (almost approaching circularization), while on the other that, while normally some of the visits miss the saddle point (since the latter's distance from the Earth changes), it is possible to adjust the semi-major axis of the orbits (in order to always encounter the saddle point) without changing too much the total cost of the shooting maneuvers.

If we combine toghether the results discussed in the last two paragraphs, we can infer that areas where the Cucker-Smale control works best involve a weak gravitational field, and this holds even for relatively large intervehicle distances. However, in the analysis performed before no study of the vector's field gradients has been done, thus it is not possible to draw a rigorous estimate of the necessary balance between the two for the application of the current version of the Cucker-Smale control. In regard to the latter, some matters about its design have to be addressed in the future. The major one concerns the control's dependence on the direct cancellation of the relative accelerations terms (subsequently substituted with a consensus algorithm). This of course restricts the control's applicability to mission scenarios satisfying the conditions above, thus it is only reasonable to ask if it is necessary to cancel the relative accelerations. On the other side, when dealing with the saddle point's visits, we have adopted a version of the control devoid of its adaptive design, and we have shown that the relative distances remain more or less fixed. Thus, since these distances are an integral part of the adaptive gains definition, it is necessary to ask if and when this design should be used for the translational control. The last matter about the control's design that has to be addressed is its lack of robustness, primarily against collisions between the spacecraft, and secondarily against failures of different kinds that

may affect the time invariance of the communication graph. However, since these add additional layers of complexity to the problem, they may be put after the other issues mentioned.

Do note that all the previous observations refer to the analytical design of the control. Practically speaking however, there is another issue in the analysis conducted up to now, and this is the fact that the control's characteristics have been explored only with leader-follower couples. Enlargening the formation is not a computational problem, since, as discussed later in this section, we can exploit parallelization and hierarchical graphs to study formations of very large dimensions. However, while the factors determining a possible application of the Cucker-Smale control are probably equal (the same characteristics of the relative accelerations, just spread over different spacecraft), this has to be verified and a proper formation for the feasible mission objectives must be established in connection with the graph used (for example, if a hierarchical graph is used it would make sense to work with a wedge formation, or with circular layers corresponding to different communication levels).

Coming to Chapter 5, here we have considered the problem of distributed attitude synchronization, that is the problem of designing distributed control laws for spacecraft in a formation to achieve the same rotational state, both in terms of attitude and angular velocity. The starting goal of this chapter has been to develop an adaptive design capable of improving the consensus rate of standard PD-like controls with constant gains. In order to do so we have parametrized the rotation group by using quaternions, and we have subsequently introduced a PD-like distributed control law aimed to synchronize the attitude dynamics of the spacecraft. This control, introduced as benchmark, has been selected among a list of possible candidates in the literature, according to the condition of being as simple as possible (thus, no additional terms are present to deal with perturbations, for example).

In light of the stated synchronization objective, the selected control rests of course on two sets of gains for consensus, one for the quaternions and one for the angular velocities. The author that first introduced this control proved consensus under it only with constant gains and an undirected connected communication graph. Furthermore, as far as we know, there have been in the literature no discussions about the associated rate of consensus. Thus, in order to introduce our adaptive design, our first contribution has been to prove that consensus under this control law can be reached even when the gains associated to the angular velocities change with time (but do not explicitly depend by it, thus keeping the controlled system autonomous). Furthermore, we have proved exponential convergence for this control, also explicitating its dependence from the formation's dimension and the gains structure. In light of these results, we have constructed our adaptive design in a manner equivalent to the Cucker-Smale control (scaling them with respect to their rotational distance, also adding some parameters to calibrate the gradient) and proved its advantage under an undirected connected communication graph.

Similarly to the translational case, the interesting instance of the control lies in driving the spacecraft towards a rotational state defined a priori through the presence of a formation's leader, and thus a digraph with a spanning tree. While an analytical, deterministic description has for

the moment eluded us, overcoming this obstacle has actually brought out a different kind of contribution from this work. Specifically, we have shown that if one reduces itself to consider only hierarchical graphs, it is possible to conduct computationally fast MonteCarlo simulations to explore the dynamics determined by the controlled equations of motions.

By considering multiple sets of initial conditions, we have defined the associated average synchronization time (where the spacecraft are assumed to be synchronized if certain magnitude thresholds for the relative quaternions and angular velocities are reached). By assuming the control gains to be constant and, for each of the two sets, equal for all the agents, we have drawn discrete heat maps representing these times for each gains couple and for different hierarchical graph structures. While this has been done for a single formation dimension, we have also proved that, thanks to the hierarchical structure of the graph, the values obtained constitute upper bounds for formations with lower ones. Starting from the minimal value obtained, we have repeated the simulations with our adaptive design and showed that it is always possible to adjust the control parameters in order to achieve a better synchronization time.

However, in the experiments above we have considered a particular uniform distribution of the initial conditions, that is, once randomly generated, we have arranged them in such a way that the farther a spacecraft is in the indexation, the larger is its rotational distance from the formation's leader. Thus, in order to show more thoroughly the advantage of our adaptive design, we have considered, for every successive, increasing formation dimension (where additional spacecraft were added to the already existing ones), multiple sets of initial conditions constructed by shuffling the previous one, and, for each of them, repeated the same simulations of the previous paragraph, working with a single gains couple for all the graphs in the constant case, and using, for each graph, the adaptive control parameters derived for the baseline configuration at largest dimension. While at first glance numerically heavy, since for each growing set of initial conditions one should integrate $N!$ equations to perform these simulations, we have shown that by exploiting the graph's hierarchical structure it is possible to reduce the computational cost to $O(N)$. Besides confirming the advantage of our adaptive control, these simulations have given us and idea of its dependence from the formation's dimension and initial conditions, and this is true both for a three-axis and spin stabilized leader (where for the latter different angular velocities have been considered and, for the gains derived by studying the baseline configuration, also the average synchronization time dependence from this velocity has been studied). The case of an accelerating leader has been also touched very briefly, with this acceleration supposed to derive from the necessity of rotating the formation's leader in order to observe a given primary. Main objective of the section has been to check the robustness of the control under this kind of acceleration, and the simulations performed seems to indicate that, as long as the formation is not too large and the graph not too sparse, synchronization can still be reached.

The major shortcoming of this chapter is of course the lack of proper analytical results supporting the simulations done. While we managed to describe completely the undirected case, the same cannot be said for the directed one. Thus, studying analytically the latter should be

the first priority of an eventual expansion, with a natural simplification of the problem lying in restricting ourselves to hierarchical graphs. Similarly to the undirected connected case, this analysis can be conducted first without assuming any limitation on the torque applicable by the spacecraft, which however should be added as a second step in order to get closer to a more realistic situation. This can be obtained also by extending the control to deal with different situations (perturbations, time-varying graphs and so on), in a manner similar to what proposed for the control of Chapter 4. Finally, each of these step should proceed in parallel with the comparison of the proposed control and adaptive design to other already existing in the literature, in order to understand if and what kind of advantages they offer with respect to those.

Bibliography

[1] Matt Long, Aaron Gage, Robin Murphy, and Kimon Valavanis. Application of the Distributed Field Robot Architecture to a Simulated Demining Task. In *Proceedings of the 2005 IEEE International Conference on Robotics and Automation*, pages 3193–3200, Barcelona, Spain, 2005.

[2] Randal W. Beard, T. W. Mclain, D. B. Nelson, Derek B. Kingston, and D. Johanson. Decentralized Cooperative Aerial Surveillance Using Fixed-Wing Miniature UAVs. In *Proceedings of the IEEE*, volume 94(7), pages 1306–1324, 2006.

[3] Daniel J. Stilwell and Bradley E. Bishop. Platoons of Underwater Vehicles: Communication, Feedback and Decentralized Control. *IEEE Control Systems Magazine*, 20(6):45–52, 2000.

[4] Stephen G. Ungar, Jay S. Pearlman, Jeffrey A. Mendenhall, and Dennis Reuter. Overview of the Earth Observing One (EO-1) Mission. *IEEE Transactions on Geoscience and Remote Sensing*, 41(6):1149–1159, 2003.

[5] C. Fridlund. The Darwin Mission. *Advances in Space Research*, 34(3):613–617, 2004.

[6] J. Christensen-Dalsgaard, K.G. Carpenter, C.J. Schrijver, and M. Karovska. The Stellar Imager (SI) - A Mission to Resolve Stellar Surfaces, Interiors, and Magnetic Activity. In *Journal of Physics: Conference Series*, volume 271, 2011.

[7] C.A. Beichman, N.J. Woolf, and C.A. Lindensmith. The Terrestrial Planet Finder (TPF): a NASA Origins Program to search for habitable planets. Technical report, JPL Publication 99-003, 1999.

[8] G. Rousset, L. Mugner, C. Frederic, and B. Sorrente. Imaging with multi-aperture optical telescopes and an application. *Comptes Rendus de l'Académie des Sciences - Series IV - Physics*, 2(1):17–25, 2001.

[9] R. Burns, C.A. McLaughlin, J. Leitner, and M. Martin. TechSat 21: formation design, control, and simulation. In *Proceedings of the 2000 IEEE Aerospace Conference*, volume 7, pages 19–25, Big Sky, MT, 2000.

[10] X.-M. Shao, W. Junor, A. Rogers, R. Zenick, and K. Dighe. Passive interferometric millimeter-wave imaging: achieving big results with a constellation of small satellites. In *SPIE Proceedings*, volume 5410, pages 270–277, 2004.

[11] A.S. Sharma and S.A. Curtis. Magnetospheric Multiscale Mission. In *Nonequilibrium Phenomena in Plasmas*, volume 321 of *Astrophysics and Space Science Library*, chapter 8, pages 179–195. Springer Netherlands, 2005.

[12] D.P. Scharf, F.Y. Hadaegh, and S.R. Ploen. A Survey of Spacecraft Formation Flying Guidance and Control (Part II): Control. In *Proceedings of the 2004 American Control Conference*, volume 4, pages 2976–2985, Boston, MA, 2004.

[13] G.J.W. Mallory. *Development and Experimental Validation of Direct Controller Tuning for Spaceborne Telescopes*. PhD thesis, Massachusetts Institute of Technology, 2000.

[14] S.-J. Chung and D.W. Miller. Propellant-Free Control of Tethered Formation Flight, Part 1: Linear Control and Experimentation. *AIAA Journal of Guidance, Control and Dynamics*, 31(3):571–584, 2008.

[15] E.M.C. Kong, D.W. Kwon, S.A. Schweighart, L.M. Elias, R.J. Sedwick, and D.W. Miller. Electromagnetic Formation Flight for Multisatellite Arrays. *Journal of Spacecraft and Rockets*, 41(4):659–666, 2004.

[16] P.K.C. Wang and F.Y. Hadaegh. Coordination and Control of Multiple Microspacecraft Moving in Formation. *Journal of the Astronautical Sciences*, 44(3):315–355, 1996.

[17] P.K.C. Wang, F.Y. Hadaegh, and K. Lau. Synchronized Formation Rotation and Attitude Control of Multiple Free-flying spacecraft. *AIAA Journal of Guidance, Control and Dynamics*, 22(1):28–35, 1999.

[18] J.R. Lawton and R.W. Beard. Synchronized Multiple Spacecraft Rotations. *Automatica*, 38(8):1359–1364, 2002.

[19] M.C. VanDyke and C.D. Hall. Decentralized Coordinated Attitude Control Within a Formation of Spacecraft. *AIAA Journal of Guidance, Control and Dynamics*, 29(5):1101–1109, 2006.

[20] V. Borkar and P. Varaiya. Asymptotic Agreement in Distributed Estimation. *IEEE Transactions on Automatic Control*, 27(3):650–655, 1982.

[21] J. Tsitsiklis. *Problems in Decentralized Decision Making and Computation*. PhD thesis, Massachusetts Institute of Technology, 1984.

[22] J. Tsitsiklis, D. Bertsekas, and M. Athans. Distributed Asynchronous Deterministic and Stochastic Gradient Optimization Algorithms. *IEEE Transactions on Automatic Control*, 31(9):803–812, 1986.

[23] A. Okubo. Dynamical aspects of animal grouping: Swarms, schools, flocks, and herds. *Advances in Biophysics*, 22:1–94, 1986.

[24] C.W. Reynolds. Flocks, herds, and schools: A distributed behavioral model. *Computer Graphics*, 21(4):25–34, 1987.

[25] C.M. Breder. Equations Descriptive of Fish Schools and Other Animal Aggregations. *Ecology*, 35(3):361–370, 1954.

[26] A. Jadbabaie, J. Lin, and A.S. Morse. Coordination of Groups of Mobile Autonomous Agents Using Nearest Neighbor Rules. *IEEE Transactions on Automatic Control*, 48(6):988–1001, 2003.

[27] J.A. Fax and R.M. Murray. Information Flow and Cooperative Control of Vehicle Formations. *IEEE Transactions on Automatic Control*, 49(9):1465–1476, 2004.

[28] Z. Lin, B. Francis, and M. Maggiore. Necessary and Sufficient Graphical Conditions for Formation Control of Unicycles. *IEEE Transactions on Automatic Control*, 50(1):121–127, 2005.

[29] L. Moreau. Stability of Multiagent Systems with Time-Dependent Communication Links. *IEEE Transactions on Automatic Control*, 50(2):169–182, 2005.

[30] W. Ren and R.W. Beard. Consensus Seeking in Multiagent Systems Under Dynamically Changing Interaction Topologies. *IEEE Transactions on Automatic Control*, 50(5):655–661, 2005.

[31] A. Olshvesky and J. Tsitsiklis. Convergence Rates in Distributed Consensus and Averaging. In *Proceedings of the 45th IEEE Conference on Decision and Control*, pages 3387–3392, San Diego, CA, 2006.

[32] V.D. Blondel, J.M. Hendrickx, A. Olshvesky, and J. Tsitsiklis. Convergence in Multiagent Coordination, Consensus, and Flocking. In *Proceedings of the 44th IEEE Conference on Decision and Control*, pages 2996–3000, Seville, Spain, 2005.

[33] R. Olfati-Saber. Flocking for Multi-Agent Dynamic Systems: Algorithms and Theory. *IEEE Transactions on Automatic Control*, 51(3):401–420, 2006.

[34] G. Cybenko. Dynamic Load Balancing for Distributed Memory Multiprocessors. *Journal of Parallel and Distributed Computing*, 7(2):279–301, 1989.

[35] D.P. Bertsekas and J.N. Tsitsiklis. *Parallel and Distributed Computation: Numerical Methods*. Prentice Hall, 1997.

[36] R. Diekmann, S. Muthukrishnan, and M.V. Nayakkankuppam. Engineering Diffusive Load Balancing Algorithms Using Experiments. In *Proceedings of the 4th International Symposium on Solving Irregularly Structured Problems in Parallel*, volume 1253 of *Lecture Notes in Computer Science*, pages 111–122. Springer Berlin/Heidelberg, 1997.

[37] J. Zhao, R. Govindan, and D. Estrin. Computing Aggregates for Monitoring Wireless Sensor Networks. In *Proceedings of the First IEEE International Workshop on Sensor Network Protocols and Applications*, pages 139–148, Anchorage, AK, 2003.

[38] D.S. Scherber and H.D. Papadopoulos. Distributed Computation of Averages Over Ad Hoc Networks. *IEEE Journal on Selected Areas in Communications*, 23(4):776–787, 2005.

[39] D.P. Spanos, R. Olfati-Saber, and R. Murray. Dynamic Consensus for Mobile Networks. In *Proceedings of the 16th IFAC World Congress*, Prague, Czech Republic, 2005.

[40] L. Xiao, S. Boyd, and S. Lall. A Scheme for Robust Distributed Sensor Fusion Based on Average Consensus. In *Fourth International Symposium on Information Processing in Sensor Networks*, pages 63–70, Los Angeles, CA, 2005.

[41] C.C. Mollaemi and B. Van Roy. Consensus Propagation. *IEEE Transactions on Information Theory*, 52(11):4753–4766, 2006.

[42] I.D. Schizas, A. Ribeiro, and G.B. Giannakis. Consensus in Ad Hoc WSNs With Noisy Links-Part I: Distributed Estimation of Deterministic Signals. *IEEE Transactions on Signal Processing*, 56(1):350–364, 2008.

[43] R.E. Mirollo and S.H. Strogatz. Synchronization of Pulse-Coupled Biological Oscillators. *SIAM Journal on Applied Mathematics*, 50(6):1645–1662, 1990.

[44] T. Vicsek, A. Czirók, E. Ben-Jacob, I. Cohen, and O. Schochet. Novel Type of Phase Transition in a System of Self-Driven Particles. *Physical Review Letters*, 75(6):1226–1229, 1995.

[45] V.N. Belykh, I.V. Belykh, and M. Hasler. Connection Graph Stability Method for Synchronized Coupled Chaotic Systems. *Physica D: Nonlinear Phenomena*, 195(1-2):159–187, 2004.

[46] Y.-W. Hong and A. Scaglione. A Scalable Synchronization Protocol for Large Scale Sensor Networks and its Applications. *IEEE Journal on Selected Areas in Communications*, 23(5):1085–1099, 2005.

[47] S. Barbarossa. Self-organizing sensor networks with information propagation based on mutual coupling of dynamic systems. In *Proceedings of the International Workshop on Wireless Ad-hoc Networks*, London, UK, 2005.

[48] S. Barbarossa and F. Celano. Self-Organizing Sensor Networks Designed as a Population of Mutually Coupled Oscillators. In *Proceedings of the IEEE Workshop on Signal Processing Advances in Wireless Communications*, pages 475–479, New York, US, 2005.

[49] M. Porfiri, D.J. Stilwell, and E.M. Bollt. Synchronization in Random Weighted Directed Networks. *IEEE Transactions on Circuits and Systems*, 55(10):3170–3177, 2008.

[50] R. Olfati-Saber and R.M. Murray. Consensus Problems in Networks of Agents with Switching Topology and Time-Delays. *IEEE Transactions on Automatic Control*, 49(9):1520–1533, 2004.

[51] P. Closas, E. Calvo, J.A. Fernández-Rubio, and A. Pagès-Zamora. Coupling noise effect in self-synchronizing wireless sensor networks. In *Proceedings of the 8th IEEE Signal Processing Workshop on Signal Processing Advances in Wireless Communications*, Helsinki, Finland, 2007.

[52] G. Scutari, S. Barbarossa, and L. Pescosolido. Optimal Decentralized Estimation Through Self-Synchronizing Networks in the Presence of Propagation Delays. In *Proceedings of the 7th IEEE Signal Processing Workshop on Signal Processing Advances in Wireless Communications*, Cannes, France, 2006.

[53] W. Ren, R.W. Beard, and E. Atkins. A survey of consensus problems in multi-agent coordination. In *Proceedings of the 2005 American Control Conference*, volume 3, pages 1859–1864, Portland, OR, 2005.

[54] R. Olfati-Saber, J.A. Fax, and R.M. Murray. Consensus and Cooperation in Networked Multi-Agent Systems. In *Proceedings of the IEEE*, volume 95 (1), pages 215–233, 2007.

[55] L. Pescosolido, S. Barbarossa, and G. Scutari. Decentralized Detection and Localization Through Sensor Networks Designed As a Population of Self-Synchronizing Oscillators. In *Proceedings of the 2006 IEEE International Conference on Acoustics Speech and Signal Processing*, volume 4, pages 981–984, Tolouse, France, 2006.

[56] S. Barbarossa, G. Scutari, and L. Pescosolido. Global Stability of a Population of Mutually Coupled Oscillators Reaching Global ML Estimate Through a Decentralized Approach. In

Proceedings of the 2006 IEEE International Conference on Acoustics Speech and Signal Processing, volume 4, pages 385–388, Tolouse, France, 2006.

[57] S. Barbarossa, G. Scutari, and A. Swami. Achieving Consensus in Self-Organizing Wireless Sensor Networks: The Impact of Network Topology on Energy Consumption. In *Proceedings of the 2007 IEEE International Conference on Acoustics Speech and Signal Processing*, pages 841–844, Honolulu, HI, 2007.

[58] S. Boyd, A. Gosh, B. Prabakhar, and D. Shah. Gossip algorithms: design, analysis and applications. In *Proceedings of the 24th Annual Joint Conference of the IEEE Computer and Communications Societies*, volume 3, pages 1653–1664, Miami, FL, 2005.

[59] A.D.G. Dimakis, A.D. Sarwate, and M.J. Wainwright. Geographic Gossip: Efficient Averaging for Sensor Networks. *IEEE Transactions on Signal Processing*, 56(3):1205–1216, 2007.

[60] T.C. Aysal, M.E. Yildiz, A.D. Sarwate, and A. Scaglione. Broadcast Gossip Algorithms for Consensus. *IEEE Transactions on Signal Processing*, 57(7):2748–2761, 2009.

[61] L. Xiao and S. Boyd. Fast linear iterations for distributed averaging. *Systems & Control Letters*, 53(1):65–78, 2004.

[62] Y. Hatano and M. Mesbahi. Agreement Over Random Networks. *IEEE Transactions on Automatic Control*, 50(11):1867–1872, 2005.

[63] S. Patterson, B. Bamieh, and A. El Abbadi. Convergence Rates of Distributed Average Consensus With Stochastic Link Failures. *IEEE Transactions on Automatic Control*, 55(4):880–892, 2010.

[64] R. Olfati-Saber and R.M. Murray. Consensus Protocols for Undirected Networks of Dynamic Agents with Communication Time-Delays. Technical report, California Institute of Technology, 2003.

[65] L. Xiao, S. Boyd, and S.-J. Kim. Distributed average consensus with least-mean-square deviation. *Journal of Parallel and Distributed Computing*, 67(1):33–46, 2007.

[66] S. Kar and J.M.F. Moura. Distributed Consensus Algorithms in Sensor Networks With Imperfect Communication: Link Failures and Channel Noise. *IEEE Transactions on Signal Processing*, 57(1):355–369, 2009.

[67] M. Porfiri and D.J. Stilwell. Consensus Seeking Over Random Weighted Directed Graphs. *IEEE Transactions on Automatic Control*, 52(9):1767–1773, 2007.

[68] A. Tahbaz-Salehi and A. Jadbabaie. A Necessary and Sufficient Condition for Consensus Over Random Networks. *IEEE Transactions on Automatic Control*, 53(3):791–795, 2008.

[69] J. Zhou and Q. Wang. Convergence speed in distributed consensus over dynamically switching random networks. *Automatica*, 45(6):1455–1461, 2009.

[70] Angelia Nedic, Alex Olshevsky, and Cesar A. Uribe. Nonasymptotic convergence rates for cooperative learning over time-varying directed graphs. In *Proceedings of the 2005 American Control Conference*, pages 5884–5889, 2015.

[71] Angelia Nedic and Alex Olshevsky. Distributed Optimization Over Time-Varying Directed Graphs. *IEEE Transactions on Automatic Control*, 60(3):601–615, 2015.

[72] A. Das and F.L. Lewis. Distributed adaptive control for synchronization of unknown nonlinear networked systems. *Automatica*, 46(12):2014–2021, 2010.

[73] J. Mei, W. Ren, and G. Ma. Distributed containment control for Lagrangian networks with parametric uncertainties under a directed graph. *Automatica*, 48(4):653–659, 2012.

[74] W. Ren and R.W. Beard. Decentralized Scheme for Spacecraft Formation Flying via the Virtual Structure Approach. *AIAA Journal of Guidance, Control and Dynamics*, 27(1):73–82, 2004.

[75] B. Wu, D. Wang, and E.K. Poh. Decentralized Robust Adaptive Control for Attitude Synchronization Under Directed Communication Topology. *AIAA Journal of Guidance, Control and Dynamics*, 34(4):1276–1282, 2011.

[76] C. McInnes. Autonomous ring formation for a planar constellation of satellites. *AIAA Journal of Guidance, Control and Dynamics*, 18(5):1215–1217, 1995.

[77] M. Ji and M. Egerstedt. Distributed Coordination Control of Multiagent Systems While Preserving Connectedness. *IEEE Transactions on Robotics*, 23(4):693–703, 2007.

[78] A.R. Pereira, H. Liu, and R. Ortega. Globally Stable Adaptive Formation Control of Euler-Lagrange Agents via Potential Functions. In *Proceedings of the 2009 American Control Conference*, pages 2606–2611, St. Louis, MI, 2009.

[79] M.A Demetriou. Design of Consensus and Adaptive-Consensus Filters for Distributed Parameter Systems. *Automatica*, 46(2):300–311, 2010.

[80] W. Yu, P. De Lellis, G. Chen, M. di Bernardo, and J. Kurths. Distributed Adaptive Control of Synchronization in Complex Networks. *IEEE Transactions on Automatic Control*, 57(8):2153–2158, 2012.

[81] Z. Zhang and M.A. Demetriou. Adaptive Attitude Synchronization Control of Spacecraft Formation with Adaptive Synchronization Gains. *AIAA Journal of Guidance, Control and Dynamics*, 37(5):1644–1651, 2014.

[82] I. Chang, S.-J. Chung, and L. Blackmore. Cooperative Control with Adaptive Graph Laplacians for Spacecraft Formation Flying. In *Proceedings of the 49th IEEE Conference on Decision and Control*, pages 4926–4933, Atlanta, GE, 2010.

[83] S.-J. Chung, S. Bandyopadhyay, I. Chang, and F.Y. Hadaegh. Phase synchronization control of complex networks of Lagrangian systems on adaptive digraphs. *Automatica*, 4(5):1148–1161, 2013.

[84] Y.C. Liu and N. Chopra. Synchronization of networked robotic systems on strongly connected graphs. In *Proceedings of the 49th IEEE Conference on Decision and Control*, pages 3194–3199, Atlanta, GE, 2010.

[85] E. Nuno, R. Ortega, L. Basañez, and D. Hill. Synchronization of Networks of Nonidentical Euler-Lagrange Systems With Uncertain Parameters and Communication Delays. *IEEE Transactions on Automatic Control*, 56(4):935–941, 2011.

[86] J.-J.E. Slotine and W. Li. *Applied Nonlinear Control*. Prentice Hall, 1991.

[87] H.K. Khalil. *Nonlinear Systems (3rd Edition)*. Prentice Hall, 2002.

[88] W. Lohmiller and J.-J.E. Slotine. On Contraction Analysis for Nonlinear Systems. *Automatica*, 34(6):683–696, 1998.

[89] Angeli D. A Lyapunov Approach to Incremental Stability Properties. *IEEE Transactions on Automatic Control*, 47(3):410–421, 2002.

[90] W. Wang and J.-J.E. Slotine. Contraction Analysis of Time-Delayed Communications Using Simplified Wave Variables. *IEEE Transactions on Automatic Control*, 51(4):712–717, 2006.

[91] J. Zhou, G. Ma, and Q. Hu. Delay Depending Decentralized Adaptive Attitude Synchronization Tracking Control of Spacecraft Formation. *Chinese Journal of Aeronautics*, 25(3):712–717, 2012.

[92] L. Perea, G. Gómez, and P. Elosegui. Extension of the Cucker-Smale Control Law to Spaceflight Formations. *AIAA Journal of Guidance, Control and Dynamics*, 32(2):527–537, 2009.

[93] F. Paita, G. Gómez, and J.J. Masdemont. On the Cucker–Smale Flocking Model Applied to a Formation Moving in a Central Force Field. In *64th International Astronautical Congress*, Beijing, China, September 2013.

[94] F. Paita, G. Gómez, and J.J. Masdemont. A Distributed Attitude Control Law for Formation Flying Based on the Cucker-Smale Model. In *65th International Astronautical Congress*, Toronto, Canada, October 2014.

[95] F. Paita, J.J. Masdemont, and G. Gómez. On the Rotational Cucker-Smale Model: Optimal Formation Configuration and Adaptive Gains Design. In *66th International Astronautical Congress*, Jerusalem, Israel, October 2015.

[96] F. Paita, G. Gómez, and J.J. Masdemont. On distributed control strategies for spacecraft formation flying. In *Astronet-II International Final Conference*, Tossa de Mar, Spain, June 2015.

[97] W. Ren and Y. Cao. *Distributed Coordination of Multi-agent Networks*. World Scientific, 2001.

[98] R.A. Horn and C.R. Johnson. *Matrix analysis*. Cambridge University Press, 2006.

[99] F.R.K. Chung. *Spectral Graph Theory*. American Mathematical Society, 1997.

[100] W. Ren, R.W. Beard, and T.W. McLain. *Cooperative Control*, volume 309 of *Lecture Notes in Control and Information Sciences*, chapter "Coordination Variables and Consensus Building in Multiple Vehicle Systems", pages 171–188. Springer-Verlag, 2005.

[101] W. Ren and R.W. Beard. *Distributed Consensus in Multi-vehicle Cooperative Control*. Springer-Verlag, 2008.

[102] C. Godsil and G. Royle. *Algebraic Graph Theory*. Springer-Verlag, 2001.

[103] R. Olfati-Saber and R.M. Murray. Consensus protocols for networks of dynamic agents. In *Proceedings of the 2003 American Control Conference*, volume 2, pages 951–956, Denver, CO, 2003.

[104] A.S. Morse. Supervisory Control of Families of Linear Set-Point Controllers, Part I: Exact Matching. *IEEE Transactions on Automatic Control*, 41(10):1413–1431, 1996.

[105] W. Ren and R.W. Beard. Consensus Seeking in Multiagent Systems Under Dynamically Changing Interaction Topologies. *IEEE Transactions on Automatic Control*, 50(5):655–661, 2005.

[106] F. Garin and L. Schenato. *Networked Control Systems*, volume 406 of *"Lecture Notes in Control and Information Sciences"*, chapter A Survey on Distributed Estimation and Control Applications Using Linear Consensus Algorithms, pages 75–107. Springer-Verlag, 2010.

[107] M. Cao, A.S. Morse, and B.D.O. Anderson. Reaching a Consensus in a Dynamically Changing Environment: A Graphical Approach. *SIAM Journal on Control and Optimization*, 47(2):575–600, 2008.

[108] F. Fagnani and S. Zampieri. Randomized Consensus Algorithms over Large Scale Networks. *IEEE Journal on Selected Areas in Communications*, 26(4):634–649, 2008.

[109] A. Tahbaz-Salehi and A. Jadbabaie. Consensus Over Ergodic Stationary Graph Processes. *IEEE Transactions on Automatic Control*, 54(12):225–230, 2009.

[110] S. Boyd, A. Ghosh, B. Prabhakar, and D. Shah. Randomized Gossip Algorithms. *IEEE Transactions on Information Theory*, 52(6):2508–2530, 2006.

[111] A. Kashyap, T. Başar, and R. Srikant. Quantized Consensus. *Automatica*, 43(7):1192–1203, 2007.

[112] P. Frasca, R. Carli, F. Fagnani, and S. Zampieri. Average consensus on networks with quantized communication. *International Journal of Robust and Nonlinear Control*, 19(16):1787–1816, 2008.

[113] P. Frasca, R. Carli, F. Fagnani, and S. Zampieri. Average consensus by gossip algorithms with quantized communication. In *Proceedings of the 47th IEEE Conference on Decision and Control*, pages 4831–4836, 2008.

[114] T.C. Aysal, M. Coates, and M. Rabbat. Distributed average consensus using probabilistic quantization. In *Proceedings of the IEEE 14th Workshop on Statistical Signal Processing*, pages 640–644, 2007.

[115] S. Kar and J.M.F. Moura. Distributed Consensus Algorithms in Sensor Networks: Quantized Data and Random Link Failures. *IEEE Transactions on Signal Processing*, 58(3):1383–1400, 2010.

[116] F. Fagnani and S. Zampieri. Average consensus with packet drop communication. *SIAM Journal on Control and Optimization*, 48(1):102–133, 2009.

[117] S. Kar and J.M.F. Moura. Distributed Consensus Algorithms in Sensor Networks with Imperfect Communication: Link Failures and Channel Noise. *IEEE Transactions on Signal Processing*, 57(5):355–369, 2009.

[118] M. Huang and J.H. Manton. Coordination and Consensus of Networked Agents with Noisy Measurements: Stochastic Algorithms and Asymptotic Behavior. *SIAM Journal on Control and Optimization*, 48(1):134–161, 2009.

[119] S. Kar, J.M.F. Moura, and K. Ramanan. Distributed Parameter Estimation in Sensor Networks: Nonlinear Observation Models and Imperfect Communication. *IEEE Transactions on Information Theory*, 58(6):3575–3605, 2012.

[120] R. Carli, G. Como, P. Frasca, and F. Garin. Average consensus on digital noisy networks. In *Proceedings of the 1st IFAC Workshop on Estimation and Control of Networked Systems*, pages 36–41, 2009.

[121] S. Roy, A. Saberi, and K. Herlugson. *Sensor Network Operations*, chapter "Formation and alignment of distributed sensing agents with double-integrator dynamics and actuator saturation", pages 126–157. IEEE Press, 2007.

[122] F. Cucker and S. Smale. Emergent Behavior in Flocks. *IEEE Transactions on Automatic Control*, 52(5):852–862, 2007.

[123] R. Olfati-Saber. Ultrafast consensus in small-world networks. In *Proceedings of the 2005 American Control Conference*, volume 4, pages 2371–2378, Portland, OR, 2005.

[124] S.A. Aldosari and J.M.F. Moura. Distributed Detection in Sensor Networks: Connectivity Graph and Small World Networks. In *Conference Record of the Thirty-Ninth Asilomar Conference on Signals, Systems and Computers*, pages 230–234, Pacific Grove, CA, 2005.

[125] S. Kar and J.M.F. Moura. Topology for Global Average Consensus. In *Conference Record of the Fourtieth Asilomar Conference onSignals, Systems and Computers*, pages 276–280, Pacific Grove, CA, 2006.

[126] D. Jakovetić, J. Xavier, and J.M.F. Moura. Weight Optimization for Consensus Algorithms With Correlated Switching Topology. *IEEE Transactions on Signal Processing*, 58(7):3788–3801, 2010.

[127] S.S. Pereira. *Distributed Consensus Algorithms for Wireless Sensor Networks (Convergence Analysis and Optimization)*. PhD thesis, Universitat Politècnica de Catalunya, 2011.

[128] Y. Hatano, A.K. Das, and M. Mesbahi. Agreement in presence of noise: pseudogradients on random geometric networks. In *Proceedings of the 44th IEEE Conference on Decision and Control and European Control Conference*, pages 6382–6387, 2005.

[129] D.S. Scherber and H.D. Papadopoulos. Locally constructed algorithms for distributed computations in ad-hoc networks. In *Proceedings of the Third International Symposium on Information Processing in Sensor Networks*, pages 11–19, 2004.

[130] M. Penrose. *Random Geometric Graphs*. Oxford University Press, 2003.

[131] J.-C. Delvenne, R. Carli, and S. Zampieri. Optimal Strategies in the Average Consensus Problem. *Systems & Control Letters*, 58(10-11):759–765, 2009.

[132] R. Carli, F. Fagnani, A. Speranzon, and S. Zampieri. Communication Constraints in the Average Consensus Problem. *Automatica*, 44(3):671–684, 2008.

[133] R. Olfati-Saber. Algebraic Connectivity Ratio of Ramanujan Graphs. In *Proceedings of the 2007 American Control Conference*, pages 4619–4624, 2007.

[134] R. Olfati-Saber. Ultrafast consensus in small-world networks. In *Proceedings of the 2005 American Control Conference*, volume 4, pages 2371–2378, 2005.

[135] A. Tahbaz-Salehi and A. Jadbabaie. Small world phenomenon, rapidly mixing Markov chains, and average consensus algorithms. In *Proceedings of the 2007 IEEE Conference on Decision and Control*, pages 276–281, 2007.

[136] F. Cucker and S. Smale. On the Mathematics of Emergence. *Japanese Journal of Mathematics*, 2(1):197–227, 2007.

[137] J.J. Shen. Cucker-Smale Flocking Under Hierarchical Leadership. *SIAM Journal on Applied Mathematics*, 68(3):694–719, 2008.

[138] F. Cucker and J.-G. Dong. On the critical exponent for flocks under hierarchical leadership. *Mathematical Models and Methods in Applied Sciences*, 19:1391–1404, 2009.

[139] S. Motsch and E. Tadmor. A New Model for Self-organized Dynamics and its Flocking Behavior. *Journal of Statistical Physics*, 144(5):923–947, 2011.

[140] J. Park and J. Kim. Cucker-Smale Flocking with Inter-Particle Bonding Forces. *IEEE Transactions on Automatic Control*, 55(11):2617–2623, 2010.

[141] F. Cucker and J.-G. Dong. Avoiding Collisions in Flocks. *IEEE Transactions on Automatic Control*, 55(5):1238–1243, 2010.

[142] F. Cucker and J.-G. Dong. A General Collision-Avoiding Flocking Framework. *IEEE Transactions on Automatic Control*, 56(5):1124–1129, 2011.

[143] J.-G. Dong. *Hierarchical Leadership and Collision Avoidance in Flocking*. PhD thesis, City University of Hong Kong, 2011.

[144] F. Dalmao and E. Mordecki. Cucker-Smale Flocking Under Hierarchical Leadership and Random Interactions. *SIAM Journal of Applied Mathematics*, 71(4):1307–1316, 2011.

[145] S. Motsch and E. Tadmor. Heterophilus Dynamics Enhances Consensus. *Preprint*, 2013. Available at arXiv:1301.4123.

[146] C. Colombo, C. Lucking, and C.R. McInnes. Orbit evolution, maintenance and disposal of SpaceChip swarms through electro-chromic control. *Acta Astronautica*, 82(1):25–37, 2013.

[147] J.A Carrillo, M. Fornasier, J. Rosado, and G. Toscani. Asymptotic Flocking Dynamics for the Kinetic Cucker–Smale Model. *SIAM Journal of Mathematical Analysis*, 42(1):218–236, 2010.

[148] S.-Y. Ha and E. Tadmor. From particle to kinetic and hydrodynamic descriptions of flocking. *Kinetic and Related Models*, 1(3):415–435, 2008.

[149] S.-Y. Ha and J.-G. Guo. A simple proof of the Cucker-Smale flocking dynamics and mean-field limit. *Communications in Mathematical Sciences*, 7(2):297–325, 2009.

[150] G. Mingotti and C.R. McInnes. Relative Orbital Dynamics of Swarms of Femto-Spacecraft. In *64th International Astronautical Congress*, Beijing, China, September 2013.

[151] G. Gómez and M. Marcote. High Order Analytical Solutions of Hill's Equations. *Celestial Mechanics and Dynamical Astronomy*, 94(2):197–211, 2006.

[152] C. Trenkel, S. Kemble, N. Bevis, and J. Magueijo. Testing Modified Newtonian Dynamics with LISA Pathfinder. *Advances in Space Research*, 50(11):1570–1580, 2012.

[153] V. Szebehely. *Theory of Orbits*. Academic Press, 1967.

[154] K. Hill, M.W. Lo, and G.H. Born. Liaison Navigation in the Sun-Earth-Moon Four-Body Problem. *Advances in the Astronautical Sciences*, 124:1909–1924, 2006.

[155] G. Gómez, J. Llibre, R. Martínez, and C. Simó. *Dynamics and Mission Design Near Libration Points (II)*. Springer-Verlag, 2011.

[156] S. Casotto. The Equations of Relative Motion in the Orbital Reference Frame. *Celestial Mechanics and Dynamical Astronomy*, 124(3):215–234, 2015.

[157] G.W. Hill. Researches in the lunar theory. *American Journal of Mathematics*, 1(1):5–26, 1878.

[158] Clohessy W. and Wiltshire R. Terminal guidance system for satellite rendezvous. *Journal of the Aerospace Sciences*, 27(9):653–658, 1960.

[159] J.P. de Vries. Elliptic Elements in Terms of Small Increments of Position and Velocity Components. *AIAA Journal*, 1(11):2626–2629, 1963.

[160] J. Tschauner and P. Hempel. Optimale Beschleunigungsprogramme für das Rendezvous–Manöver. *Astronautica Acta*, 10:339–343, 1964.

[161] B. Wie. *Space Vehicle Dynamics and Control*. American Institute of Aeronautics and Astronautics, 1998.

[162] D. Andreis and E.S. Canuto. Orbit dynamics and kinematics with full quaternions. In *Proceedings of the 2004 American Control Conference*, volume 4, pages 3660–3665, Boston, MA, 2004.

[163] C.G. Mayhew, R.G. Sanfelice, and A.R. Teel. On quaternion-based attitude control and the unwinding phenomenon. In *Proceedings of the 20011 American Control Conference*, pages 299–304, San Francisco, CA, 2011.

[164] P.C. Hughes. *Spacecraft Attitude Dynamics*. Wiley, 1986.

[165] W. Ren. Distributed Attitude Alignment in Spacecraft Formation Flying. *International Journal of Adaptive Control and Signal Processing*, 21(2-3):95–113, 2007.

[166] D.Q. Huynh. Metrics for 3D Rotations: Comparison and Analysis. *Journal of Mathematical Imaging and Vision*, 35(2):155–164, 2009.

[167] W. Ren. Distributed Attitude Consensus Among Multiple Networked Spacecraft. In *Proceedings of the 2006 American Control Conference*, pages 1760–1765, Minneapolis, MI, 2006.

[168] K. Shoemake. Uniform random rotations. In *Graphics Gems III*, pages 124–132. Academic Press, 1992.

[169] A.K. Misra and Y. Panchenko. Attitude Dynamics of Satellites Orbiting an Asteroid. *The Journal of Astronautical Sciences*, 54(3-4):369–381, 2006.